Mechanisms of Neurodegeneration in Niemann-Pick Type C Disease

by

Elaine A. Liu

A dissertation submitted in partial fulfillment
of the requirements for the degree of
Doctor of Philosophy
(Cellular and Molecular Biology)
in the University of Michigan
2021

Doctoral Committee:

Professor Andrew P. Lieberman, Chair
Professor Peter Arvan
Associate Professor Sami J. Barmada
Professor Malini Raghavan

Elaine A. Liu

ealiu@med.umich.edu

ORCID iD: 0000-0003-2730-1690

Acknowledgements

First, I would like to thank my mentor, Dr. Andrew Lieberman. Through all these years, he has always been kind, supportive and encouraging. The care and investment he puts into his students is evident as he fosters a positive and collaborative environment where we can pursue science with joy and curiosity. I am so grateful for the growth I could experience under his mentorship and to have him as role model for my own career.

I would also like to thank the members of my thesis committee, Dr. Peter Arvan, Dr. Sami Barmada and Dr. Malini Raghavan, who always challenged me with important questions and provided enlightening insight, comments, and suggestions at each committee meeting. Their expertise and support played an essential role in propelling my work.

This dissertation is also dedicated to my family. Without them, I could not be where I am today. Their constant encouragement, support and prayers always lift my spirits, open my perspectives, and remind me of what is most important. Whether near or far, I always feel their love and presence in my life.

I would also like to thank my friends and my church family. They have always been there for me, providing a space to check-in and talk about how I'm doing, enjoy our hobbies and diverse interests, and pray for me. Spending time with them is always refreshing and brings joy to my life.

Finally, I would like to thank God. He is my source of strength, purpose, and hope and provides me with peace that transcends understanding through all things.

Table of Contents

List of Figures

Abstract

Lysosomal storage diseases (LSDs) are a heterogeneous group of more than 70 inherited disorders characterized by the accumulation of lysosomal substrates due organellar dysfunction. This accumulation of substrates compromises lysosomal function and leads to a variety secondary effects, including defects in autophagy, calcium homeostasis, oxidative stress and activation of cell death pathways. LSDs manifest in a wide spectrum of clinical phenotypes. Notably, two-thirds of patients across LSDs display significant neurological symptoms. Niemann-Pick C disease (NPC) is an autosomal recessive LSD that primarily affects children and causes severe, progressive neurodegeneration and early death. NPC is caused by mutations in NPC1 or NPC2, proteins that function in concert to export cholesterol from the lysosome; defects in either of these two proteins leads to abnormal cholesterol trafficking and storage within the lysosomal compartment. Although we have increased our understanding of the function of NPC1 and NPC2 in cholesterol trafficking, the mechanisms that underlie neurodegeneration in NPC are not well understood, and there are currently no FDA approved treatments for this disease. This dissertation aims to characterize mechanisms of neurodegeneration in NPC and identify potential targets for therapeutic intervention.

In Chapter 1, this thesis outlines LSDs and focuses in on the genetics and pathology of NPC. It discusses what is known about key pathways that contribute to disease pathogenesis, including autophagy, lysosomal membrane permeabilization, and TDP-43 proteinopathy. In Chapter 2, this thesis describes the intersection between altered calcium homeostasis and

dysfunctional autophagy in lysosomal diseases. In Chapter 3, this thesis provides primary data

demonstrating that NPC cells are more sensitive to lysosomal damage as a consequence of lipid

storage. Furthermore, the data presented identify a role for Fbxo2 in CNS lysophagy and

establishes its functional importance in NPC. In Chapter 4, this thesis presents primary data that

examines the connection between dysfunctional neuron autophagy and TDP-43 proteinopathy in

the NPC brain. Furthermore, these data provide the first evidence nuclear pathology in an LSD.

Finally, Chapter 5 summarizes these findings and discusses remaining questions and suggests

future directions. The work presented in this dissertation seeks to understand mechanisms

underlying neurodegeneration in NPC, and I hope that this work will contribute to the

identification of novel therapeutic strategies.

Chapter 1

Introduction

1.1 The Lysosome

The lysosome was discovered serendipitously in 1955 by Christian de Duve [1]. While he initially set out to investigate the localization of hepatic glucose 6-phosphatase utilizing recently developed fractionation assays, de Duve made a surprising discovery of a new cellular compartment that contained his control enzyme, acid phosphatase. This enzyme localized to a new cellular compartment he termed the "lysosome [2]." Since then, more than 60 acid hydrolases have been discovered, and the lysosome has been shown to play an essential role in recycling of cellular waste and degradation of biological macromolecules, including proteins, lipids, carbohydrates and nucleic acids. As such, the lysosome has been termed the "garbage disposal" of the cell.

Although degradation of substrates is an essential function of the lysosome, it has become increasingly clear that the lysosome is involved in significant cellular processes beyond digestion. Far from being a mere "garbage disposal," the lysosome is an essential metabolic signaling hub. Mechanistic target of rapamycin complex 1 (mTORC1), a key regulator of cellular biosynthetic pathways [3] associates with the lysosome under specific conditions, including in response to changes in amino acid and lysosomal cholesterol [4] levels. The association of mTORC1 with the lysosome, mediated by RAG GTPases [5-7], leads to mTORC1 activation and support of cell anabolism and suppression of autophagy [8]. In this way, the

lysosome, a catabolic organelle, interfaces with regulation of anabolic pathways and cellular homeostasis.

Rag GTPases also facilitate the recruitment of TFEB, a master regulator of lysosome biogenesis and autophagy [9], to the lysosome, which leads to mTORC1 dependent phosphorylation and inhibition TFEB [10]. Activity and localization of TFEB is also regulated by lysosomal Ca^{2+}, as release of Ca^{2+} from the lysosomal TRPML1 channel activates calcineurin, which dephosphorylates TFEB and promotes its nuclear translocation [11]. Further, lysosomes participate in additional functions including gene regulation and plasma membrane repair, interact with other organelles through membrane contact sites, and are dynamic in changing their size, shape and number in response to environmental cues [12].

With such a vital role of the lysosome in cellular function, it follows that lysosomal dysfunction leads to human disease, from rare, inherited lysosomal storage disorders (LSDs) to more common neurodegenerative diseases, cancer and metabolic disorders. Here, we focus on examining mechanisms of pathology in LSDs.

1.2 Lysosomal Storage Disorders

LSDs are a heterogeneous group of more than 70 inherited disorders characterized by the accumulation of lysosomal substrates due to organellar dysfunction. The majority of LSDs exhibit autosomal recessive inheritance, though three are X-linked. As LSDs are characterized by the accumulation of substrates, many are caused by mutations in genes that encode lysosomal proteases. However, LSDs are also caused by mutations in lysosomal transporters, integral membrane proteins and enzyme modifiers. The accumulation of substrates compromises lysosomal function and leads to a variety of secondary effects, including deficits in degradation

pathways such as autophagy, alterations in calcium homeostasis, oxidative stress, and activation of cell death pathways [13].

Collectively, the prevalence of LSDs is quite high compared to other rare diseases at approximately 1 in 5,000 live births [13,14]. LSDs lead to a wide spectrum of clinical phenotypes, but most often present in childhood with visceromegaly. LSDs progress to affect a variety of organs from the heart and lung, to the gastrointestinal system, muscle, bones, skin, kidney and the immune system [13]. Despite the wide clinical variability among different LSDs, it is notable that two-thirds of patients across LSDs display significant neurological symptoms.

Some LSDs are treatable, but for many, treatment strategies are still limited and they are managed symptomatically. A diverse array of approaches has been tested in hopes of developing disease modifying therapies for LSDs. One strategy for treatment is enzyme replacement therapy (ERT) to exogenously provide the missing or defective enzyme. ERT can only be done with soluble enzymes and has other limitations, including difficulty of uptake into certain organs. Additionally, patients may develop antibodies against the therapeutic enzyme, which leads to adverse side effects [15]. Another strategy for the treatment of LSDs is substrate reduction therapy (SRT), which inhibits the buildup of the storage material in the lysosome. SRTs are non-immunogenic and can be given orally, but design of SRTs can be challenging depending on the accumulated substrate. Currently, it is only available for two LSDs [16]. Further, treatment strategies are also being developed aimed at stabilizing the mutant enzyme, promoting its folding or preventing its degradation, with the idea that if properly folded, the mutant enzymes could retain at least partial activity. Still, these strategies may be mutation specific and targeting the optimal enzyme activity level remains a challenge.

Although we have greatly progressed in our understanding of lysosomal function and of mechanisms involved in LSD pathogenesis, our understanding is still limited, and development of effective treatment strategies remains a necessary and critical task.

1.3 Niemann-Pick C

Niemann-Pick C disease (NPC) is an autosomal recessive LSD characterized by the accumulation of unesterified cholesterol in lysosomes and late endosomes [17]. NPC is part of a group of Niemann-Pick Diseases (types A, B, C), which are characterized by altered intracellular lipid metabolism or trafficking, leading to lipid accumulation.

Niemann-Pick type A and B are caused by deficiency in the enzyme acid sphingomyelinase, which functions to hydrolyze sphingomyelin into ceramide and phosphocholine [18,19]. Thus, they are characterized by the accumulation of sphingomyelin and other lipids in the lysosome. The diagnosis is established when the activity of the enzyme is less than 10% of controls [20]. Niemann-Pick type A patients are the most severely affected, have nearly complete loss of enzyme activity (<1%), and exhibit hepatosplenomegaly plus neuronopathic disease. These patients show a failure to thrive, and 50% of infants present with a cherry-red spot in the macula. Niemann-Pick A patients develop rapid, progressive neurodegeneration and death in infancy, often from respiratory failure [21]. In contrast, Niemann-Pick type B patients do not exhibit neurodegeneration, but can have prominent hepatosplenomegaly and liver failure. Children have growth restriction and gradually worsening pulmonary function [21]. Forms intermediate to these extremes occur as a continuum of neurological findings (so-called type A-B patients).

Niemann-Pick C (NPC) is characterized by the accumulation of unesterified cholesterol in late endosomes and lysosomes [17,22]. This cholesterol represents LDL cholesterol that is

endocytosed through the LDL-receptor pathway and delivered to the lysosome. In the lysosome, cholesterol esters are hydrolyzed, and in normal conditions, cholesterol is liberated and used by the cell [23]. NPC is caused by mutations in NPC1 and NPC2, proteins that function in concert to export cholesterol from the lysosome; defects in either of these two proteins leads to abnormal cholesterol trafficking and storage within the lysosomal compartment.

The majority of cases of NPC (~95%) are due to mutations in the *NPC1* gene [24], although a small subset (~5%) are due to mutations in *NPC2* [25]. NPC1 is a large, 1278-residue protein with 13 transmembrane domains found in the limiting membrane of late endosomes and lysosomes. It contains a luminal amino terminus, cytosolic carboxyl-terminal tail, 3 large and 4 small luminal loops, 6 small cytoplasmic loops and a sterol sensing domain [26]. NPC1 binds cholesterol at the first luminal loop, which is designated the N-terminal domain [27], and a functioning sterol sensing domain is required for its interaction with cholesterol [28] (Figure 1.1).

NPC2 is a small, 131-residue protein found in the lumen of the lysosome, and contains a deep hydrophobic pocket that binds cholesterol [29]. NPC1 and NPC2 bind cholesterol in opposite orientations [30], and a mechanism has been identified in which NPC2 binds to free cholesterol in its hydrophobic pocket and transfers cholesterol to the N-terminal domain of NPC1 in a "hand-off" mechanism [31-36]. Still, the mechanism by which NPC1 then transfers cholesterol across the lysosomal membrane is incompletely understood. It has been proposed that through interaction of the N-terminal domain with the C-terminal domain, NPC1 transfers cholesterol to its sterol sensing domain in the lysosomal membrane, or directly to the lysosomal membrane to facilitate egress [31,35]. However, it has also been shown that NPC1 can transfer cholesterol to neighboring NPC1 molecules [37], and another mechanistic possibility has been proposed such that NPC1 could function as a transporter by which cholesterol can pass through the protein [38] (Figure 1.1).

Mutations in NPC1 or NPC2 impair cholesterol trafficking and cause NPC disease. The incidence of NPC is estimated in a range from 1/150,000 to 1/50,000 [39,40]. It is a devastating illness that is clinically heterogeneous. While primarily affecting children, the age of onset can range from the perinatal period into adulthood, and lifespan can range from a few days to over 60 years of age, although the majority of individuals die between 10 and 25 years of age [41]. Clinically, it often begins with liver disease, followed by a gradually worsening neurological course, with loss of motor skills, cognitive decline, seizures, and death [39].
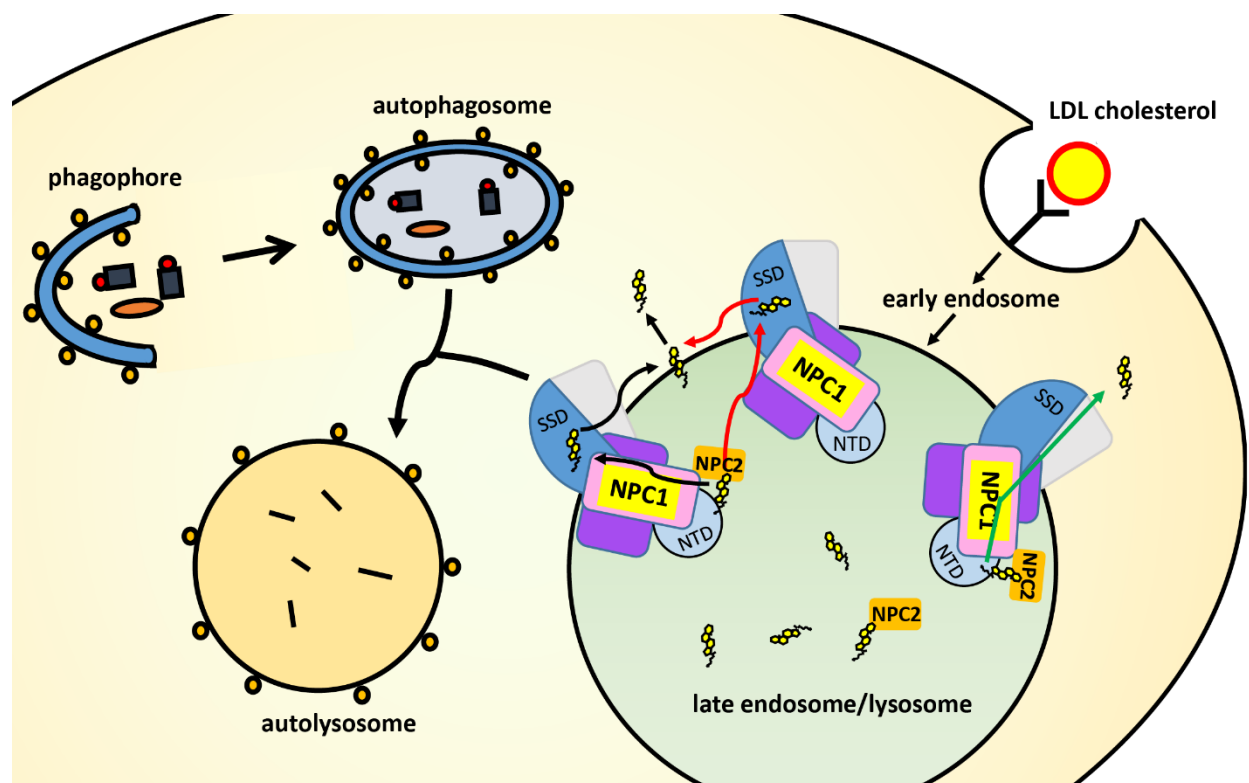
Figure 1.1 Lysosome function in cholesterol trafficking and autophagy. Endocytosed LDL cholesterol is trafficked to the lysosome, where NPC1 and NPC2 function to export cholesterol out of the lysosome. Luminal NPC2 passes cholesterol to the N-terminal domain (NTD) of NPC1, a large transmembrane protein. Several mechanisms have been proposed for how this cholesterol can then exit the lysosome. This cholesterol may be transferred to the sterol sensing domain (SSD) intramolecularly (black arrows) or intermolecularly (red arrows), where it is then inserted into the lysosome's limiting membrane and released through poorly characterized mechanisms. Alternatively, cholesterol may pass through the NPC1 protein (green arrows), possibly followed by handoff to cholesterol binding proteins in other organelles such as the endoplasmic reticulum. The lysosome is also critical for autophagy, where a double membrane phagophore surrounds substrates and encloses as the autophagosome. The autophagosome fuses with the lysosome, forming the autolysosome, leading to degradation of substrates.

Currently, treatment for NPC remains largely symptomatic, including through use of antiepileptic drugs for seizures or anticholinergic agents to improve dystonia. Miglustat, a

reported inhibitor of glucosylceramide synthase, partially stabilizes disease but does not alter the disease course [42] and has been approved in the European Union for treatment of NPC. The involvement of cholesterol storage in neurodegeneration has spurred the development of substrate reduction therapeutics such as hydroxypropyl-beta-dextrin (cyclodextrin). In mice and cats, peripheral administration of cyclodextrin corrects liver enzyme activity and weight defects but has no effects on neurodegeneration. This was found to be caused by the low blood brain permeability of cyclodextrin [43]. Alternatively, intrathecal administration of cyclodextrin circumvents this challenge and dramatically improves lifespan and slows the disease course. These promising results have moved cyclodextrin through stage 1 and 2 clinical trials. Although neurological defects are slowed, cyclodextrin has limitations, including challenges associated with intrathecal injections, severe hearing loss [44], and more recently described, temporary paralysis. The mechanism by which cyclodextrin exerts therapeutic effects is controversial, and may include liberation of stored cholesterol from the lysosome by circumventing the need for NPC1/NPC2, promotion of lysosomal exocytosis, or redistribution of cholesterol following its extraction from the plasma membrane [45-48].

Although our understanding of NPC has progressed, increased mechanistic understanding of disease pathogenesis is essential to uncover new treatment strategies.

1.4 Autophagy

One pathway that has been implicated in the pathogenesis of NPC is altered autophagy. Autophagy, literally meaning 'self-eating,' is an essential process for cellular quality control that relies on the lysosome to degrade misfolded proteins, protein aggregates or dysfunctional organelles. It is divided into three main subtypes – macroautophagy, microautophagy, and

chaperone mediated autophagy – based on the mechanism of delivery of cytosolic components.

In macroautophagy, cytoplasmic cargo is delivered to the lysosome through fusion with a double membrane-bound vesicle known as the autophagosome [49]. In microautophagy, cytosolic components are taken up by the lysosome directly through invagination of the lysosomal membrane [50]. In chaperone mediated autophagy, chaperones identify cargo that contain a pentapeptide KFERQ consensus motif, and these substrates are then unfolded and translocated across the lysosomal membrane [51].

In this thesis, I focus on macroautophagy, which I will herein refer to as autophagy. Autophagy begins with the formation of a pre-autophagosomal structure (PAS) that is initiated through the function of several autophagy-related (*ATG*) genes and signaling complexes. The PAS gives rise to an isolation membrane or phagophore, which elongates, recruits microtubule-associated protein 1 light chain 3 (LC3), and envelopes a portion of the cytosol to enclose and become a double-membrane vesicle, the autophagosome. During formation of the autophagosome, ubiquitinated proteins are recognized by p62, which binds directly to LC3 to facilitate delivery of cargo to autophagosomes [52]. The autophagosome then fuses to the lysosome to form an autolysosome, ultimately leading to the degradation of substrates by the action of lysosomal hydrolases [53].

A subset of these Atg proteins, termed the 'core molecular machinery,' are essential for autophagosome formation [54]. This core machinery consists of 1) the Atg1/ULK complex, 2) two ubiquitin-like protein conjugation systems (Atg12 and Atg8/LC3), 3) the class III phosphatidylinositol 3-kinase/Vps34 complex I and 4) two transmembrane proteins Atg9/mAtg9 and VMP1 [55].

The ULK complex, which contains ULK1/2, mAtg13 and FIP200, is important for autophagy initiation. In addition, hVps34 forms a complex with Beclin-1 and p150, which also promotes autophagosome formation and maturation. For elongation and expansion of the phagophore, Atg12 is conjugated to Atg5 through the action of Atg7 (an E1-like enzyme) and Atg10 (an E2-like enzyme). The Atg12-Atg5 conjugate then interacts with Atg16L, which oligomerizes to form the Atg16L complex. In parallel, Atg8/LC3 is cleaved by Atg4 at its C-terminus to generate cytosolic LC3-I. LC3-I is conjugated to phosphatidylethanolamine (PE) to form LC3-II through the action of Atg7 and Atg3 (an E2-like enzyme). LC3-II is then attached to the phagophore membrane. These two ubiquitination-like systems appear to be closely connected, as inhibition of either system prevents progression of the other [55].

Upstream, autophagy is regulated by several signaling pathways. mTORC1, when activated under nutrient-rich conditions, phosphorylates the Ulk complex with Atg13, which inactivates them and inhibits autophagy. Conversely, inactivation of mTORC1 leads to dephosphorylation of the Ulk complex and induction of autophagy [8]. In addition, calcium plays a role in autophagy regulation, and altered calcium homeostasis is also implicated in several LSDs. This is the topic of discussion in Chapter 2.

Autophagy is critical for cellular function, including as a response against metabolic stress such as starvation, and eliminating defective proteins and organelles. Thus, it follows that dysfunction in autophagy leads to human disease across many organ systems, including cardiac disease, cancer, aging, inflammatory disease, and muscle disease [56]. Notably, autophagy has been found to play an increasingly important role in many neurodegenerative diseases, such as Alzheimer and Huntington Disease, where it is essential for degrading disease-related protein aggregations [57]. Autophagy is particularly important in neurons, as they are non-dividing cells

and cannot clear waste through cell division [58]. Without functioning autophagy, neurons accumulate ubiquitinated proteins and degenerate; mice with neural-specific knockouts of essential autophagy genes develop accumulation of cytoplasmic ubiquitin-containing inclusion bodies in neurons and develop progressive neurodegeneration [59-62].

As the lysosome plays an essential role in autophagy by fusing with autophagosomes and digesting their content, autophagy dysfunction is also seen across LSDs, and they can be seen primarily as "autophagy disorders [63]." Although the specifics of autophagic dysfunction vary, a common theme includes accumulation of lysosomal storage material, impairment of autophagic flux, and secondary accumulation of autophagic substrates and damaged mitochondria, leading to cellular damage and cell death [63].

In NPC, there is a striking accumulation of LC3, p62 and autophagic vesicles in multiple tissues of *Npc1-/-* mice and cultured patient fibroblasts [64-66]. Studies in our lab and others have found defects in autophagy in patient fibroblasts at multiple steps of the pathway, including increased induction of autophagy through Beclin-1 [65], decreased autophagic flux and lysosomal fusion [67] and impaired cargo degradation in lysosomes due to altered enzyme activity [65,68]. Studies in neuronal models of NPC disease also support activation of autophagy and a block in autophagy flux that contributes to defective clearance of mitochondria and mitochondrial fragmentation [69-71].

Although some work characterized neuronal autophagy in NPC, it is noteworthy that prior studies have been done primarily on non-neuronal cells. This is important considering that studies done in our lab have shown that deleting *Npc1* specifically in neurons but not in astrocytes is capable of recapitulating the neurological phenotype of a global *Npc1* null mouse [72]. In addition, autophagy is regulated differently in neurons compared to non-neuronal cells [73].

Neurons exhibit low basal levels of autophagosomes and lack of autophagy induction in response to starvation, which is seen in the heart and liver [73-75]. Furthermore, the polarized structure of neurons adds another layer of complexity to autophagy dynamics. In neurons, autophagosomes are formed in the distal axon and undergo retrograde transport towards the cell body where they are degraded [76]. Thus, autophagy in neurons exhibits spatial and temporal regulation. Impairments in neuron autophagy lead to accumulation of autophagosomes within swollen axons [77]. In *Npc1* deficient mice, there is a striking accumulation of swollen axons throughout the brainstem [78], a pathology reminiscent of the effects of neuron autophagic dysfunction. In Chapter 4, I characterize these axonal swellings and show that they accumulate autophagic cargo, including damaged mitochondria.

1.5 Lysosomal Damage and Lysophagy

Soon after lysosomes were discovered by de Duve, the possibility that they could act as 'suicide bags' was proposed [79]. As lysosomes sequester potent lytic enzymes, such as cathepsins, it was thought that integrity of the lysosomal membrane must be critical to protect the cell against autolytic injuries. Indeed, this hypothesis has been shown to be accurate; on top of the plethora of other cellular functions involving lysosomes, they also play a key role in cell death.

Lysosomal cell death is preceded by lysosomal membrane permeabilization (LMP). In this process, damage to the lysosomal membrane leads to leakage of lysosomal contents, including cathepsins, which triggers cell death pathways. LMP can be induced by numerous endogenous and exogenous factors, including oxidative stress, iron-catalysed Fenton reactions, endocytosed materials such as silica crystals, lipids, pathogens and lysosomotropic drugs [80].

Inhibition of cathepsins enhances cell survival, supporting the role that leaked cathepsins play in mediating cell death [81].

LMP can trigger a variety of cell death processes depending on the cellular context and cell type. There are varying degrees of LMP, from massive leakage that leads to acidification of the cytosol, breakdown of cell components and necrosis, to partial and selective leakage of cathepsins that initiate alternative cell death pathways, including apoptosis or pyroptosis [82]. One of the main cell death pathways triggered by LMP involves cathepsin mediated cleavage of Bid, which activates pro-apoptotic Bcl-2 family members Bax and Bak, and induces mitochondrial outer membrane permeabilization, cytochrome c release and caspase-dependent apoptosis. However, caspase-independent apoptosis can also occur, as lysosomal cell death induced by certain infections or microtubule poisons cannot be prevented by caspase inhibitors [83].

LMP-induced cell death can occur under physiologic conditions as a homeostatic response, such as during mammary gland involution or to maintain neutrophil numbers during inflammation [83]. However, LMP has also been observed in several neurodegenerative diseases, including Alzheimer and Parkinson diseases, and an increasing number of LSDs [83]. In a mouse model of Gaucher disease, changes in the levels and distribution of cathepsins were observed in the brain and neurons, indicating release from the lysosome [84]. In late-infantile neuronal ceroid lipofuscinosis, subunit c of mitochondrial ATP synthase, one of the stored catabolites, was found in extra-lysosomal aggregates in neurons, consistent with LMP [85]. LMP has also been observed in Niemann Pick disease type A, where accumulated sphingomyelin levels induce lysosomal damage [86,87], and lysosomal instability can be corrected by treatment with Hsp70 [88]. Altered levels, activity and localization of cathepsins has also been observed in NPC; inhibition of

cathepsins attenuates neuron death, whereas activation of cathepsins enhances the degenerative phenotype in NPC mice [89,90].

To limit cytotoxic consequences of LMP, cells can either repair or degrade the damaged lysosomes. Lysosomes that have undergone more limited permeabilization can be repaired through the function of ESCRT (endosomal sorting complex required for transport) machinery [91,92]. However, upon more significant lysosomal damage, lysosomes are degraded through a form of selective autophagy known as lysophagy. In this process, damaged lysosomes are sensed, and subsequent ubiquitination of lysosomal proteins leads to recruitment of autophagic machinery, engulfment by autophagic membranes, and clearance of the damaged organelles [80].

Sensing of damaged lysosomes involves the exposure of glycans that are normally on the luminal side of lysosomes. These glycans are recognized by cytosolic galectins, including galectin-1, -3, -8 and -9 [93-96]. In addition to their sensing function, galectins also play more active roles in lysophagy by recruiting autophagy adapters; galectin-3 interacts with TRIM16 [94], and galectin-8 recruits NDP52 [96], which contributes to ubiquitination of damaged lysosomes and recruitment of autophagic membranes, respectively. Further, galectin-8 inhibits mTOR signaling through its Ragulator-Rag signaling machinery and galectin-9 activates AMPK, both of which activate autophagy after lysosomal damage [97].

A key intermediate step for lysophagy progression is ubiquitination of lysosomal proteins. Polyubiquitination of organelle membrane proteins is a feature of many forms of selective autophagy, which mediates recruitment of autophagic machinery, allowing for efficient organelle turnover [80,98]. LRSAM1 [99], TRIM16 [94] and the SCF^{FBXO27} ubiquitin ligase complex [100] are ubiquitin ligases that have been implicated in lysophagy. In addition, the ubiquitin-directed AAA-ATPase p97 is also recruited to damaged lysosomes. Deficiency in p97 delays lysophagy

and is thought to extract ubiquitinated proteins from the lysosomal membrane to facilitate binding to autophagy receptors [101,102].

Although components of lysophagy have been identified in recent studies, aspects of the machinery that function in organ and cell type specific regulation remain incompletely understood. Notably, LMP has been observed in an increasing number of neurodegenerative diseases, yet brain specific lysophagy machinery remains unknown. Understanding the role that lysosomal damage plays in NPC and uncovering mechanisms of lysophagy in the brain is the focus of Chapter 3.

1.6 Autophagy and TDP-43 proteinopathy

Dysfunctional autophagy has also been associated with the cytoplasmic mislocalization and aggregation of TAR-DNA binding protein of 43 kDa (TDP-43). TDP-43 is a ubiquitous, highly conserved RNA/DNA- binding protein that belongs to the heterogeneous nuclear ribonucleoprotein (hnRNP) family and functions in RNA metabolism. It contains two RNA recognition motifs, a nuclear localization sequence at the N-terminus, a nuclear export signal, and a C-terminal glycine-rich low complexity domain. Though TDP-43 is primarily nuclear, it can shuttle between the nucleus and cytoplasm [103], and plays key roles in RNA processing, including splicing, translation and degradation [104,105].

TDP-43 expression levels and localization are critical for normal cellular function, and cytoplasmic inclusions of TDP-43 are a pathological hallmark of amyotrophic lateral sclerosis (ALS) and frontotemporal degeneration (FTD). Pathologic TDP-43 forms ubiquitinated cytoplasmic aggregates, is hyper-phosphorylated, cleaved to generate C-terminal fragments, and is depleted from the nucleus [106,107]. Although ALS and FTD are biochemically, genetically and

clinically heterogeneous, pathological TDP-43 cytoplasmic inclusions are observed in over 90% of ALS and over 50% of FTD patients, highlighting its role in disease pathogenesis [108]. Corresponding to nuclear exclusion, TDP-43 loss-of-function mechanisms have been indicated in neurodegeneration. Loss of TDP-43 in diverse model systems from C. elegans to Drosophila and zebrafish results in behavioral and neurodegenerative phenotypes [109-111]. Furthermore, homozygous loss of TDP-43 in mice is embryonic lethal and heterozygous mutants display motor deficits and muscle weakness [112], revealing the essential role of TDP-43 in development and neuromuscular function. On the flip side, gain-of-function mechanisms have also been described. Increased levels of TDP-43 have been detected in ALS patients [113-115], overexpression of TDP-43 causes neurodegeneration [116-119], and cytoplasmic mislocalization of TDP-43 is sufficient to drive neuron death [120].

Despite increased understanding of both gain- and loss-of-function pathological mechanisms of TDP-43 mislocalization [121], the processes that mediate the formation of these pathological aggregates remain incompletely understood. TDP-43 contains a C-terminal low complexity domain, which renders it aggregation prone [122]. Disordered domains can drive dynamic self-assembly into intracellular membraneless organelles. In cell culture, TDP-43 undergoes liquid-liquid phase separation and forms cytosolic liquid droplets in response to stress. These then progressively convert into gels/solids that show characteristics of TDP-43 aggregates in vivo and cause neuron death [123]. Almost all ALS-associated TDP-43 mutations are concentrated in the low complexity domain, which promote its cytoplasmic mislocalization [124-126]. However, they contribute to only 2%-5% of ALS cases [121,122]. An alternative mechanism of TDP-43 aggregation is thought to arise from its role in stress granule assembly, as TDP-43 recruitment to stress granules may increase its propensity to form pathological aggregates [127-129].

Still, the role of stress granules in TDP-43 aggregation is unclear, as TDP-43 mislocalization has also been shown to occur independently of stress granule formation [123,130]. More recently, neuroinflammation has also been implicated in TDP-43 proteinopathy, as neurotoxic microglia and complement activation promote TDP-43 proteinopathy in progranulin deficient neurons [131]. This is in agreement with prior studies that also pointed to the role of inflammation in TDP-43 pathology, and an immune response with astrocytes and microglia is seen in both ALS patients and mouse models [132,133].

Of particular interest, impaired clearance of TDP-43 has also been implicated in TDP-43 pathology. TDP-43 is degraded by both the ubiquitin-proteasome system and by autophagy. Dysfunction in the clearance of TDP-43 aggregates by autophagy has been linked to disease pathogenesis [134-136]. Inhibition of autophagy contributes to TDP-43 cytoplasmic accumulation [135-137], and autophagy induction reduces cytoplasmic mislocalization and enhances neuronal survival in ALS models [73]. Consistent with this idea, multiple ALS- and FTD-associated genes are linked to autophagy and the lysosomal pathway [138], including *C9ORF72*, *TBK1*, *UBQLN2*, *VCP*, *SQSTM1*, and *OPTN*, and mutations in these genes result in TDP-43 pathology [139-144]. This link between dysfunctional autophagy and TDP-43 proteinopathy is of particular interest to LSDs, in which autophagic dysfunction is prominent [63]. Mouse and patient brains with progranulin mutations accumulate TDP-43 inclusions and exhibit pathologic hallmarks of the lysosomal storage disease (LSD) neuronal ceroid lipofuscinosis [145], highlighting a link between lysosomal dysfunction and TDP-43 pathology. Altered expression and localization of TDP-43 has also been reported in NPC [146]. However, the extent to which impaired autophagy in NPC is sufficient to drive TDP-43 mislocalization is unclear. Furthermore, a detailed characterization of TDP-43 proteinopathy and its pathological state from early stage cytoplasmic droplets towards aggregates

16

and nuclear depletion in vivo is lacking. Characterization of TDP-43 mislocalization in NPC and examination of factors that drive TDP-43 proteinopathy, including impaired autophagy and neuroinflammation is the focus of Chapter 4.

Increasingly associated with TDP-43 proteinopathy is the disruption of nucleocytoplasmic transport [147]. Nucleocytoplasmic transport involves the regulated exchange of proteins and RNAs between the nucleus and the cytoplasm, which is essential for cellular function. The nuclear envelope is composed of an outer and an inner nuclear membrane, and the inner membrane is associated with a network of intermediate filaments composed of lamin. The gatekeeper of this barrier is the nuclear pore complex, a large structure composed of an assembly of nucleoporins (Nups) that form a cylindrical channel and diffusion barrier between the cytoplasm and nucleus [148]. The import and export of proteins utilizes nuclear transport receptors of the karyopherin family, also known as importins and exportins, which recognize nuclear localization signals or nuclear export signals [149]. Furthermore, the small GTPase Ran forms a gradient of RanGTP in the nucleus and RanGDP in the cytoplasm, which allows for directionality in nuclear transport [150]. In classical nuclear import, importin α binds to NLS-containing cargo proteins, which then forms a ternary complex with importin β. This complex is targeted to the nuclear pore complex and translocates into the nucleus. In the nucleus, RanGTP binding triggers dissociation of the complex and release of cargo proteins. RanGTP bound importin α and importin β are then exported back to the cytoplasm where RanGTP is converted to RanGDP, releasing the importins to be reused for another round of transport [151]. The export of RNAs also requires transport machinery, including the transcription-export (TREX) complex for mRNAs [147].

Disruption of nucleocytoplasmic transport has emerged as an important mechanism of neurodegeneration in ALS/FTD. A plethora of abnormalities have been observed in patient tissue and animal and cell models of ALS/FTD, including irregular nuclear membrane morphology, loss of the Ran gradient, protein import defects, RNA export defects, and mislocalization or aggregation of Nups or importins [152]. Notably, mislocalization of TDP-43 has been associated with all of these pathologies, and mislocalized transport factors, including importin α and Nups, co-localize with cytoplasmic TDP-43 [123,153,154]. The impact of TDP-43 proteinopathy on nucleocytoplasmic transport and nuclear membrane morphology in NPC is explored in Chapter 4.

1.7 Remaining questions in NPC

Although we have progressed in our understanding of NPC disease and the functions of NPC1 and NPC2 in cholesterol trafficking, there are still no FDA approved treatments for this disease. Further, studies done in NPC neurons are still lacking, which is a significant gap as neurons are a critical cell type in disease. This thesis focuses on examining alterations in autophagy in NPC neurons and their impact in disease pathogenesis. In Chapter 2, I discuss the intersection between altered calcium homeostasis and dysfunctional autophagy in lysosomal diseases. In Chapter 3, I explore the role of lysosomal damage in NPC disease pathogenesis and investigate mechanisms of lysophagy in the brain. I discuss data showing that NPC cells are more sensitive to lysosomal damage and highlight a role for Fbxo2 in lysophagy in the brain. In Chapter 4, I characterize axonal pathology in the NPC mouse brain and reinforce its connection to impaired autophagy. Furthermore, I investigate the relationship between dysfunctional autophagy and TDP-43 proteinopathy and show that TDP-43 mislocalization in NPC persists for

months without progression to aggregates and occurs independently of autophagic substrate

accumulation. I also highlight vulnerable neuron populations and provide evidence of abnormal

nucleocytoplasmic transport in NPC neurons. The work presented in this dissertation seeks to

understand mechanisms underlying neurodegeneration in NPC, and I hope that this work will

contribute to the identification of novel therapeutic strategies.

References

1   De Duve, C., Pressman, B. C., Gianetto, R., Wattiaux, R. & Appelmans, F. Tissue fractionation studies. 6. Intracellular distribution patterns of enzymes in rat-liver tissue. *Biochem J* **60**, 604-617 (1955).

2   de Duve, C. The lysosome turns fifty. *Nat Cell Biol* **7**, 847-849, doi:10.1038/ncb0905-847 (2005).

3   Saxton, R. A. & Sabatini, D. M. mTOR Signaling in Growth, Metabolism, and Disease. *Cell* **168**, 960-976, doi:10.1016/j.cell.2017.02.004 (2017).

4   Castellano, B. M. *et al.* Lysosomal cholesterol activates mTORC1 via an SLC38A9-Niemann-Pick C1 signaling complex. *Science* **355**, 1306-1311, doi:10.1126/science.aag1417 (2017).

5   Kim, E., Goraksha-Hicks, P., Li, L., Neufeld, T. P. & Guan, K. L. Regulation of TORC1 by Rag GTPases in nutrient response. *Nat Cell Biol* **10**, 935-945, doi:10.1038/ncb1753 (2008).

6   Lawrence, R. E. *et al.* A nutrient-induced affinity switch controls mTORC1 activation by its Rag GTPase-Ragulator lysosomal scaffold. *Nat Cell Biol* **20**, 1052-1063, doi:10.1038/s41556-018-0148-6 (2018).

7   Sancak, Y. *et al.* The Rag GTPases bind raptor and mediate amino acid signaling to mTORC1. *Science* **320**, 1496-1501, doi:10.1126/science.1157535 (2008).

8   Hosokawa, N. *et al.* Nutrient-dependent mTORC1 association with the ULK1-Atg13-FIP200 complex required for autophagy. *Mol Biol Cell* **20**, 1981-1991, doi:10.1091/mbc.E08-12-1248 (2009).

9   Settembre, C. *et al.* TFEB links autophagy to lysosomal biogenesis. *Science* **332**, 1429-1433, doi:10.1126/science.1204592 (2011).

10   Martina, J. A. & Puertollano, R. Rag GTPases mediate amino acid-dependent recruitment of TFEB and MITF to lysosomes. *J Cell Biol* **200**, 475-491, doi:10.1083/jcb.201209135 (2013).

11   Medina, D. L. *et al.* Lysosomal calcium signalling regulates autophagy through calcineurin and TFEB. *Nat Cell Biol* **17**, 288-299, doi:10.1038/ncb3114 (2015).

12   Ballabio, A. & Bonifacino, J. S. Lysosomes as dynamic regulators of cell and organismal homeostasis. *Nat Rev Mol Cell Biol* **21**, 101-118, doi:10.1038/s41580-019-0185-4 (2020).

13   Platt, F. M., d'Azzo, A., Davidson, B. L., Neufeld, E. F. & Tifft, C. J. Lysosomal storage diseases. *Nat Rev Dis Primers* **4**, 27, doi:10.1038/s41572-018-0025-4 (2018).

14   Meikle, P. J., Hopwood, J. J., Clague, A. E. & Carey, W. F. Prevalence of lysosomal storage disorders. *JAMA* **281**, 249-254 (1999).

15   Broomfield, A., Jones, S. A., Hughes, S. M. & Bigger, B. W. The impact of the immune system on the safety and efficiency of enzyme replacement therapy in lysosomal storage disorders. *J Inherit Metab Dis* **39**, 499-512, doi:10.1007/s10545-016-9917-1 (2016).

16   Beck, M. Treatment strategies for lysosomal storage disorders. *Dev Med Child Neurol* **60**, 13-18, doi:10.1111/dmcn.13600 (2018).

17   Pentchev, P. G. *et al.* A defect in cholesterol esterification in Niemann-Pick disease (type C) patients. *Proc Natl Acad Sci U S A* **82**, 8247-8251, doi:10.1073/pnas.82.23.8247 (1985).

18   Brady, R. O., Kanfer, J. N., Mock, M. B. & Fredrickson, D. S. The metabolism of sphingomyelin. II. Evidence of an enzymatic deficiency in Niemann-Pick diseae. *Proc Natl Acad Sci U S A* **55**, 366-369, doi:10.1073/pnas.55.2.366 (1966).

19   Kanfer, J. N., Young, O. M., Shapiro, D. & Brady, R. O. The metabolism of sphingomyelin. I. Purification and properties of a sphingomyelin-cleaving enzyme from rat liver tissue. *J Biol Chem* **241**, 1081-1084 (1966).

20   Wasserstein, M. P. & Schuchman, E. H. in *GeneReviews((R))*   (eds M. P. Adam *et al.*) (1993).

21   Schuchman, E. H. & Desnick, R. J. Types A and B Niemann-Pick disease. *Mol Genet Metab* **120**, 27-33, doi:10.1016/j.ymgme.2016.12.008 (2017).

22   Pentchev, P. G. *et al.* The Niemann-Pick C lesion and its relationship to the intracellular distribution and utilization of LDL cholesterol. *Biochim Biophys Acta* **1225**, 235-243, doi:10.1016/0925-4439(94)90001-9 (1994).

23   Brown, M. S. & Goldstein, J. L. A receptor-mediated pathway for cholesterol homeostasis. *Science* **232**, 34-47, doi:10.1126/science.3513311 (1986).

24   Carstea, E. D. *et al.* Niemann-Pick C1 disease gene: homology to mediators of cholesterol homeostasis. *Science* **277**, 228-231 (1997).

25   Naureckiene, S. *et al.* Identification of HE1 as the second gene of Niemann-Pick C disease. *Science* **290**, 2298-2301, doi:10.1126/science.290.5500.2298 (2000).

26   Davies, J. P. & Ioannou, Y. A. Topological analysis of Niemann-Pick C1 protein reveals that the membrane orientation of the putative sterol-sensing domain is identical to those of 3-hydroxy-3-methylglutaryl-CoA reductase and sterol regulatory element binding protein cleavage-activating protein. *J Biol Chem* **275**, 24367-24374, doi:10.1074/jbc.M002184200 (2000).

27   Infante, R. E. *et al.* Purified NPC1 protein: II. Localization of sterol binding to a 240-amino acid soluble luminal loop. *J Biol Chem* **283**, 1064-1075, doi:10.1074/jbc.M707944200 (2008).

28   Ohgami, N. *et al.* Binding between the Niemann-Pick C1 protein and a photoactivatable cholesterol analog requires a functional sterol-sensing domain. *Proc Natl Acad Sci U S A* **101**, 12473-12478, doi:10.1073/pnas.0405255101 (2004).

29   Xu, S., Benoff, B., Liou, H. L., Lobel, P. & Stock, A. M. Structural basis of sterol binding by NPC2, a lysosomal protein deficient in Niemann-Pick type C2 disease. *J Biol Chem* **282**, 23525-23531, doi:10.1074/jbc.M703848200 (2007).

30   Infante, R. E. *et al.* NPC2 facilitates bidirectional transfer of cholesterol between NPC1 and lipid bilayers, a step in cholesterol egress from lysosomes. *Proc Natl Acad Sci U S A* **105**, 15287-15292, doi:10.1073/pnas.0807328105 (2008).

31   Kwon, H. J. *et al.* Structure of N-terminal domain of NPC1 reveals distinct subdomains for binding and transfer of cholesterol. *Cell* **137**, 1213-1224, doi:10.1016/j.cell.2009.03.049 (2009).

32   Gong, X. *et al.* Structural Insights into the Niemann-Pick C1 (NPC1)-Mediated Cholesterol Transfer and Ebola Infection. *Cell* **165**, 1467-1478, doi:10.1016/j.cell.2016.05.022 (2016).

33   Li, X. *et al.* Structure of human Niemann-Pick C1 protein. *Proc Natl Acad Sci U S A* **113**, 8212-8217, doi:10.1073/pnas.1607795113 (2016).

34   Li, X., Saha, P., Li, J., Blobel, G. & Pfeffer, S. R. Clues to the mechanism of cholesterol transfer from the structure of NPC1 middle lumenal domain bound to NPC2. *Proc Natl Acad Sci U S A* **113**, 10079-10084, doi:10.1073/pnas.1611956113 (2016).

35   Li, X. *et al.* 3.3 A structure of Niemann-Pick C1 protein reveals insights into the function of the C-terminal luminal domain in cholesterol transport. *Proc Natl Acad Sci U S A* **114**, 9116-9121, doi:10.1073/pnas.1711716114 (2017).

36   Li, X. *et al.* A molecular mechanism to regulate lysosome motility for lysosome positioning and tubulation. *Nat Cell Biol* **18**, 404-417, doi:10.1038/ncb3324 (2016).

37   Trinh, M. N., Brown, M. S., Seemann, J., Goldstein, J. L. & Lu, F. Lysosomal cholesterol export reconstituted from fragments of Niemann-Pick C1. *Elife* **7**, doi:10.7554/eLife.38564 (2018).

38   Pfeffer, S. R. NPC intracellular cholesterol transporter 1 (NPC1)-mediated cholesterol export from lysosomes. *J Biol Chem* **294**, 1706-1709, doi:10.1074/jbc.TM118.004165 (2019).

39   Vanier, M. T. & Millat, G. Niemann-Pick disease type C. *Clin Genet* **64**, 269-281 (2003).

40   Wassif, C. A. *et al.* High incidence of unrecognized visceral/neurological late-onset Niemann-Pick disease, type C1, predicted by analysis of massively parallel sequencing data sets. *Genet Med* **18**, 41-48, doi:10.1038/gim.2015.25 (2016).

41   Vanier, M. T. Niemann-Pick disease type C. *Orphanet J Rare Dis* **5**, 16, doi:10.1186/1750-1172-5-16 (2010).

42   Patterson, M. C., Vecchio, D., Prady, H., Abel, L. & Wraith, J. E. Miglustat for treatment of Niemann-Pick C disease: a randomised controlled study. *Lancet Neurol* **6**, 765-772, doi:10.1016/S1474-4422(07)70194-1 (2007).

43   Liu, B. *et al.* Reversal of defective lysosomal transport in NPC disease ameliorates liver dysfunction and neurodegeneration in the npc1-/- mouse. *Proc Natl Acad Sci U S A* **106**, 2377-2382, doi:10.1073/pnas.0810895106 (2009).

44   Ward, S., O'Donnell, P., Fernandez, S. & Vite, C. H. 2-hydroxypropyl-beta-cyclodextrin raises hearing threshold in normal cats and in cats with Niemann-Pick type C disease. *Pediatr Res* **68**, 52-56, doi:10.1203/00006450-201011001-00099 10.1203/PDR.0b013e3181df4623 (2010).

45   Chen, F. W., Li, C. & Ioannou, Y. A. Cyclodextrin induces calcium-dependent lysosomal exocytosis. *PLoS One* **5**, e15054, doi:10.1371/journal.pone.0015054 (2010).

46   McCauliff, L. A., Xu, Z. & Storch, J. Sterol transfer between cyclodextrin and membranes: similar but not identical mechanism to NPC2-mediated cholesterol transfer. *Biochemistry* **50**, 7341-7349, doi:10.1021/bi200574f (2011).

47   Rosenbaum, A. I., Zhang, G., Warren, J. D. & Maxfield, F. R. Endocytosis of beta-cyclodextrins is responsible for cholesterol reduction in Niemann-Pick type C mutant cells. *Proc Natl Acad Sci U S A* **107**, 5477-5482, doi:10.1073/pnas.0914309107 (2010).

48   Vance, J. E. & Karten, B. Niemann-Pick C disease and mobilization of lysosomal cholesterol by cyclodextrin. *J Lipid Res* **55**, 1609-1621, doi:10.1194/jlr.R047837 (2014).

49   Parzych, K. R. & Klionsky, D. J. An overview of autophagy: morphology, mechanism, and regulation. *Antioxid Redox Signal* **20**, 460-473, doi:10.1089/ars.2013.5371 (2014).

50   Mijaljica, D., Prescott, M. & Devenish, R. J. Microautophagy in mammalian cells: revisiting a 40-year-old conundrum. *Autophagy* **7**, 673-682, doi:10.4161/auto.7.7.14733 (2011).

51   Massey, A., Kiffin, R. & Cuervo, A. M. Pathophysiology of chaperone-mediated autophagy. *Int J Biochem Cell Biol* **36**, 2420-2434, doi:10.1016/j.biocel.2004.04.010 (2004).

52   Pankiv, S. *et al.* p62/SQSTM1 binds directly to Atg8/LC3 to facilitate degradation of ubiquitinated protein aggregates by autophagy. *J Biol Chem* **282**, 24131-24145, doi:10.1074/jbc.M702824200 (2007).

53   Klionsky, D. J. & Emr, S. D. Autophagy as a regulated pathway of cellular degradation. *Science* **290**, 1717-1721 (2000).

54   Xie, Z. & Klionsky, D. J. Autophagosome formation: core machinery and adaptations. *Nat Cell Biol* **9**, 1102-1109, doi:10.1038/ncb1007-1102 (2007).

55   Yang, Z. & Klionsky, D. J. Mammalian autophagy: core molecular machinery and signaling regulation. *Curr Opin Cell Biol* **22**, 124-131, doi:10.1016/j.ceb.2009.11.014 (2010).

56   Levine, B. & Kroemer, G. Autophagy in the pathogenesis of disease. *Cell* **132**, 27-42, doi:10.1016/j.cell.2007.12.018 (2008).

57   Rubinsztein, D. C. The roles of intracellular protein-degradation pathways in neurodegeneration. *Nature* **443**, 780-786, doi:10.1038/nature05291 (2006).

58   Nixon, R. A. The role of autophagy in neurodegenerative disease. *Nat Med* **19**, 983-997, doi:10.1038/nm.3232 (2013).

59   Hara, T. *et al.* Suppression of basal autophagy in neural cells causes neurodegenerative disease in mice. *Nature* **441**, 885-889, doi:10.1038/nature04724 (2006).

60   Komatsu, M. *et al.* Homeostatic levels of p62 control cytoplasmic inclusion body formation in autophagy-deficient mice. *Cell* **131**, 1149-1163, doi:10.1016/j.cell.2007.10.035 (2007).

61   Komatsu, M. *et al.* Loss of autophagy in the central nervous system causes neurodegeneration in mice. *Nature* **441**, 880-884, doi:10.1038/nature04723 (2006).

62   Wong, E. & Cuervo, A. M. Autophagy gone awry in neurodegenerative diseases. *Nat Neurosci* **13**, 805-811, doi:10.1038/nn.2575 (2010).

63   Lieberman, A. P. *et al.* Autophagy in lysosomal storage disorders. *Autophagy* **8**, 719-730, doi:10.4161/auto.19469 (2012).

64   Ko, D. C. *et al.* Cell-autonomous death of cerebellar purkinje neurons with autophagy in Niemann-Pick type C disease. *PLoS Genet* **1**, 81-95, doi:10.1371/journal.pgen.0010007 (2005).

65   Pacheco, C. D., Kunkel, R. & Lieberman, A. P. Autophagy in Niemann-Pick C disease is dependent upon Beclin-1 and responsive to lipid trafficking defects. *Hum Mol Genet* **16**, 1495-1503, doi:10.1093/hmg/ddm100 (2007).

66   Liao, G. *et al.* Cholesterol accumulation is associated with lysosomal dysfunction and autophagic stress in Npc1 -/- mouse brain. *Am J Pathol* **171**, 962-975, doi:10.2353/ajpath.2007.070052 (2007).

67   Sarkar, S. *et al.* Impaired autophagy in the lipid-storage disorder Niemann-Pick type C1 disease. *Cell Rep* **5**, 1302-1315, doi:10.1016/j.celrep.2013.10.042 (2013).

68   Elrick, M. J., Yu, T., Chung, C. & Lieberman, A. P. Impaired proteolysis underlies autophagic dysfunction in Niemann-Pick type C disease. *Hum Mol Genet* **21**, 4876-4887, doi:10.1093/hmg/dds324 (2012).

69   Maetzel, D. *et al.* Genetic and chemical correction of cholesterol accumulation and impaired autophagy in hepatic and neural cells derived from Niemann-Pick Type C patient-specific iPS cells. *Stem Cell Reports* **2**, 866-880, doi:10.1016/j.stemcr.2014.03.014 (2014).

70   Meske, V., Erz, J., Priesnitz, T. & Ohm, T. G. The autophagic defect in Niemann-Pick disease type C neurons differs from somatic cells and reduces neuronal viability. *Neurobiol Dis* **64**, 88-97, doi:10.1016/j.nbd.2013.12.018 (2014).

71   Ordonez, M. P. *et al.* Disruption and therapeutic rescue of autophagy in a human neuronal model of Niemann Pick type C1. *Hum Mol Genet* **21**, 2651-2662, doi:10.1093/hmg/dds090 (2012).

72   Yu, T., Shakkottai, V. G., Chung, C. & Lieberman, A. P. Temporal and cell-specific deletion establishes that neuronal Npc1 deficiency is sufficient to mediate neurodegeneration. *Hum Mol Genet* **20**, 4440-4451, doi:10.1093/hmg/ddr372 (2011).

73   Barmada, S. J. *et al.* Autophagy induction enhances TDP43 turnover and survival in neuronal ALS models. *Nat Chem Biol* **10**, 677-685, doi:10.1038/nchembio.1563 (2014).

74   Thestrup, T. *et al.* Optimized ratiometric calcium sensors for functional in vivo imaging of neurons and T lymphocytes. *Nat Methods* **11**, 175-182, doi:10.1038/nmeth.2773 (2014).

75   Yue, Z., Friedman, L., Komatsu, M. & Tanaka, K. The cellular pathways of neuronal autophagy and their implication in neurodegenerative diseases. *Biochim Biophys Acta* **1793**, 1496-1507, doi:10.1016/j.bbamcr.2009.01.016 (2009).

76   Hill, S. E. & Colon-Ramos, D. A. The Journey of the Synaptic Autophagosome: A Cell Biological Perspective. *Neuron* **105**, 961-973, doi:10.1016/j.neuron.2020.01.018 (2020).

77   Nixon, R. A. *et al.* Extensive involvement of autophagy in Alzheimer disease: an immuno-electron microscopy study. *J Neuropathol Exp Neurol* **64**, 113-122, doi:10.1093/jnen/64.2.113 (2005).

78   Yu, T. & Lieberman, A. P. Npc1 acting in neurons and glia is essential for the formation and maintenance of CNS myelin. *PLoS Genet* **9**, e1003462, doi:10.1371/journal.pgen.1003462 (2013).

79   de Duve, C. Lysosomes revisited. *Eur J Biochem* **137**, 391-397, doi:10.1111/j.1432-1033.1983.tb07841.x (1983).

80   Papadopoulos, C. & Meyer, H. Detection and Clearance of Damaged Lysosomes by the Endo-Lysosomal Damage Response and Lysophagy. *Curr Biol* **27**, R1330-R1341, doi:10.1016/j.cub.2017.11.012 (2017).

81   Boya, P. & Kroemer, G. Lysosomal membrane permeabilization in cell death. *Oncogene* **27**, 6434-6451, doi:10.1038/onc.2008.310 (2008).

82   Wang, F., Gomez-Sintes, R. & Boya, P. Lysosomal membrane permeabilization and cell death. *Traffic* **19**, 918-931, doi:10.1111/tra.12613 (2018).

83   Serrano-Puebla, A. & Boya, P. Lysosomal membrane permeabilization in cell death: new evidence and implications for health and disease. *Ann N Y Acad Sci* **1371**, 30-44, doi:10.1111/nyas.12966 (2016).

84   Vitner, E. B. *et al.* Altered expression and distribution of cathepsins in neuronopathic forms of Gaucher disease and in other sphingolipidoses. *Hum Mol Genet* **19**, 3583-3590, doi:10.1093/hmg/ddq273 (2010).

85   Micsenyi, M. C., Sikora, J., Stephney, G., Dobrenis, K. & Walkley, S. U. Lysosomal membrane permeability stimulates protein aggregate formation in neurons of a lysosomal disease. *J Neurosci* **33**, 10815-10827, doi:10.1523/JNEUROSCI.0987-13.2013 (2013).

86   Gabande-Rodriguez, E., Boya, P., Labrador, V., Dotti, C. G. & Ledesma, M. D. High sphingomyelin levels induce lysosomal damage and autophagy dysfunction in Niemann Pick disease type A. *Cell Death Differ* **21**, 864-875, doi:10.1038/cdd.2014.4 (2014).

87   Gabande-Rodriguez, E. *et al.* Lipid-induced lysosomal damage after demyelination corrupts microglia protective function in lysosomal storage disorders. *EMBO J* **38**, doi:10.15252/embj.201899553 (2019).

88   Kirkegaard, T. *et al.* Hsp70 stabilizes lysosomes and reverts Niemann-Pick disease-associated lysosomal pathology. *Nature* **463**, 549-553, doi:10.1038/nature08710 (2010).

89   Amritraj, A. *et al.* Increased activity and altered subcellular distribution of lysosomal enzymes determine neuronal vulnerability in Niemann-Pick type C1-deficient mice. *Am J Pathol* **175**, 2540-2556, doi:10.2353/ajpath.2009.081096 (2009).

90   Chung, C., Puthanveetil, P., Ory, D. S. & Lieberman, A. P. Genetic and pharmacological evidence implicates cathepsins in Niemann-Pick C cerebellar degeneration. *Hum Mol Genet* **25**, 1434-1446, doi:10.1093/hmg/ddw025 (2016).

91   Radulovic, M. *et al.* ESCRT-mediated lysosome repair precedes lysophagy and promotes cell survival. *EMBO J* **37**, doi:10.15252/embj.201899753 (2018).

92   Skowyra, M. L., Schlesinger, P. H., Naismith, T. V. & Hanson, P. I. Triggered recruitment of ESCRT machinery promotes endolysosomal repair. *Science* **360**, doi:10.1126/science.aar5078 (2018).

93   Aits, S. *et al.* Sensitive detection of lysosomal membrane permeabilization by lysosomal galectin puncta assay. *Autophagy* **11**, 1408-1424, doi:10.1080/15548627.2015.1063871 (2015).

94   Chauhan, S. *et al.* TRIMs and Galectins Globally Cooperate and TRIM16 and Galectin-3 Co-direct Autophagy in Endomembrane Damage Homeostasis. *Dev Cell* **39**, 13-27, doi:10.1016/j.devcel.2016.08.003 (2016).

95   Paz, I. *et al.* Galectin-3, a marker for vacuole lysis by invasive pathogens. *Cell Microbiol* **12**, 530-544, doi:10.1111/j.1462-5822.2009.01415.x (2010).

96   Thurston, T. L., Wandel, M. P., von Muhlinen, N., Foeglein, A. & Randow, F. Galectin 8 targets damaged vesicles for autophagy to defend cells against bacterial invasion. *Nature* **482**, 414-418, doi:10.1038/nature10744 (2012).

97   Jia, J. *et al.* Galectins Control mTOR in Response to Endomembrane Damage. *Mol Cell* **70**, 120-135 e128, doi:10.1016/j.molcel.2018.03.009 (2018).

98   Hung, Y. H., Chen, L. M., Yang, J. Y. & Yang, W. Y. Spatiotemporally controlled induction of autophagy-mediated lysosome turnover. *Nat Commun* **4**, 2111, doi:10.1038/ncomms3111 (2013).

99   Huett, A. *et al.* The LRR and RING domain protein LRSAM1 is an E3 ligase crucial for ubiquitin-dependent autophagy of intracellular Salmonella Typhimurium. *Cell Host Microbe* **12**, 778-790, doi:10.1016/j.chom.2012.10.019 (2012).

100   Yoshida, Y. *et al.* Ubiquitination of exposed glycoproteins by SCF(FBXO27) directs damaged lysosomes for autophagy. *Proc Natl Acad Sci U S A* **114**, 8574-8579, doi:10.1073/pnas.1702615114 (2017).

101   Papadopoulos, C. *et al.* VCP/p97 cooperates with YOD1, UBXD1 and PLAA to drive clearance of ruptured lysosomes by autophagy. *EMBO J* **36**, 135-150, doi:10.15252/embj.201695148 (2017).

102   Papadopoulos, C., Kravic, B. & Meyer, H. Repair or Lysophagy: Dealing with Damaged Lysosomes. *J Mol Biol* **432**, 231-239, doi:10.1016/j.jmb.2019.08.010 (2020).

103   Ayala, Y. M. *et al.* Structural determinants of the cellular localization and shuttling of TDP-43. *J Cell Sci* **121**, 3778-3785, doi:10.1242/jcs.038950 (2008).

104   Polymenidou, M. *et al.* Long pre-mRNA depletion and RNA missplicing contribute to neuronal vulnerability from loss of TDP-43. *Nat Neurosci* **14**, 459-468, doi:10.1038/nn.2779 (2011).

105   Tollervey, J. R. *et al.* Characterizing the RNA targets and position-dependent splicing regulation by TDP-43. *Nat Neurosci* **14**, 452-458, doi:10.1038/nn.2778 (2011).

106   Arai, T. *et al.* TDP-43 is a component of ubiquitin-positive tau-negative inclusions in frontotemporal lobar degeneration and amyotrophic lateral sclerosis. *Biochem Biophys Res Commun* **351**, 602-611, doi:10.1016/j.bbrc.2006.10.093 (2006).

107   Neumann, M. *et al.* Ubiquitinated TDP-43 in frontotemporal lobar degeneration and amyotrophic lateral sclerosis. *Science* **314**, 130-133, doi:10.1126/science.1134108 (2006).

108   Ling, S. C., Polymenidou, M. & Cleveland, D. W. Converging mechanisms in ALS and FTD: disrupted RNA and protein homeostasis. *Neuron* **79**, 416-438, doi:10.1016/j.neuron.2013.07.033 (2013).

109   Feiguin, F. *et al.* Depletion of TDP-43 affects Drosophila motoneurons terminal synapsis and locomotive behavior. *FEBS Lett* **583**, 1586-1592, doi:10.1016/j.febslet.2009.04.019 (2009).

110   Schmid, B. *et al.* Loss of ALS-associated TDP-43 in zebrafish causes muscle degeneration, vascular dysfunction, and reduced motor neuron axon outgrowth. *Proc Natl Acad Sci U S A* **110**, 4986-4991, doi:10.1073/pnas.1218311110 (2013).

111   Zhang, T., Hwang, H. Y., Hao, H., Talbot, C., Jr. & Wang, J. Caenorhabditis elegans RNA-processing protein TDP-1 regulates protein homeostasis and life span. *J Biol Chem* **287**, 8371-8382, doi:10.1074/jbc.M111.311977 (2012).

112   Kraemer, B. C. *et al.* Loss of murine TDP-43 disrupts motor function and plays an essential role in embryogenesis. *Acta Neuropathol* **119**, 409-419, doi:10.1007/s00401-010-0659-0 (2010).

113   Kasai, T. *et al.* Increased TDP-43 protein in cerebrospinal fluid of patients with amyotrophic lateral sclerosis. *Acta Neuropathol* **117**, 55-62, doi:10.1007/s00401-008-0456-1 (2009).

114   Noto, Y. *et al.* Elevated CSF TDP-43 levels in amyotrophic lateral sclerosis: specificity, sensitivity, and a possible prognostic value. *Amyotroph Lateral Scler* **12**, 140-143, doi:10.3109/17482968.2010.541263 (2011).

115   Verstraete, E. *et al.* TDP-43 plasma levels are higher in amyotrophic lateral sclerosis. *Amyotroph Lateral Scler* **13**, 446-451, doi:10.3109/17482968.2012.703208 (2012).

116   Barmada, S. J. *et al.* Amelioration of toxicity in neuronal models of amyotrophic lateral sclerosis by hUPF1. *Proc Natl Acad Sci U S A* **112**, 7821-7826, doi:10.1073/pnas.1509744112 (2015).

117   Kabashi, E. *et al.* Gain and loss of function of ALS-related mutations of TARDBP (TDP-43) cause motor deficits in vivo. *Hum Mol Genet* **19**, 671-683, doi:10.1093/hmg/ddp534 (2010).

118   Wang, D. B. *et al.* Expansive gene transfer in the rat CNS rapidly produces amyotrophic lateral sclerosis relevant sequelae when TDP-43 is overexpressed. *Mol Ther* **18**, 2064-2074, doi:10.1038/mt.2010.191 (2010).

119   Wils, H. *et al.* TDP-43 transgenic mice develop spastic paralysis and neuronal inclusions characteristic of ALS and frontotemporal lobar degeneration. *Proc Natl Acad Sci U S A* **107**, 3858-3863, doi:10.1073/pnas.0912417107 (2010).

120   Barmada, S. J. *et al.* Cytoplasmic mislocalization of TDP-43 is toxic to neurons and enhanced by a mutation associated with familial amyotrophic lateral sclerosis. *J Neurosci* **30**, 639-649, doi:10.1523/JNEUROSCI.4988-09.2010 (2010).

121   Lee, E. B., Lee, V. M. & Trojanowski, J. Q. Gains or losses: molecular mechanisms of TDP43-mediated neurodegeneration. *Nat Rev Neurosci* **13**, 38-50, doi:10.1038/nrn3121 (2011).

122   Johnson, B. S. *et al.* TDP-43 is intrinsically aggregation-prone, and amyotrophic lateral sclerosis-linked mutations accelerate aggregation and increase toxicity. *J Biol Chem* **284**, 20329-20339, doi:10.1074/jbc.M109.010264 (2009).

123   Gasset-Rosa, F. *et al.* Cytoplasmic TDP-43 De-mixing Independent of Stress Granules Drives Inhibition of Nuclear Import, Loss of Nuclear TDP-43, and Cell Death. *Neuron* **102**, 339-357 e337, doi:10.1016/j.neuron.2019.02.038 (2019).

124   Gitcho, M. A. *et al.* TDP-43 A315T mutation in familial motor neuron disease. *Ann Neurol* **63**, 535-538, doi:10.1002/ana.21344 (2008).

125   Guo, W. *et al.* An ALS-associated mutation affecting TDP-43 enhances protein aggregation, fibril formation and neurotoxicity. *Nat Struct Mol Biol* **18**, 822-830, doi:10.1038/nsmb.2053 (2011).

126   Nonaka, T., Kametani, F., Arai, T., Akiyama, H. & Hasegawa, M. Truncation and pathogenic mutations facilitate the formation of intracellular aggregates of TDP-43. *Hum Mol Genet* **18**, 3353-3364, doi:10.1093/hmg/ddp275 (2009).

127   Colombrita, C. *et al.* TDP-43 is recruited to stress granules in conditions of oxidative insult. *J Neurochem* **111**, 1051-1061, doi:10.1111/j.1471-4159.2009.06383.x (2009).

128   Li, Y. R., King, O. D., Shorter, J. & Gitler, A. D. Stress granules as crucibles of ALS pathogenesis. *J Cell Biol* **201**, 361-372, doi:10.1083/jcb.201302044 (2013).

129   Parker, S. J. *et al.* Endogenous TDP-43 localized to stress granules can subsequently form protein aggregates. *Neurochem Int* **60**, 415-424, doi:10.1016/j.neuint.2012.01.019 (2012).

130   Mann, J. R. *et al.* RNA Binding Antagonizes Neurotoxic Phase Transitions of TDP-43. *Neuron* **102**, 321-338 e328, doi:10.1016/j.neuron.2019.01.048 (2019).

131   Zhang, J. *et al.* Neurotoxic microglia promote TDP-43 proteinopathy in progranulin deficiency. *Nature* **588**, 459-465, doi:10.1038/s41586-020-2709-7 (2020).

132   Correia, A. S., Patel, P., Dutta, K. & Julien, J. P. Inflammation Induces TDP-43 Mislocalization and Aggregation. *PLoS One* **10**, e0140248, doi:10.1371/journal.pone.0140248 (2015).

133   Jara, J. H. *et al.* MCP1-CCR2 and neuroinflammation in the ALS motor cortex with TDP-43 pathology. *J Neuroinflammation* **16**, 196, doi:10.1186/s12974-019-1589-y (2019).

134   Scotter, E. L. *et al.* Differential roles of the ubiquitin proteasome system and autophagy in the clearance of soluble and aggregated TDP-43 species. *J Cell Sci* **127**, 1263-1278, doi:10.1242/jcs.140087 (2014).

135   Urushitani, M., Sato, T., Bamba, H., Hisa, Y. & Tooyama, I. Synergistic effect between proteasome and autophagosome in the clearance of polyubiquitinated TDP-43. *J Neurosci Res* **88**, 784-797, doi:10.1002/jnr.22243 (2010).

136   Wang, X. *et al.* Degradation of TDP-43 and its pathogenic form by autophagy and the ubiquitin-proteasome system. *Neurosci Lett* **469**, 112-116, doi:10.1016/j.neulet.2009.11.055 (2010).

137   Chang, M. C. *et al.* Progranulin deficiency causes impairment of autophagy and TDP-43 accumulation. *J Exp Med* **214**, 2611-2628, doi:10.1084/jem.20160999 (2017).

138   Deng, Z., Sheehan, P., Chen, S. & Yue, Z. Is amyotrophic lateral sclerosis/frontotemporal dementia an autophagy disease? *Mol Neurodegener* **12**, 90, doi:10.1186/s13024-017-0232-6 (2017).

139   Deng, H. X. *et al.* Mutations in UBQLN2 cause dominant X-linked juvenile and adult-onset ALS and ALS/dementia. *Nature* **477**, 211-215, doi:10.1038/nature10353 (2011).

140   Fecto, F. *et al.* SQSTM1 mutations in familial and sporadic amyotrophic lateral sclerosis. *Arch Neurol* **68**, 1440-1446, doi:10.1001/archneurol.2011.250 (2011).

141   Johnson, J. O. *et al.* Exome sequencing reveals VCP mutations as a cause of familial ALS. *Neuron* **68**, 857-864, doi:10.1016/j.neuron.2010.11.036 (2010).

142   Maruyama, H. *et al.* Mutations of optineurin in amyotrophic lateral sclerosis. *Nature* **465**, 223-226, doi:10.1038/nature08971 (2010).

143   Murray, M. E. *et al.* Clinical and neuropathologic heterogeneity of c9FTD/ALS associated with hexanucleotide repeat expansion in C9ORF72. *Acta Neuropathol* **122**, 673-690, doi:10.1007/s00401-011-0907-y (2011).

144   Van Mossevelde, S. *et al.* Clinical features of TBK1 carriers compared with C9orf72, GRN and non-mutation carriers in a Belgian cohort. *Brain* **139**, 452-467, doi:10.1093/brain/awv358 (2016).

145   Gotzl, J. K. *et al.* Common pathobiochemical hallmarks of progranulin-associated frontotemporal lobar degeneration and neuronal ceroid lipofuscinosis. *Acta Neuropathol* **127**, 845-860, doi:10.1007/s00401-014-1262-6 (2014).

146   Dardis, A. *et al.* Altered localization and functionality of TAR DNA Binding Protein 43 (TDP-43) in niemann- pick disease type C. *Acta Neuropathol Commun* **4**, 52, doi:10.1186/s40478-016-0325-4 (2016).

147   Kim, H. J. & Taylor, J. P. Lost in Transportation: Nucleocytoplasmic Transport Defects in ALS and Other Neurodegenerative Diseases. *Neuron* **96**, 285-297, doi:10.1016/j.neuron.2017.07.029 (2017).

148   Hampoelz, B., Andres-Pons, A., Kastritis, P. & Beck, M. Structure and Assembly of the Nuclear Pore Complex. *Annu Rev Biophys* **48**, 515-536, doi:10.1146/annurev-biophys-052118-115308 (2019).

149   Cautain, B., Hill, R., de Pedro, N. & Link, W. Components and regulation of nuclear transport processes. *FEBS J* **282**, 445-462, doi:10.1111/febs.13163 (2015).

150   Gorlich, D., Pante, N., Kutay, U., Aebi, U. & Bischoff, F. R. Identification of different roles for RanGDP and RanGTP in nuclear protein import. *EMBO J* **15**, 5584-5594 (1996).

151   Oka, M. & Yoneda, Y. Importin alpha: functions as a nuclear transport factor and beyond. *Proc Jpn Acad Ser B Phys Biol Sci* **94**, 259-274, doi:10.2183/pjab.94.018 (2018).

152   Fallini, C., Khalil, B., Smith, C. L. & Rossoll, W. Traffic jam at the nuclear pore: All roads lead to nucleocytoplasmic transport defects in ALS/FTD. *Neurobiol Dis* **140**, 104835, doi:10.1016/j.nbd.2020.104835 (2020).

153   Chou, C. C. *et al.* TDP-43 pathology disrupts nuclear pore complexes and nucleocytoplasmic transport in ALS/FTD. *Nat Neurosci* **21**, 228-239, doi:10.1038/s41593-017-0047-3 (2018).

154   Woerner, A. C. *et al.* Cytoplasmic protein aggregates interfere with nucleocytoplasmic transport of protein and RNA. *Science* **351**, 173-176, doi:10.1126/science.aad2033 (2016).

Chapter 2

The Intersection of Lysosomal and ER Calcium with Autophagy Defects in Lysosomal Diseases

2.1 Introduction

The lysosomal storage disorders (LSDs) are a group of more than 50 inherited diseases characterized by the accumulation of lysosomal substrates due to organellar dysfunction. As lysosomes are ubiquitous cellular organelles, LSDs lead to pathology in many different tissues and organ systems. Notably, two-thirds of patients experience significant neurological symptoms. However, the mechanisms of neurodegeneration are not well understood, and this contributes to the lack of available and effective treatments for these devastating illnesses. As the lysosome plays a critical role in autophagy, a wide range of LSDs give rise to defects in autophagic flux, which disrupt the ability of the cell to degrade and recycle damaged or sequestered materials. As such, LSDs can be seen as "autophagy disorders [1,2]." Still, LSDs exhibit a wide range of other cellular defects, including altered Ca^{2+} homeostasis [3]. It is of interest that LSDs share defects in both autophagy and Ca^{2+} regulation, as Ca^{2+} itself is a critical regulator of autophagy. The question arises as to whether the dysregulation in these pathways is connected. To address this question, we focus on one class of LSDs, the sphingolipidoses, which are disorders of sphingolipid trafficking or metabolism. Included in this group are Niemann-Pick type C disease (NPC) and Gaucher disease (GD). Studies in NPC and GD have established dysregulation in both autophagy and Ca^{2+} homeostasis, but further work is required to elucidate

possible links between the two. In this review, we discuss the roles of endoplasmic reticulum (ER) and lysosomal Ca^{2+} in autophagy regulation, and we highlight what is known about altered ER and lysosomal Ca^{2+} homeostasis and autophagy in NPC and GD.

2.2 ER calcium and autophagy

The endoplasmic reticulum (ER) is a major intracellular store of Ca^{2+}, with a resting Ca^{2+} concentration of several hundred μM [4]. This composes a dynamic pool of Ca^{2+} that functions in processes ranging from proliferation to cell death, and of note, autophagy. Calcium has been implicated in the regulation of autophagy since 1993, when a first report suggested the dependence of autophagy on the presence of Ca^{2+} in an intracellular storage compartment [5]. Since then, much work has been done to gain insight into this question, and while much progress has been made, controversy still remains.

ER Ca^{2+} is regulated through various channels and pumps (Table 2.1), including the inositol 1,4,5-triphosphate receptors (IP3Rs), ryanodine receptors (RyRs) and the sarcoendoplasmic reticulum Ca^{2+} transport ATPase (SERCA) pumps. These facilitate movement of Ca^{2+} both into (SERCA) and out of (IP3Rs and RyRs) the ER (Figure 2.1) [6]. In vertebrates, there are three IP3R isoforms, IP3R1, 2 and 3. Most cell types express two or even all three isoforms, but IP3R1 is found predominantly in neuronal cells, IP3R2 in liver and muscle, and IP3R3 in most cultured cells [7]. RyRs also exist as three isoforms, RyR1, 2 and 3. RyR1 is primarily expressed in skeletal muscle. RyR2 is expressed in cardiac muscle and also in cerebellar Purkinje neurons and the cerebral cortex. RyR3 is expressed in hippocampal neurons, Purkinje neurons, skeletal muscle, lung, kidney and various other tissues [8].

Table 2.1. Calcium channels and pumps of the ER and lysosome

	Channel	Autophagy	Refs.	NPC	Refs.	GD	Refs.
Endoplasmic Reticulum	**RyR**			Inhibition of RyRs enhances NPC1 proteostasis and ameliorates cholesterol storage	68	Increased Ca^{2+} release	80-83
						Inhibition of RyRs enhances GCase proteostasis	84
						Dantrolene corrects Ca^{2+} signaling and autophagy defects	91
	IP3R	Inhibiting IP3Rs induces autophagy	13-17				
		Inhibition of IP3R releases Beclin-1 to stimulate autophagy	14-15				
		Ca^{2+} transfer to mitochondria inhibits autophagy	16				
		Ca^{2+} release important for starvation induced autophagy	23				
	SERCA	Inhibiting SERCA activates autophagy	19-21	Thapsigargin induces fusion between late endosomes and lysosomes	69		
		CaMKK-b activation of AMPK	20				
		Activation of PKCθ	21				
Lysosome	**TPC**	TPC Ca^{2+} release induces autophagy	32, 52				
		mTOR reactivation and autophagy termination in prolonged starvation	53				
		Inhibiting TPCs diminishes autophagic flux	54				
	TRPML-1	Loss of TRPML-1 function leads to accumulation of autophagosomes and delays autophagosome-lysosome fusion	46-47	Sphingomyelin inhibits Ca^{2+} release; increased Ca^{2+} channel activity corrects late endosome and lysosome to Golgi transport	70		
		Activation of mTORC1	48-49				
		Promotion of lysosomal motility	51				
		Activation of calcineurin and TFEB	56, 57				

Similarly, there are three SERCA isoforms, SERCA1, 2 and 3, which form more than 10 different splice variants. SERCA1 is expressed in fast-twitch skeletal muscle. SERCA2a is expressed primarily in cardiac and slow-twitch muscle, and SERCA2b is found in all tissues at low levels, including muscle, brain, kidney and stomach. SERCA3 isoforms are also expressed in several tissues, including hematopoietic cells, fibroblasts and endothelial cells [9].
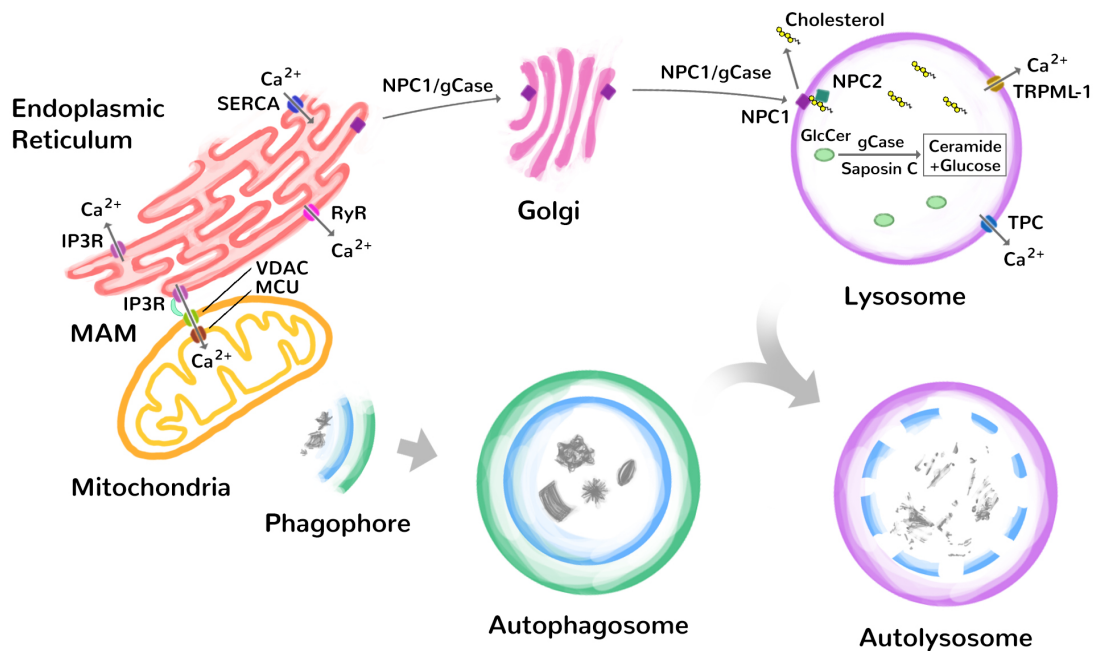
Figure 2.1 Ca^{2+} regulation and autophagy. NPC1 and gCase are synthesized in the ER and traffic through the Golgi to the lysosome, where they function to export cholesterol or hydrolyze GlcCer, respectively. Mutations in these proteins lead to accumulation of lysosomal substrates and disease. Altered Ca^{2+} homeostasis and autophagy have been implicated in both NPC and GD. ER Ca^{2+} is regulated through IP3Rs, RyRs and SERCA pumps. IP3Rs and RyRs move Ca^{2+} out while SERCA pumps move Ca^{2+} into the ER. IP3Rs are also found in MAMs, where they function with VDAC and MCU to transfer Ca^{2+} from the ER to the mitochondria. Lysosomal Ca^{2+} is regulated by TRPML-1 and TPC, which both facilitate movement of Ca^{2+} out of the lysosome. Autophagy is a process in which a double membraned phagophore surrounds substrates, elongates, and encloses to form the autophagosome. The autophagosome fuses with the lysosome to form the autolysosome and degrade substrates. The connection between altered Ca^{2+} regulation and autophagy is of particular interest in lysosomal storage diseases.

Early work examining the role of ER Ca^{2+} in autophagy centered on the IP3R, which releases Ca^{2+} from the ER in response to elevations in inositol 1,4,5-triphosphate (IP3) [10,11]. IP3 is generated after external signals activate G protein-coupled or tyrosine-kinase linked receptors. These in turn activate phospholipase C to hydrolyze phosphatidylinositol 4,5-bisphosphate

(PIP2) to form diacylglycerol (DAG) and IP3, which then binds IP3R [12]. PIP2 is generated in a pathway from inositol, which forms when inositol monophosphatase (IMP) hydrolyzes phosphatidylinositol (PI) [10]. A continuous supply of PIP2 is necessary to generate IP3.

Interest in the role of inositol phosphate signaling as a regulator of autophagy was prompted by an initial study which showed that lithium induced autophagy by inhibiting IMP, leading to decreased IP3 and implicating an inhibitory role of IP3Rs on autophagy [13]. Subsequent studies from several different groups showed that reducing IP3 levels or inhibiting IP3Rs with either the chemical inhibitor xestospongin B or siRNA knockdown induced autophagy, supporting the notion that IP3Rs are inhibitory on autophagy [13,14]. The mechanism of inhibition remains a topic of debate, as some groups attribute it to altered interactions between IP3R and Bcl2. In this model, IP3Rs serve as a scaffold to complex Bcl2 and Beclin1, and inhibitory treatments alter the interaction of IP3R and Bcl2, which releases Beclin-1 and stimulates autophagy [14,15]. While this model does not support a role for Ca^{2+}, a variety of other Ca^{2+} dependent mechanisms of autophagy regulation have been proposed. Using IP3R pore-dead mutants, IP3R channel activity was found to be essential for autophagy suppression [16,17]. Suggested underlying mechanisms include the notion that IP3R dependent Ca^{2+} signals maintain mTORC1 activity to inhibit autophagy [17]. Alternative possibilities build on the observation that IP3Rs are essential for Ca^{2+} transfer from the ER to mitochondria for normal bioenergetics. This function keeps autophagy at basal levels; absence of Ca^{2+} transfer compromises mitochondrial respiration and leads to AMPK dependent activation of autophagy [16]. Furthermore, L-type Ca^{2+} channel mediated Ca^{2+} release was shown to activate calpain, which increases cAMP and IP3, creating a cyclical loop of autophagy inhibition [18].

Despite studies implicating an inhibitory role of IP3R-mediated Ca^{2+} release on autophagy, others have described, in contrast, an activating role. Many of these studies utilized agents that elevate cytosolic Ca^{2+} through independent mechanisms, such as the SERCA inhibitor thapsigargin [19-21] or other Ca^{2+} mobilizing agents such as cadmium [22]. These studies described multiple mechanisms for autophagy regulation, including Ca^{2+} calmodulin-dependent kinase kinase-beta (CaMKK-b) dependent activation of AMPK and inhibition of mTOR [20] and Ca^{2+} activation of PKCθ [21]. While these studies perturbed Ca^{2+} in their methodology, even without disturbing intracellular Ca^{2+} homeostasis with drug treatments, starvation induced autophagy was found to be dependent on IP3R Ca^{2+} release [23], and rapamycin induced autophagy was shown to require cytosolic Ca^{2+} [24].

Various explanations have been proposed to reconcile these seemingly conflicting views of the role of Ca^{2+} in autophagy, including use of different cell types, different forms of autophagy and autophagy checkpoints, and differing roles of Ca^{2+} in basal versus stress conditions [25]. In particular, stress conditions may increase cytosolic Ca^{2+}, activating autophagy through mechanisms described above, while in the basal state, constitutively released Ca^{2+} from ER IP3Rs is taken up by mitochondria, which allows for the production of ATP and inhibits autophagy [26].

The exchange of critical regulatory signals between the ER and mitochondria has received increasing interest. ER and mitochondria make close contact at sites known as mitochondrial associated membranes (MAMs), which function in Ca^{2+} signaling, lipid exchange and synthesis, and control of mitochondrial bioenergetics. Ca^{2+} transfer is proposed to occur through IP3Rs on the ER membrane to the voltage-dependent anion-selective channel protein 1 (VDAC) on the outer mitochondrial membrane and the mitochondrial calcium uniporter (MCU)

on the inner mitochondrial membrane (Figure 2.1). This Ca^{2+} exchange is essential for ATP generation, which keeps autophagy at basal levels, while excessive Ca^{2+} uptake leads to apoptosis [27]. Additionally, it was recently shown that the integral ER protein vesicle-associated membrane protein-associated protein B (VAPB) binds to protein tyrosine phosphatase interacting protein 51 (PTPIP51) on the outer mitochondrial membrane at MAMs; manipulating this tethering between ER and mitochondria was sufficient to regulate autophagy in a Ca^{2+} dependent manner [28]. In fact, ER-mitochondria contact sites themselves have been found to serve as a membrane origin for autophagosomes [29]. Thus, alterations in MAMs are well positioned to contribute to both ER Ca^{2+} and autophagic dysregulation in LSDs.

2.3 Lysosomal calcium and autophagy

Lysosomes are essential for the efficient degradation of complex macromolecules and spent organelles and have emerged as key nodes in the regulation of cellular energy metabolism. In their function to maintain cellular quality control, their direct role in autophagy is apparent as the endpoint for digestion of substrates. In studying autophagy, small molecules such as bafilomycin and chloroquine are commonly used inhibitors, and it is known that the ability of these compounds to neutralize lysosomal pH impairs substrate degradation and disrupts autophagosome-lysosome fusion [30,31]. However, the observation that disruption of lysosomal pH also alters lysosomal Ca^{2+} homeostasis has prompted investigations into the extent to which lysosomal Ca^{2+} regulates autophagy [32]. As this question has been pursued, the importance of lysosomal Ca^{2+} has been increasingly revealed.

Due to the acidic nature of lysosomes, measuring lysosomal Ca^{2+} is difficult, as many fluorescent probes are sensitive to pH. However, experiments controlling for pH found that free

Ca^{2+} in lysosomes is in the 400-600 µM range, which is comparable to ER Ca^{2+} levels [33]. Using sea urchin eggs, it was demonstrated that nicotinic acid adenine dinucleotide phosphate (NAADP) mobilizes Ca^{2+} from a lysosome equivalent organelle [34]. Both transient receptor potential mucolipin-1 (TRPML-1) [35] and the two-pore channel (TPC) have been implicated as NAADP receptors that release Ca^{2+} from lysosomes (Figure 2.1, Table 2.1) [36,37].

TPCs, which include TPC1-3, are localized on endosomes and lysosomes and belong to the superfamily of voltage-gated ion channels. In contrast to plasma membrane-localized voltage-gated Na^+ and Ca^{2+} channels, which contain four 6-transmembrane domains, TPCs are likely dimeric, with two 6-transmembrane domains [38]. There has been considerable controversy regarding their ion selectivity and gating. The bulk of evidence suggests that NAADP activates TPC channel activity to release Ca^{2+}. However, some reports identify TPCs as Na^+ channels that are activated by phosphatidylinositol-3,5-bisphosphate (PI(3,5)P$_2$) and not NAADP [39]. In addition, other reports indicate that TPCs associate with mTOR, and that this complex is involved with ATP-mediated inhibition of Na^+ currents [40]. Indeed, TPC activation and permeability are complex, and they are likely to be co-regulated by NAADP and PI(3,5)P$_2$ and permeable to both Na^+ and Ca^{2+} [38].

TRPML-1 is part of the mucolipin family of TRP ion channels, so named because mutations in its founding member, TRPML-1, lead to the lysosomal storage disease mucolipidosis type IV [41]. TRPML-1 is a major Ca^{2+} release channel composed of 6-transmembrane domains with two di-leucine motifs that target TRPML-1 to late endosomes and lysosomes. In addition to Ca^{2+}, TRPML-1 has been shown to be permeable to many ions, including Fe^{2+}, Zn^{2+}, Na^+ and K^+ [42]. Like TPCs, regulation of TRPML-1 is likely complex, but PI(3,5)P$_2$ has been shown to activate TRPML-1, while PI(4,5)P$_2$ inhibits TRPML-1 [43]. While

these Ca^{2+} release channels have become better characterized, the mechanism of lysosomal Ca^{2+} filling is less well understood. The hypothesis that the acidic pH of the lysosome drives Ca^{2+} filling from cytosolic stores has been widely accepted [44], but a recent study suggests that the ER is a critical source of lysosomal Ca^{2+} [45].

Loss of TRPML-1 function leads to changes in autophagic flux, including increased accumulation of autophagosomes and delayed autophagosome-lysosome fusion [46,47]. However, it was initially unclear whether TRPML-1 and its Ca^{2+} channel activity are directly involved in these changes or if they occur secondary to alterations in intracellular lipids. Further studies resolved this question, showing that TRPML-1 mediated Ca^{2+} release is important for amphisome-lysosome fusion and that the subsequent degradation of proteins promotes TORC1 activation to inhibit autophagy [48]. These effects occur through a cascade in which Ca^{2+} released from TRPML-1 binds calmodulin, which in turn binds mTORC1 to stimulate its kinase activity [49]. In addition, starvation-induced autophagy leads to upregulation of TRPML-1 and increases Ca^{2+} currents to enhance autophagic degradation [50]. TRPML-1 Ca^{2+} release has also been shown to regulate lysosome motility, promoting lysosome movement towards autophagosomes [51].

Like TRPML-1, TPCs have been implicated in autophagy regulation. Modulating lysosomal Ca^{2+} by delivery of NAADP showed that Ca^{2+} release from TPCs induces autophagy [32]. This was confirmed by work investigating mechanisms of autophagy dysregulation caused by mutations in leucine-rich repeat kinase-2 (LRRK2), a gene mutated in familial Parkinson disease. LRRK2 over-expression has been found to induce autophagy via the CaMKK-b/AMPK pathway, mediated by NAADP dependent release of lysosomal Ca^{2+} [52]. In contrast, in studies of *Tpcn2* null mice, it was shown that TPC2 regulates mTOR reactivation and autophagy termination in response to prolonged starvation [53]. In cardiomyocytes, genetically inhibiting TPCs diminishes

autophagic flux and decreases cell viability under starvation [54]. These studies support an important role for lysosomal Ca^{2+} channels in the regulation of autophagy, and suggest that additional levels of complexity influence outcomes dependent upon the cell type studied and induction paradigm utilized.

Lysosomal Ca^{2+} is also implicated in the regulation of autophagy that occurs through transcription factor EB (TFEB). TFEB is an important regulator of lysosomal and autophagic function by controlling expression of many genes critical to these pathways. Phosphorylation retains TFEB in the cytoplasm, but when dephosphorylated, TFEB translocates to the nucleus to activate autophagy and lysosomal genes [55]. In identifying phosphatases that promote TFEB's nuclear localization, it was found that TRPML-1 mediated Ca^{2+} release activates calcineurin, which dephosphorylates TFEB and leads to its nuclear localization and induction of autophagy genes [56]. Upstream of this pathway, increased reactive oxygen species (ROS) activate TRPML-1, which leads to lysosomal Ca^{2+} release and calcineurin-dependent TFEB nuclear translocation [57].

As we are still progressing in our understanding of mechanisms controlling lysosomal Ca^{2+}, there is much to clarify regarding the role of lysosomal Ca^{2+} in the regulation of autophagy. Modulation of Ca^{2+} release by TPCs and TRPML-1 impacts autophagy, but further understanding of pathways that regulate the activity of these channels is needed. In addition, clarifying cell type specific differences, how these channels respond in situations of autophagy induction, and their contribution to autophagy dysfunction in LSDs are critical questions to be addressed.

2.4 LSDs and ER/lysosomal calcium

Lysosomal storage disorders (LSDs) are a heterogeneous group of inherited diseases resulting from deficiency of lysosomal proteins or non-lysosomal proteins critical for trafficking or post-translational modification of lysosomal proteins. Alterations in lysosomal function result in the accumulation of lysosomal substrates, a pathological hallmark of disease. Collectively, the prevalence of LSDs is quite high compared to other rare diseases, at approximately 1 in 8,000 live births [58]. LSDs lead to a wide spectrum of clinical phenotypes, but notably, two-thirds of patients display significant neurological symptoms. A persistent question in the field is why and how defects in lysosomal function contribute to organ dysfunction, particularly neurodegeneration. Studies of LSDs have revealed impairments in several critical cellular functions, including Ca^{2+} homeostasis and autophagy [1,3]. These pathways are increasingly shown to be important contributors to disease pathogenesis, and as Ca^{2+} has been implicated in autophagy regulation, alterations in these pathways may be functionally related. Here we discuss data from studies of two LSDs, Niemann-Pick type C (NPC) and Gaucher disease (GD), both of which exhibit Ca^{2+} and autophagy defects. These disorders are discussed as exemplars of the potential role of lysosomal and ER Ca^{2+} in autophagy dysregulation in this larger group of disorders.

2.4.1 Niemann-Pick C disease

NPC is an autosomal recessive LSD characterized by the accumulation of unesterified cholesterol in lysosomes and late endosomes [59]. The incidence of NPC is estimated to be in a range of 1/150,000 to 1/50,000 [60,61]. It is a devastating, progressive illness that often begins in infancy with liver disease, followed by a gradually worsening neurological course, with loss of motor skills, cognitive decline, seizures and most often death in early adolescence [60]. Later

symptomatic onset can occur in adolescents and adults, complicating the clinical spectrum of disease phenotypes. Most cases of NPC (~95%) are due to mutations in the *NPC1* gene [62], although a small subset (~5%) is due to mutations in *NPC2* [63]. NPC1 is a multipass transmembrane protein found in the limiting membrane of the lysosome while NPC2 is a soluble protein in the lysosomal lumen. It is thought that NPC1 and NPC2 function in concert to export cholesterol from lysosomes (Figure 2.1) [64]. Crystal structures and cryogenic electron microscopy studies have identified a mechanism by which NPC2 binds cholesterol and hands it off to NPC1, which then inserts it into the lysosomal membrane [65-67]. Although we have progressed in our understanding of NPC1's role in intracellular lipid trafficking, the precise mechanisms by which lipid accumulation leads to severe neurodegeneration are not well understood.

Studies using proteostasis regulators targeting the ER suggest that the ER Ca^{2+} concentration could be altered in NPC disease (Table 2.1). Increasing ER Ca^{2+} levels with the ryanodine receptor antagonist DHBP (1,1'-diheptyl-4,4'-bipyridium) increased steady state levels and trafficking of mutant NPC1 containing a substitution of isoleucine at position 1061 for threonine (I1061T); this treatment also ameliorated lipid storage [68]. The same study also found that overexpression of calnexin, a Ca^{2+} dependent molecular chaperone in the ER, reduced lipid storage by similarly impacting NPC1 I1061T proteostasis. It is not currently known whether these effects of modulating the ER environment reflect a baseline alteration in ER Ca^{2+} concentration in disease or merely benefits from activating Ca^{2+} dependent molecular chaperones. Direct measures of ER Ca^{2+} in NPC1 mutant cells have not been reported. Nonetheless, indirect analyses using Fura-2AM measurements of cytosolic Ca^{2+} after thapsigargin induced ER Ca^{2+} depletion found no difference between WT and NPC1 deficient cells [69]. Notably, this same study found that lysosomal Ca^{2+} was decreased in NPC1 mutant

fibroblasts and human B lymphoblasts. While diminished lysosomal Ca^{2+} could reflect disruptions in ER Ca^{2+} homeostasis, as the ER is required for lysosomal Ca^{2+} refilling [45], further work is needed to clarify this point. In addition to alterations in lysosomal Ca^{2+} concentration, channels regulating lysosomal Ca^{2+} release may be dysfunctional in NPC disease. This notion is supported by the observation that sphingomyelin in lysosomes of NPC1 deficient Chinese hamster ovary (CHO) cells inhibited TRPML-1 mediated Ca^{2+} release [70].

Multiple studies have demonstrated autophagy dysregulation in NPC disease. There is a striking accumulation of LC3, p62 and autophagic vesicles in multiple tissues of Npc1 deficient mice and cultured patient fibroblasts [71-73]. Defects in autophagy have been found at multiple steps of the pathway, including increased Beclin-1 dependent induction of autophagy [73], decreased autophagic flux, defective amphisome-lysosomal fusion [74] and impaired cargo degradation in lysosomes [73,75]. Studies in neuronal models of NPC disease also support activation of autophagy and a block in autophagy progression that contributes to defective clearance of mitochondria and mitochondrial fragmentation [76]. Although it is clear that autophagy defects exist in NPC, how autophagy can be modulated to impact disease progression is not well understood, and both autophagy induction and inhibition have been found to be beneficial and detrimental, depending on the model system and readout [74-77].

The relationship between impaired Ca^{2+} homeostasis and autophagy in NPC is not well characterized, but tantalizing data suggest an important link. Modulation of Ca^{2+} has been shown to impact intracellular trafficking in models of NPC. Treating NPC1-mutant CHO cells with thapsigargin elevated cytosolic Ca^{2+}, induced fusion between late endosomes and lysosomes and corrected endocytic uptake of horseradish peroxidase, which is normally defective due to annexin A2 mislocalization [69]. In addition, increased expression of TRPML-1 increased

TRPML-1 Ca^{2+} channel activity and corrected late endosome and lysosome to Golgi transport and reduced cholesterol storage [70]. Whether modulation of Ca^{2+} could correct autophagy and clearance of damaged substrates is an interesting question to pursue.

2.4.2 Gaucher disease

GD is the most common LSD, with an incidence of 1/40,000 to 1/50,000 [58]. It is an autosomal recessive sphingolipidosis caused by mutations in the lysosomal enzyme glucocerebrosidase (GCase) or its activator protein saposin C, which are responsible for hydrolysis of glucosylceramide (GlcCer) to ceramide and glucose (Figure 2.1). It is divided clinically into three variants – type 1 mainly involves viscera and bones while types 2 and 3 are neuronopathic. Type 1 ranges from childhood to adult-onset disorders and can manifest with hematological, visceral and bony involvement. Type 2 is most severe and presents within the first few months of life with rapid neurodegeneration and median death by 9 months. Type 3 exhibits varied levels of peripheral and CNS involvement, but leads to death within the first two decades [78]. GD is characterized by accumulation of GlcCer particularly in macrophages, which contain large amounts of glycosphingolipids. The activation of these macrophages is thought to underlie disease pathogenesis, as they infiltrate bone marrow, spleen, liver and other organs. The pathogenesis of neurodegeneration and neuron death is less well understood [79].

Using hippocampal neuron cultures treated with a small molecule inhibitor of GCase, it was shown that accumulation of GlcCer in neurons increases ER Ca^{2+} release in response to glutamate and caffeine, and that this increased the susceptibility of neurons to glutamate-induced death [80]. A subsequent study showed that GlcCer did not directly affect Ca^{2+} release, but augmented agonist-stimulated Ca^{2+} release through RyRs but not IP3Rs [81]. Microsomes from brains of type 2 GD patients also exhibited increased Ca^{2+} release via RyRs compared to type 1

and control patients, supporting the notion that altered Ca^{2+} signaling may play a role in neuronopathic forms of disease [81,82]. Confirming prior studies, GD iPSC-derived neurons had significantly higher cytosolic calcium levels compared to controls, increased RyR mediated ER Ca^{2+} release, and increased vulnerability to ER stress [83]. Additionally, studies have shown that correcting ER Ca^{2+} defects alters the disease phenotype. Knockdown or inhibition of RyRs increased ER Ca^{2+} in GD patient fibroblasts and enhanced GCase proteostasis and function [84]. Notably, the extent to which lysosomal Ca^{2+} is altered in GD is not well characterized. As ER Ca^{2+} levels impact lysosomal Ca^{2+} [45], it is reasonable to speculate that these levels are altered in GD.

Similarly to NPC, autophagy is dysregulated in GD. A mouse model deficient in saposin C and harboring mutant V394L GCase exhibited axonal degeneration and accumulation of p62 and Lamp2, suggesting impairment of autophagosome/lysosome fusion [85]. In addition, saposin C deficient fibroblasts exhibit enhanced autophagy and an accumulation of autophagic vesicles [86]. Likewise, a block in autophagy in GD macrophages leads to increased inflammasome activation [87]. Other mouse models of neuronopathic GD also show defective autophagy, as evidenced by accumulation of p62, ubiquitinated proteins and dysfunctional mitochondria [88]. Similarly, iPSC-derived neurons from GD patients exhibit an accumulation of autophagosomes and impaired autophagosome-lysosome fusion [83,89]. Notably, TFEB is significantly downregulated in GD iPSC-derived neurons, an alteration that impairs lysosomal biogenesis and likely contributes to autophagy defects. Furthermore, impaired lysosomal clearance increased susceptibility to death following rapamycin-induced autophagy [89]. A study in a *Drosophila* model of GD also showed a block in autophagy flux. In contrast to iPSC neurons, the fly model demonstrated increased expression of *Mitf*, the fly ortholog of TFEB, and showed that rapamycin ameliorated rather than

exacerbated disease phenotypes [90]. The reasons for these discrepancies are unclear, but could reflect differences *in vitro* versus *in vivo* or different stages of disease. The connection between Ca^{2+} and autophagy dysregulation is not well characterized in GD. However, the RyR antagonist dantrolene corrected altered Ca^{2+} signaling and autophagy defects in a GD mouse model, suggesting that stabilizing Ca^{2+} signaling is a potentially promising therapeutic target for GD [91].

Taken together, many LSDs share similar cellular defects, and altered Ca^{2+} homeostasis and autophagy have been separately characterized in both NPC and GD. As our understanding of the role of Ca^{2+} in autophagy regulation continues to increase, it will be interesting to explore how these processes intertwine to contribute to disease pathogenesis, thereby providing new mechanistic insights and suggesting novel therapeutic strategies.

2.5 Conclusion

Significant advances have been made in our understanding of the pathophysiology of LSDs. Studies in NPC and GD have established defects in autophagic flux that lead to accumulation of p62, LC3 and damaged organelles. In addition, altered Ca^{2+} homeostasis in NPC and GD likely contribute to defects in protein folding and intracellular trafficking that have been associated with the disease phenotype. As ER and lysosomal Ca^{2+} are critical regulators of autophagy, there is an intriguing possibility that these alterations are connected. Further studies examining how impaired Ca^{2+} homeostasis is related to and modulates autophagy in LSDs will likely reveal important insights into cellular mechanisms of disease.

2.6 Acknowledgements

References

1   Lieberman, A. P. *et al.* Autophagy in lysosomal storage disorders. *Autophagy* **8**, 719-730, doi:10.4161/auto.19469 (2012).
2   Settembre, C., Fraldi, A., Rubinsztein, D. C. & Ballabio, A. Lysosomal storage diseases as disorders of autophagy. *Autophagy* **4**, 113-114 (2008).
3   Ballabio, A. & Gieselmann, V. Lysosomal disorders: from storage to cellular damage. *Biochim Biophys Acta* **1793**, 684-696, doi:10.1016/j.bbamcr.2008.12.001 (2009).
4   Miyawaki, A. *et al.* Fluorescent indicators for Ca2+ based on green fluorescent proteins and calmodulin. *Nature* **388**, 882-887, doi:10.1038/42264 (1997).
5   Gordon, P. B., Holen, I., Fosse, M., Rotnes, J. S. & Seglen, P. O. Dependence of hepatocytic autophagy on intracellularly sequestered calcium. *J Biol Chem* **268**, 26107-26112 (1993).
6   Clapham, D. E. Calcium signaling. *Cell* **131**, 1047-1058, doi:10.1016/j.cell.2007.11.028 (2007).
7   Ivanova, H. *et al.* Inositol 1,4,5-trisphosphate receptor-isoform diversity in cell death and survival. *Biochim Biophys Acta* **1843**, 2164-2183, doi:10.1016/j.bbamcr.2014.03.007 (2014).
8   Lanner, J. T., Georgiou, D. K., Joshi, A. D. & Hamilton, S. L. Ryanodine receptors: structure, expression, molecular details, and function in calcium release. *Cold Spring Harb Perspect Biol* **2**, a003996, doi:10.1101/cshperspect.a003996 (2010).
9   Periasamy, M. & Kalyanasundaram, A. SERCA pump isoforms: their role in calcium transport and disease. *Muscle Nerve* **35**, 430-442, doi:10.1002/mus.20745 (2007).
10   Berridge, M. J. Inositol trisphosphate and calcium signalling mechanisms. *Biochim Biophys Acta* **1793**, 933-940, doi:10.1016/j.bbamcr.2008.10.005 (2009).
11   Foskett, J. K., White, C., Cheung, K. H. & Mak, D. O. Inositol trisphosphate receptor Ca2+ release channels. *Physiol Rev* **87**, 593-658, doi:10.1152/physrev.00035.2006 (2007).
12   Berridge, M. J. Inositol trisphosphate and calcium signalling. *Nature* **361**, 315-325, doi:10.1038/361315a0 (1993).
13   Sarkar, S. *et al.* Lithium induces autophagy by inhibiting inositol monophosphatase. *J Cell Biol* **170**, 1101-1111, doi:10.1083/jcb.200504035 (2005).
14   Criollo, A. *et al.* Regulation of autophagy by the inositol trisphosphate receptor. *Cell Death Differ* **14**, 1029-1039, doi:10.1038/sj.cdd.4402099 (2007).
15   Vicencio, J. M. *et al.* The inositol 1,4,5-trisphosphate receptor regulates autophagy through its interaction with Beclin 1. *Cell Death Differ* **16**, 1006-1017, doi:10.1038/cdd.2009.34 (2009).

16   Cardenas, C. *et al.* Essential regulation of cell bioenergetics by constitutive InsP3 receptor Ca2+ transfer to mitochondria. *Cell* **142**, 270-283, doi:10.1016/j.cell.2010.06.007 (2010).

17   Khan, M. T. & Joseph, S. K. Role of inositol trisphosphate receptors in autophagy in DT40 cells. *J Biol Chem* **285**, 16912-16920, doi:10.1074/jbc.M110.114207 (2010).

18   Williams, A. *et al.* Novel targets for Huntington's disease in an mTOR-independent autophagy pathway. *Nat Chem Biol* **4**, 295-305, doi:10.1038/nchembio.79 (2008).

19   Grotemeier, A. *et al.* AMPK-independent induction of autophagy by cytosolic Ca2+ increase. *Cell Signal* **22**, 914-925, doi:10.1016/j.cellsig.2010.01.015 (2010).

20   Hoyer-Hansen, M. *et al.* Control of macroautophagy by calcium, calmodulin-dependent kinase kinase-beta, and Bcl-2. *Mol Cell* **25**, 193-205, doi:10.1016/j.molcel.2006.12.009 (2007).

21   Sakaki, K., Wu, J. & Kaufman, R. J. Protein kinase Ctheta is required for autophagy in response to stress in the endoplasmic reticulum. *J Biol Chem* **283**, 15370-15380, doi:10.1074/jbc.M710209200 (2008).

22   Wang, S. H., Shih, Y. L., Ko, W. C., Wei, Y. H. & Shih, C. M. Cadmium-induced autophagy and apoptosis are mediated by a calcium signaling pathway. *Cell Mol Life Sci* **65**, 3640-3652, doi:10.1007/s00018-008-8383-9 (2008).

23   Decuypere, J. P. *et al.* Ins(1,4,5)P3 receptor-mediated Ca2+ signaling and autophagy induction are interrelated. *Autophagy* **7**, 1472-1489 (2011).

24   Decuypere, J. P. *et al.* mTOR-Controlled Autophagy Requires Intracellular Ca(2+) Signaling. *PLoS One* **8**, e61020, doi:10.1371/journal.pone.0061020 (2013).

25   La Rovere, R. M., Roest, G., Bultynck, G. & Parys, J. B. Intracellular Ca(2+) signaling and Ca(2+) microdomains in the control of cell survival, apoptosis and autophagy. *Cell Calcium* **60**, 74-87, doi:10.1016/j.ceca.2016.04.005 (2016).

26   Decuypere, J. P., Bultynck, G. & Parys, J. B. A dual role for Ca(2+) in autophagy regulation. *Cell Calcium* **50**, 242-250, doi:10.1016/j.ceca.2011.04.001 (2011).

27   Rowland, A. A. & Voeltz, G. K. Endoplasmic reticulum-mitochondria contacts: function of the junction. *Nat Rev Mol Cell Biol* **13**, 607-625, doi:10.1038/nrm3440 (2012).

28   Gomez-Suaga, P. *et al.* The ER-Mitochondria Tethering Complex VAPB-PTPIP51 Regulates Autophagy. *Curr Biol* **27**, 371-385, doi:10.1016/j.cub.2016.12.038 (2017).

29   Hamasaki, M. *et al.* Autophagosomes form at ER-mitochondria contact sites. *Nature* **495**, 389-393, doi:10.1038/nature11910 (2013).

30   Rubinsztein, D. C., Gestwicki, J. E., Murphy, L. O. & Klionsky, D. J. Potential therapeutic applications of autophagy. *Nat Rev Drug Discov* **6**, 304-312, doi:10.1038/nrd2272 (2007).

31   Yamamoto, A. *et al.* Bafilomycin A1 prevents maturation of autophagic vacuoles by inhibiting fusion between autophagosomes and lysosomes in rat hepatoma cell line, H-4-II-E cells. *Cell Struct Funct* **23**, 33-42 (1998).

32   Pereira, G. J. *et al.* Nicotinic acid adenine dinucleotide phosphate (NAADP) regulates autophagy in cultured astrocytes. *J Biol Chem* **286**, 27875-27881, doi:10.1074/jbc.C110.216580 (2011).

33   Christensen, K. A., Myers, J. T. & Swanson, J. A. pH-dependent regulation of lysosomal calcium in macrophages. *J Cell Sci* **115**, 599-607 (2002).

34   Churchill, G. C. *et al.* NAADP mobilizes Ca(2+) from reserve granules, lysosome-related organelles, in sea urchin eggs. *Cell* **111**, 703-708 (2002).

35   Zhang, F. & Li, P. L. Reconstitution and characterization of a nicotinic acid adenine dinucleotide phosphate (NAADP)-sensitive Ca2+ release channel from liver lysosomes of rats. *J Biol Chem* **282**, 25259-25269, doi:10.1074/jbc.M701614200 (2007).

36   Brailoiu, E. *et al.* Essential requirement for two-pore channel 1 in NAADP-mediated calcium signaling. *J Cell Biol* **186**, 201-209, doi:10.1083/jcb.200904073 (2009).

37   Calcraft, P. J. *et al.* NAADP mobilizes calcium from acidic organelles through two-pore channels. *Nature* **459**, 596-600, doi:10.1038/nature08030 (2009).

38   Patel, S. Function and dysfunction of two-pore channels. *Sci Signal* **8**, re7, doi:10.1126/scisignal.aab3314 (2015).

39   Wang, X. *et al.* TPC proteins are phosphoinositide- activated sodium-selective ion channels in endosomes and lysosomes. *Cell* **151**, 372-383, doi:10.1016/j.cell.2012.08.036 (2012).

40   Cang, C. *et al.* mTOR regulates lysosomal ATP-sensitive two-pore Na(+) channels to adapt to metabolic state. *Cell* **152**, 778-790, doi:10.1016/j.cell.2013.01.023 (2013).

41   Puertollano, R. & Kiselyov, K. TRPMLs: in sickness and in health. *Am J Physiol Renal Physiol* **296**, F1245-1254, doi:10.1152/ajprenal.90522.2008 (2009).

42   Wang, W., Zhang, X., Gao, Q. & Xu, H. TRPML1: an ion channel in the lysosome. *Handb Exp Pharmacol* **222**, 631-645, doi:10.1007/978-3-642-54215-2_24 (2014).

43   Zhang, X., Li, X. & Xu, H. Phosphoinositide isoforms determine compartment-specific ion channel activity. *Proc Natl Acad Sci U S A* **109**, 11384-11389, doi:10.1073/pnas.1202194109 (2012).

44   Morgan, A. J., Platt, F. M., Lloyd-Evans, E. & Galione, A. Molecular mechanisms of endolysosomal Ca2+ signalling in health and disease. *Biochem J* **439**, 349-374, doi:10.1042/BJ20110949 (2011).

45   Garrity, A. G. *et al.* The endoplasmic reticulum, not the pH gradient, drives calcium refilling of lysosomes. *Elife* **5**, doi:10.7554/eLife.15887 (2016).

46   Curcio-Morelli, C. *et al.* Macroautophagy is defective in mucolipin-1-deficient mouse neurons. *Neurobiol Dis* **40**, 370-377, doi:10.1016/j.nbd.2010.06.010 (2010).

47   Vergarajauregui, S. & Puertollano, R. Mucolipidosis type IV: the importance of functional lysosomes for efficient autophagy. *Autophagy* **4**, 832-834 (2008).

48   Wong, C. O., Li, R., Montell, C. & Venkatachalam, K. Drosophila TRPML is required for TORC1 activation. *Curr Biol* **22**, 1616-1621, doi:10.1016/j.cub.2012.06.055 (2012).

49   Li, R. J. *et al.* Regulation of mTORC1 by lysosomal calcium and calmodulin. *Elife* **5**, doi:10.7554/eLife.19360 (2016).

50   Wang, W. *et al.* Up-regulation of lysosomal TRPML1 channels is essential for lysosomal adaptation to nutrient starvation. *Proc Natl Acad Sci U S A* **112**, E1373-1381, doi:10.1073/pnas.1419669112 (2015).

51   Li, X. *et al.* A molecular mechanism to regulate lysosome motility for lysosome positioning and tubulation. *Nat Cell Biol* **18**, 404-417, doi:10.1038/ncb3324 (2016).

52   Gomez-Suaga, P. *et al.* Leucine-rich repeat kinase 2 regulates autophagy through a calcium-dependent pathway involving NAADP. *Hum Mol Genet* **21**, 511-525, doi:10.1093/hmg/ddr481 (2012).

53   Lin, P. H. *et al.* Lysosomal two-pore channel subtype 2 (TPC2) regulates skeletal muscle autophagic signaling. *J Biol Chem* **290**, 3377-3389, doi:10.1074/jbc.M114.608471 (2015).

54   Garcia-Rua, V. *et al.* Endolysosomal two-pore channels regulate autophagy in cardiomyocytes. *J Physiol* **594**, 3061-3077, doi:10.1113/JP271332 (2016).

55   Settembre, C. *et al.* TFEB links autophagy to lysosomal biogenesis. *Science* **332**, 1429-1433, doi:10.1126/science.1204592 (2011).

56   Medina, D. L. *et al.* Lysosomal calcium signalling regulates autophagy through calcineurin and TFEB. *Nat Cell Biol* **17**, 288-299, doi:10.1038/ncb3114 (2015).

57   Zhang, X. *et al.* MCOLN1 is a ROS sensor in lysosomes that regulates autophagy. *Nat Commun* **7**, 12109, doi:10.1038/ncomms12109 (2016).

58   Meikle, P. J., Hopwood, J. J., Clague, A. E. & Carey, W. F. Prevalence of lysosomal storage disorders. *JAMA* **281**, 249-254 (1999).

59   Pentchev, P. G. *et al.* A defect in cholesterol esterification in Niemann-Pick disease (type C) patients. *Proc Natl Acad Sci U S A* **82**, 8247-8251, doi:10.1073/pnas.82.23.8247 (1985).

60   Vanier, M. T. & Millat, G. Niemann-Pick disease type C. *Clin Genet* **64**, 269-281 (2003).

61   Wassif, C. A. *et al.* High incidence of unrecognized visceral/neurological late-onset Niemann-Pick disease, type C1, predicted by analysis of massively parallel sequencing data sets. *Genet Med* **18**, 41-48, doi:10.1038/gim.2015.25 (2016).

62   Carstea, E. D. *et al.* Niemann-Pick C1 disease gene: homology to mediators of cholesterol homeostasis. *Science* **277**, 228-231 (1997).

63   Naureckiene, S. *et al.* Identification of HE1 as the second gene of Niemann-Pick C disease. *Science* **290**, 2298-2301, doi:10.1126/science.290.5500.2298 (2000).

64   Infante, R. E. *et al.* NPC2 facilitates bidirectional transfer of cholesterol between NPC1 and lipid bilayers, a step in cholesterol egress from lysosomes. *Proc Natl Acad Sci U S A* **105**, 15287-15292, doi:10.1073/pnas.0807328105 (2008).

65   Gong, X. *et al.* Structural Insights into the Niemann-Pick C1 (NPC1)-Mediated Cholesterol Transfer and Ebola Infection. *Cell* **165**, 1467-1478, doi:10.1016/j.cell.2016.05.022 (2016).

66   Kwon, H. J. *et al.* Structure of N-terminal domain of NPC1 reveals distinct subdomains for binding and transfer of cholesterol. *Cell* **137**, 1213-1224, doi:10.1016/j.cell.2009.03.049 (2009).

67   Li, X. *et al.* Structure of human Niemann-Pick C1 protein. *Proc Natl Acad Sci U S A* **113**, 8212-8217, doi:10.1073/pnas.1607795113 (2016).

68   Yu, T., Chung, C., Shen, D., Xu, H. & Lieberman, A. P. Ryanodine receptor antagonists adapt NPC1 proteostasis to ameliorate lipid storage in Niemann-Pick type C disease fibroblasts. *Hum Mol Genet* **21**, 3205-3214, doi:10.1093/hmg/dds145 (2012).

69   Lloyd-Evans, E. *et al.* Niemann-Pick disease type C1 is a sphingosine storage disease that causes deregulation of lysosomal calcium. *Nat Med* **14**, 1247-1255, doi:10.1038/nm.1876 (2008).

70   Shen, D. *et al.* Lipid storage disorders block lysosomal trafficking by inhibiting a TRP channel and lysosomal calcium release. *Nat Commun* **3**, 731, doi:10.1038/ncomms1735 (2012).

71   Ko, D. C. *et al.* Cell-autonomous death of cerebellar purkinje neurons with autophagy in Niemann-Pick type C disease. *PLoS Genet* **1**, 81-95, doi:10.1371/journal.pgen.0010007 (2005).

72   Liao, G. *et al.* Cholesterol accumulation is associated with lysosomal dysfunction and autophagic stress in Npc1 -/- mouse brain. *Am J Pathol* **171**, 962-975, doi:10.2353/ajpath.2007.070052 (2007).

73   Pacheco, C. D., Kunkel, R. & Lieberman, A. P. Autophagy in Niemann-Pick C disease is dependent upon Beclin-1 and responsive to lipid trafficking defects. *Hum Mol Genet* **16**, 1495-1503, doi:10.1093/hmg/ddm100 (2007).

74   Sarkar, S. *et al.* Impaired autophagy in the lipid-storage disorder Niemann-Pick type C1 disease. *Cell Rep* **5**, 1302-1315, doi:10.1016/j.celrep.2013.10.042 (2013).

75   Elrick, M. J., Yu, T., Chung, C. & Lieberman, A. P. Impaired proteolysis underlies autophagic dysfunction in Niemann-Pick type C disease. *Hum Mol Genet* **21**, 4876-4887, doi:10.1093/hmg/dds324 (2012).

76   Ordonez, M. P. *et al.* Disruption and therapeutic rescue of autophagy in a human neuronal model of Niemann Pick type C1. *Hum Mol Genet* **21**, 2651-2662, doi:10.1093/hmg/dds090 (2012).

77   Maetzel, D. *et al.* Genetic and chemical correction of cholesterol accumulation and impaired autophagy in hepatic and neural cells derived from Niemann-Pick Type C patient-specific iPS cells. *Stem Cell Reports* **2**, 866-880, doi:10.1016/j.stemcr.2014.03.014 (2014).

78   Grabowski, G. A. Phenotype, diagnosis, and treatment of Gaucher's disease. *Lancet* **372**, 1263-1271, doi:10.1016/S0140-6736(08)61522-6 (2008).

79   Stirnemann, J. *et al.* A Review of Gaucher Disease Pathophysiology, Clinical Presentation and Treatments. *Int J Mol Sci* **18**, doi:10.3390/ijms18020441 (2017).

80   Korkotian, E. *et al.* Elevation of intracellular glucosylceramide levels results in an increase in endoplasmic reticulum density and in functional calcium stores in cultured neurons. *J Biol Chem* **274**, 21673-21678 (1999).

81   Lloyd-Evans, E. *et al.* Glucosylceramide and glucosylsphingosine modulate calcium mobilization from brain microsomes via different mechanisms. *J Biol Chem* **278**, 23594-23599, doi:10.1074/jbc.M300212200 (2003).

82   Pelled, D. *et al.* Enhanced calcium release in the acute neuronopathic form of Gaucher disease. *Neurobiol Dis* **18**, 83-88, doi:10.1016/j.nbd.2004.09.004 (2005).

83   Schondorf, D. C. *et al.* iPSC-derived neurons from GBA1-associated Parkinson's disease patients show autophagic defects and impaired calcium homeostasis. *Nat Commun* **5**, 4028, doi:10.1038/ncomms5028 (2014).

84   Ong, D. S., Mu, T. W., Palmer, A. E. & Kelly, J. W. Endoplasmic reticulum Ca2+ increases enhance mutant glucocerebrosidase proteostasis. *Nat Chem Biol* **6**, 424-432, doi:10.1038/nchembio.368 (2010).

85   Sun, Y. *et al.* Neuronopathic Gaucher disease in the mouse: viable combined selective saposin C deficiency and mutant glucocerebrosidase (V394L) mice with glucosylsphingosine and glucosylceramide accumulation and progressive neurological deficits. *Hum Mol Genet* **19**, 1088-1097, doi:10.1093/hmg/ddp580 (2010).

86   Vaccaro, A. M. *et al.* Saposin C mutations in Gaucher disease patients resulting in lysosomal lipid accumulation, saposin C deficiency, but normal prosaposin processing and sorting. *Hum Mol Genet* **19**, 2987-2997, doi:10.1093/hmg/ddq204 (2010).

87   Aflaki, E. *et al.* Lysosomal storage and impaired autophagy lead to inflammasome activation in Gaucher macrophages. *Aging Cell* **15**, 77-88, doi:10.1111/acel.12409 (2016).

88   Osellame, L. D. *et al.* Mitochondria and quality control defects in a mouse model of Gaucher disease--links to Parkinson's disease. *Cell Metab* **17**, 941-953, doi:10.1016/j.cmet.2013.04.014 (2013).

89   Awad, O. *et al.* Altered TFEB-mediated lysosomal biogenesis in Gaucher disease iPSC-derived neuronal cells. *Hum Mol Genet* **24**, 5775-5788, doi:10.1093/hmg/ddv297 (2015).

90   Kinghorn, K. J. *et al.* A Drosophila Model of Neuronopathic Gaucher Disease Demonstrates Lysosomal-Autophagic Defects and Altered mTOR Signalling and Is Functionally Rescued by Rapamycin. *J Neurosci* **36**, 11654-11670, doi:10.1523/JNEUROSCI.4527-15.2016 (2016).

91   Liou, B. *et al.* Modulating ryanodine receptors with dantrolene attenuates neuronopathic phenotype in Gaucher disease mice. *Hum Mol Genet* **25**, 5126-5141, doi:10.1093/hmg/ddw322 (2016).

This work has been published in *Neuroscience Letters* (2019):

Liu, E. A. & Lieberman, A. P. The intersection of lysosomal and endoplasmic reticulum calcium with autophagy defects in lysosomal diseases. *Neurosci Lett* **697**, 10-16, doi:10.1016/j.neulet.2018.04.049 (2019).

Chapter 3

Fbxo2 Mediates Clearance of Damaged Lysosomes and Modifies Neurodegeneration in the Niemann-Pick C Brain

3.1 Abstract

A critical response to lysosomal membrane permeabilization (LMP) is the clearance of damaged lysosomes through a selective form of macroautophagy known as lysophagy. Although regulators of this process are emerging, whether organ and cell specific components contribute to the control of lysophagy remains incompletely understood. Here, we examine LMP and lysophagy in Niemann-Pick type C disease (NPC), an autosomal recessive disorder characterized by the accumulation of unesterified cholesterol within late endosomes and lysosomes, leading to neurodegeneration and early death. We demonstrate that NPC patient fibroblasts show enhanced sensitivity to lysosomal damage as a consequence of lipid storage. Moreover, we describe a role for the glycan binding F-box protein Fbxo2 in CNS lysophagy. Fbxo2 functions as a component of the SCF ubiquitin ligase complex. Loss of Fbxo2 in mouse primary cortical cultures delays clearance of damaged lysosomes and decreases viability following lysosomal damage. Moreover, Fbxo2 deficiency in a mouse model of NPC exacerbates deficits in motor function, enhances neurodegeneration, and reduces survival. Collectively, our data identify a role for Fbxo2 in CNS lysophagy and establish its functional importance in NPC.

3.2 Introduction

Lysosomes are critical organelles that function in degrading and recycling cellular waste and play broader roles in signaling, membrane repair and metabolism [1]. As lysosomes contain diverse hydrolytic enzymes, lysosomal membrane integrity is essential for organelle function and for containing enzymes within the lysosomal compartment. A variety of factors, including lysosomotropic drugs and oxidative stress, lead to lysosomal membrane permeabilization (LMP), releasing lysosomal enzymes and triggering cellular processes from inflammasome activation to apoptosis [2]. LMP-induced cell death can occur under physiologic conditions as a homeostatic response, such as during mammary gland involution or to maintain neutrophil numbers during inflammation [3]. However, LMP has also been observed in several neurodegenerative diseases, including Alzheimer and Parkinson diseases and lysosomal storage disorders (LSDs) [3].

One protective measure against LMP is the clearance of damaged lysosomes through a selective form of macroautophagy known as lysophagy. In this process, damaged lysosomes are sensed, and subsequent ubiquitination of lysosomal proteins leads to recruitment of autophagic machinery, engulfment by autophagic membranes, and clearance of the damaged organelles [2]. Cytosolic galectins, including galectin-1, -3, -8 and -9, serve as sensors of lysosomal damage [4-7]. In addition to their sensing function, galectins also play more active roles in lysophagy by recruiting autophagy adapters; galectin-3 interacts with TRIM16 [5], and galectin-8 recruits NDP52 [7]. A key intermediate step for lysophagy progression is ubiquitination of lysosomal proteins. Polyubiquitination of organelle membrane proteins is a feature of many forms of selective autophagy, which mediates recruitment of autophagic machinery, allowing for efficient organelle turnover [2,8]. LRSAM1 [9], TRIM16 [5] and the SCF[FBXO27] ubiquitin ligase complex [10] are ubiquitin ligases that have been implicated in lysophagy. Although components of lysophagy

have been identified in recent studies, aspects of the machinery that function in organ and cell type specific regulation remain incompletely understood. Notably, LMP has been observed in an increasing number of neurodegenerative diseases, yet brain specific lysophagy machinery remains unknown.

Here, we probe LMP and lysophagy in Niemann-Pick C, an autosomal recessive LSD characterized by accumulation of unesterified cholesterol in lysosomes and late endosomes [11]. LSDs are a heterogeneous group of more than 70 inherited disorders characterized by the accumulation of lysosomal substrates due to organellar dysfunction and frequently cause neurodegeneration [12]. LMP has been implicated in an increasing number of lysosomal diseases, including Gaucher disease [13], late-infantile neuronal ceroid lipofuscinosis [14], Niemann-Pick A [15-17] and Niemann-Pick C [18,19].

Niemann-Pick C is a devastating illness that often begins with liver disease, followed by a gradually worsening neurological course, with loss of motor skills, cognitive decline, seizures and most often death by early adolescence [20]. Most cases of Niemann-Pick C (~95%) are due to mutations in the *NPC1* gene [21], although a small subset (~5%) is due to mutations in *NPC2* [22]. NPC1 is a multi-pass transmembrane protein in the limiting membrane of lysosomes, while NPC2 is a soluble protein in the lysosomal lumen. NPC1 and NPC2 function in concert to export cholesterol from lysosomes [23]; thus, mutations in either of these proteins lead to cholesterol accumulation. Although lipid accumulation is a hallmark of disease, the pathogenesis of neurodegeneration in Niemann-Pick C remains incompletely understood. Prior studies have demonstrated mislocalization of lysosomal cathepsins outside of the lysosomal compartment in neurons in the Niemann-Pick C mouse brain, suggestive of LMP [18,19]. In addition, NPC1-deficient cells experience increased toxicity with oxidative stress, a known inducer of LMP, and

Niemann-Pick C mice deficient in cystatin B, an inhibitor of cathepsins, exhibit exacerbated cerebellar degeneration [19].

Here, we sought to further establish the role of LMP in Niemann-Pick C pathogenesis and define mechanisms of lysophagy, a critical response to lysosomal damage. We show that Niemann-Pick C patient fibroblasts exhibit increased lysosomal damage after exposure to lysosome damaging agents, and that this sensitivity is dependent upon the presence of stored lipids. Furthermore, we describe a novel role for Fbxo2 in CNS lysophagy. Fbxo2 is a glycan binding F-box protein that functions in the S phase kinase-associated protein 1 (SKP1)-cullin 1 (CUL1)-F-box protein (SCF) ubiquitin ligase complex, one of the largest classes of E3 ubiquitin protein ligases. We demonstrate that Fbxo2 localizes to damaged lysosomes, and that Fbxo2 deficiency impairs clearance of damaged lysosomes and exacerbates the Niemann-Pick C disease phenotype.

3.3 Results

3.3.1 I1061T NPC1 patient fibroblasts are more sensitive to lysosomal damage

Prior work has described LMP in Purkinje neurons and cerebellar lysates of Niemann-Pick C mice, as evidenced by cytosolic mislocalization of cathepsins outside of the lysosomal compartment [18,19]. To further investigate the role of LMP in Niemann-Pick C disease pathogenesis, we utilized control (Ctrl) fibroblasts homozygous for WT NPC1 and Niemann-Pick C patient fibroblasts homozygous for I1061T NPC1 (I1061T), the most common disease-causing allele in patients of Western European ancestry [24]. Cells were treated with increasing doses of the lysosomotropic compound L-leucyl-L-leucine methyl ester (LLOMe), a widely used lysosomal damaging agent that accumulates in lysosomes and is converted to a membranolytic

form, (Leu-Leu)n-OME (n>3), by a lysosomal thiol protease, dipeptidyl peptidase I (DPPI) [4,25,26]. To detect damaged lysosomes, we quantified the number of galectin-3 (Gal3) puncta, which accumulate on damaged lysosomes and are a sensitive indicator of LMP [4,6]. Even at the lowest doses of LLOMe, I1061T patient fibroblasts exhibited significantly higher levels of Gal3 puncta per cell (Figure 3.1A). As accumulated storage of lysosomal substrates leads to an increase in both size and number of lysosomes [27], we wondered if the greater number of damaged lysosomes also reflected a greater proportion of damaged lysosomes in Niemann-Pick C cells. To address this, we treated Ctrl and I1061T patient fibroblasts with LLOMe, stained for both Gal3 and LAMP-1, and quantified their co-localization (Figure 3.1B). A significantly higher portion of LAMP-1 signal co-localized with Gal3 in I1061T patient fibroblasts (~40%) compared to Ctrl (~10%), indicating a higher percentage of damaged lysosomes.

To limit cytotoxic consequences of LMP, damaged lysosomes are eliminated by a form of selective macroautophagy known as lysophagy [5,7,8,10,25,28]. As impairments in autophagic flux have been characterized in Niemann-Pick C [29-35], we wondered whether the increased lysosomal damage was due to deficient autophagic clearance. Thus, we performed a time course, treating Ctrl and I1061T patient fibroblasts with LLOMe for 1 hr followed by washout, and Gal3 puncta were quantified up to 24 hrs. Cells that are deficient in autophagy exhibit impaired clearance of Gal3 puncta [25,28]. Our time course confirmed significantly increased Gal3 puncta per cell in I1061T patient fibroblasts but showed that these puncta were cleared through time, decreasing markedly by 16 and 24 hrs (Figure 3.2A) and indicating functioning lysophagy. To assess if markers of autophagy also correlated with the transient accumulation and subsequent clearance of Gal3 puncta, we quantified LC3 puncta after LLOMe treatment. Similar to the pattern seen with Gal3 (Figure 3.2A), I1061T patient fibroblasts exhibited significantly higher numbers of

LC3 puncta per cell compared to Ctrl, and these puncta were cleared out by 24 hrs (Figure 3.2B).

Plotting the percentage of Gal3 and LC3 puncta clearance through time also showed that both

Ctrl and I1061T patient fibroblasts clear Gal3 and LC3 puncta at similar rates (Figure 3.3). These

data support the induction of lysophagy and clearance of damaged lysosomes following
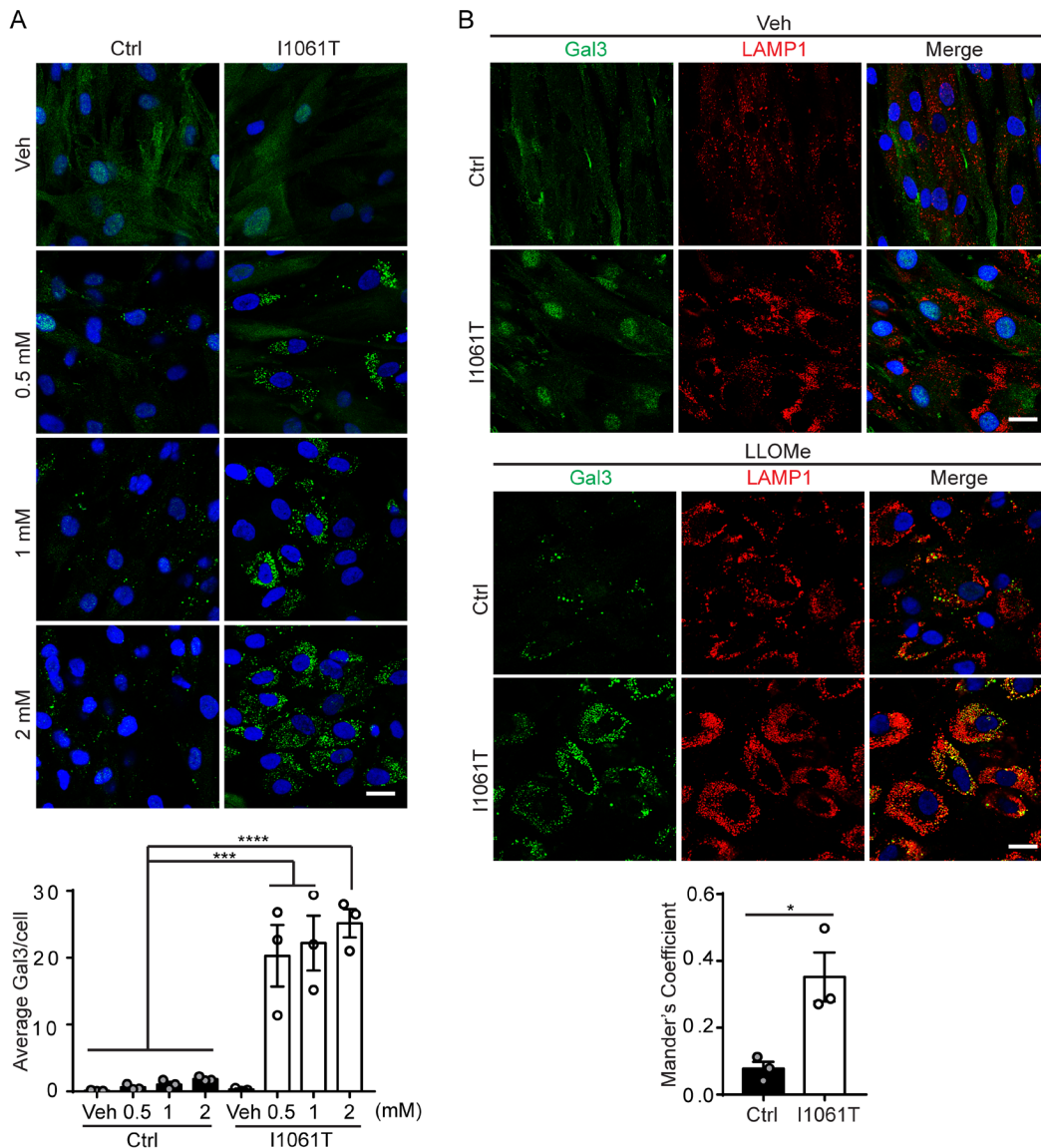
treatment with LLOMe.

Figure 3.1 I1061T NPC1 patient fibroblasts are more sensitive to lysosomal damage. (A) Primary human fibroblasts
homozygous for WT NPC1 (Ctrl) or I1061T NPC1 (I1061T) were treated with vehicle (Veh) or indicated doses of LLOMe for
1hr and stained for Gal3 to detect damaged lysosomes. Gal3 puncta per cell quantified below. (B) Ctrl and I1061T patient
fibroblasts were treated with Veh or 2mM LLOMe for 1 hr and stained for Gal3 and LAMP-1. Co-localization was performed on
4 fields each from 3 independent experiments, with 100-200 cells per experiment. Data are shown as mean ± s.e.m. from 3

independent experiments. *P ≤ 0.05, **P ≤ 0.01, ***P ≤ 0.001, ****P ≤ 0.0001 by (A) one-way ANOVA with Tukey's multiple comparisons (B) t-test ((A) F=24.04; (B) F=12.78). Scale bar: 25μm
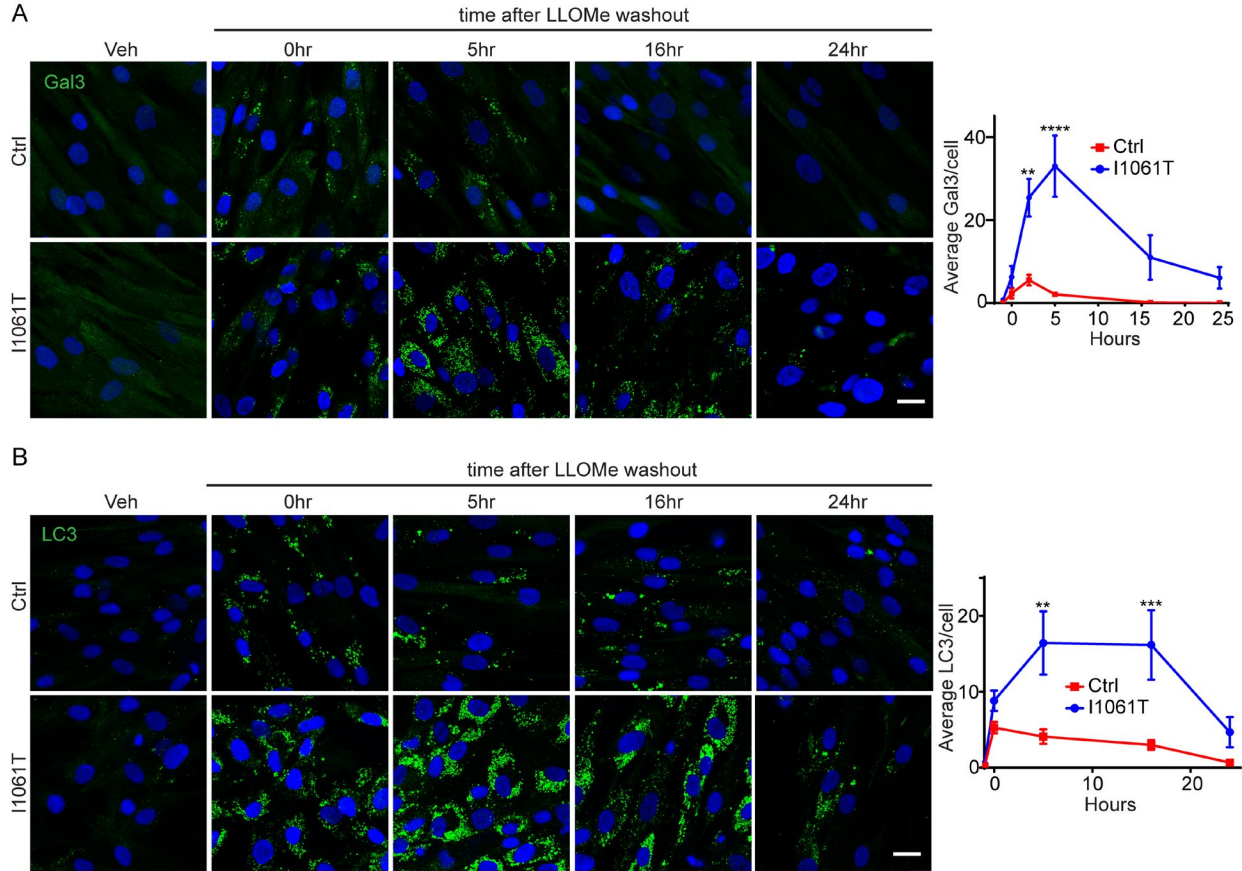

Figure 3.2 Gal3 and LC3 puncta induced by lysosomal damage are cleared in I1061T NPC1 patient fibroblasts. (A) Ctrl and I1061T patient fibroblasts were treated with Veh or 2mM LLOMe for 1 hr and stained for Gal3 at indicated times after washout. Quantified at the right. (B) Ctrl and I1061T patient fibroblasts were treated with Veh or 0.5mM LLOMe for 1 hr and stained for LC3 at indicated times. LC3 puncta per cell quantified at the right. Data are shown as mean ± s.e.m. from (A) 3 or (B) 4 independent experiments. *P ≤ 0.05, **P ≤ 0.01, ***P ≤ 0.001, ****P ≤ 0.0001 by two-way ANOVA with Sidak's test. Scale bar: 25μm
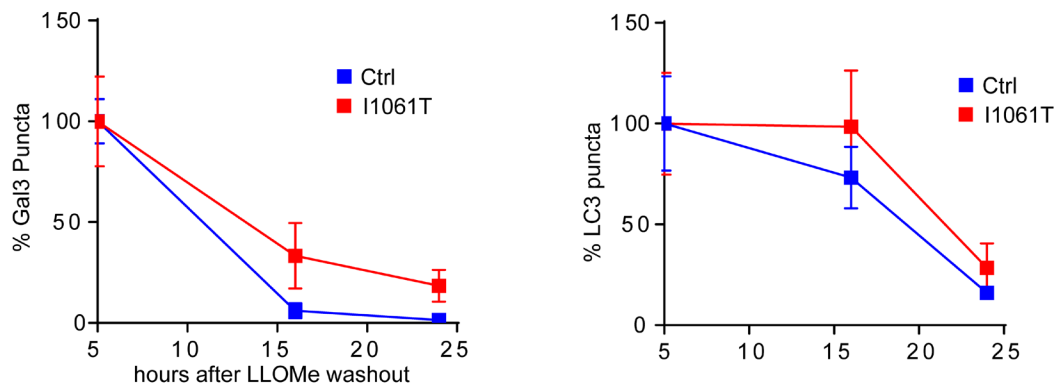

Figure 3.3 I1061T patient fibroblasts exhibit similar rates of Gal3 and LC3 clearance. CTRL and I1061T patient fibroblasts were treated with Veh or 2mM LLOMe for 1hr and stained for Gal3 or LC3 at indicated times after washout. % of Gal3 or LC3 puncta clearance is plotted. Data are shown as mean ± s.e.m. from 3-4 independent experiments. Clearance of Gal3 and LC3 are not significantly different (P>0.5) by two-way ANOVA with Sidak's test.

3.3.2 Increased lysosomal damage is dependent upon lipid storage

In addition to the marked accumulation of Gal3 puncta in NPC patient fibroblasts after inducing lysosomal damage with LLOMe, we also observed lysosomal damage in Npc1-I1061T knock-in mice [36]. These mice develop age-dependent phenotypes including cholesterol accumulation, neuron loss, motor impairment, and early death. Wild type (WT) and mutant mice were treated with vinblastine for 2 hrs to slow autophagosome maturation [37]. This facilitated the identification of Gal3+, Lamp-2+ vesicles in liver macrophages of Npc1-I1061T mutants (Mander's coefficient = 0.76 for I1061T), suggesting the occurrence of lysosomal damage in vivo (Figure 3.4A).
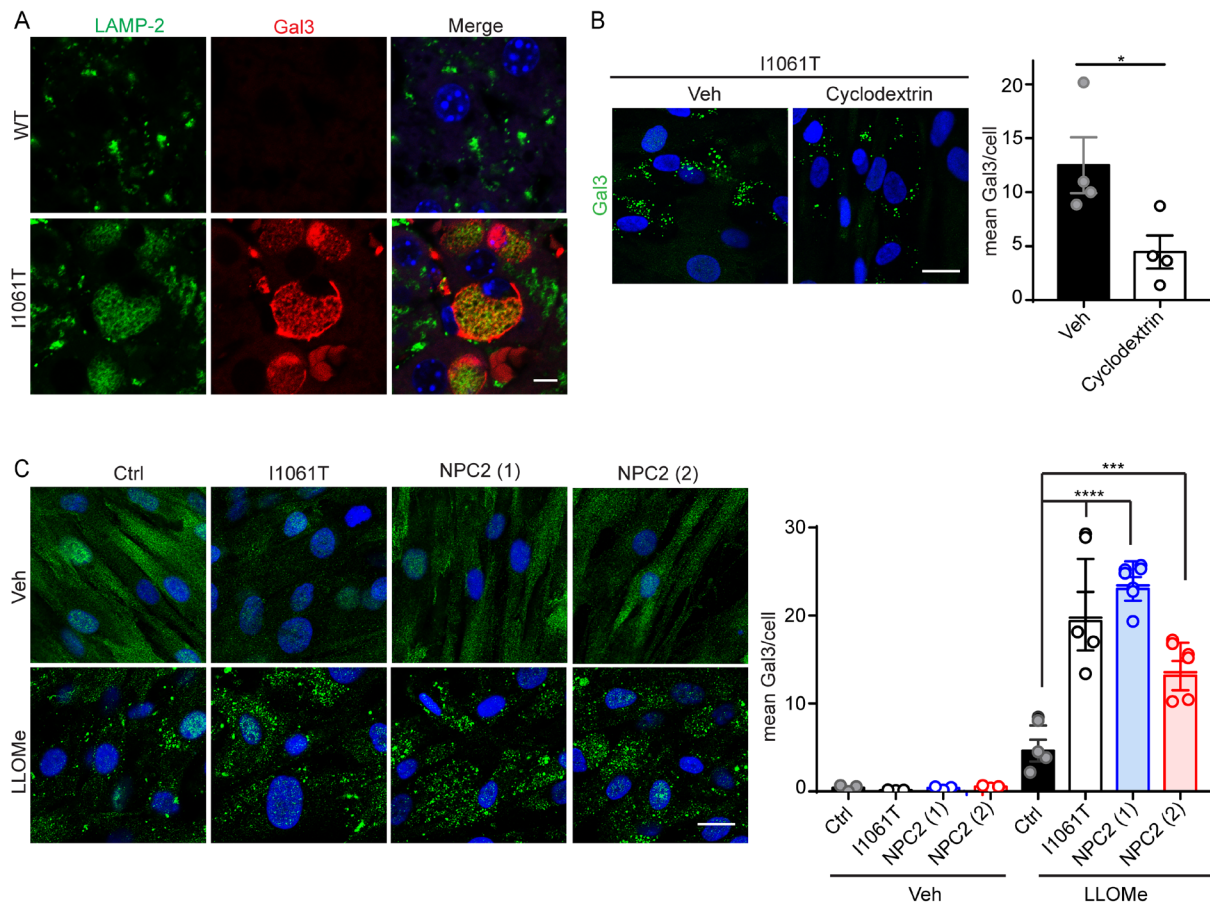

Figure 3.4 Increased lysosomal damage is dependent upon lipid storage. **(A)** Seven-week-old WT and I1061T mice were treated with vinblastine for 2 hr. Liver was collected and stained for Gal3 and LAMP-2. Mander's coefficient in I1061T liver: 0.76. Scale bar: 5µm **(B)** Ctrl and I1061T patient fibroblasts were treated with Veh or 1mM cyclodextrin (Cyclo) for 48 hrs, then

treated with 2mM LLOMe for 1 hr and stained for Gal3. Quantified at the right. Scale bar: 25μm **(C)** Ctrl, I1061T and two independent lines of NPC2 patient fibroblasts were treated with Veh or 2mM LLOMe for 1 hr and stained for Gal3. Quantified at the right. Scale bar: 25μm**.** Data are shown as mean ± s.e.m. from **(B-C)** 4 independent experiments. n.s., not significant, *P ≤ 0.05, **P ≤ 0.01, ***P ≤ 0.001, ****P ≤ 0.0001 by **(B)** t-test **(C)** one-way ANOVA with Tukey's multiple comparisons (**(B)** F=2.845, **(C)** F=30.99).

As accumulated lipids contribute to LMP [15-17,38-40], we reasoned that lipid storage in I1061T patient fibroblasts could increase sensitivity to lysosomal damage. To test this notion, we treated I1061T patient fibroblasts with hydroxypropyl-β-cyclodextrin to remove stored lipids including unesterified cholesterol. Treatment with cyclodextrin for 48 hrs did not significantly change levels of LAMP-1 (Figure 3.5) indicating that lysosome number was unaltered during the experiment. However, cyclodextrin treatment significantly reduced Gal3 puncta per cell in I1061T patient fibroblasts following treatment with LLOMe, demonstrating that sensitivity to lysosomal damage was dependent upon lipid storage (Figure 3.4B). The mutant I1061T NPC1 protein is known to misfold in the endoplasmic reticulum and be degraded, preventing its trafficking to the lysosome [37,41]. To examine whether loss of NPC1 at the lysosomal membrane plays a role in sensitivity to lysosomal damage, we treated NPC2-mutant patient fibroblasts with LLOMe. These cells express WT NPC1 yet accumulate lipids due to functional deficiency of NPC2 [42-44]. Similar to I1061T patient fibroblasts, two independent lines of NPC2-mutant fibroblasts (g.IVS1+2T>C/g.IVS1+2T>C and c.58G>T/c.140G>T) also exhibited significantly increased lysosomal damage (Figure 3.4C). These data corroborate our findings from NPC1-I1061T patient fibroblasts that lipid accumulation is linked to lysosomal damage. Further, they support the notion that lipid accumulation, independent of loss of NPC1 at the lysosomal membrane, contributes to increased lysosomal damage.
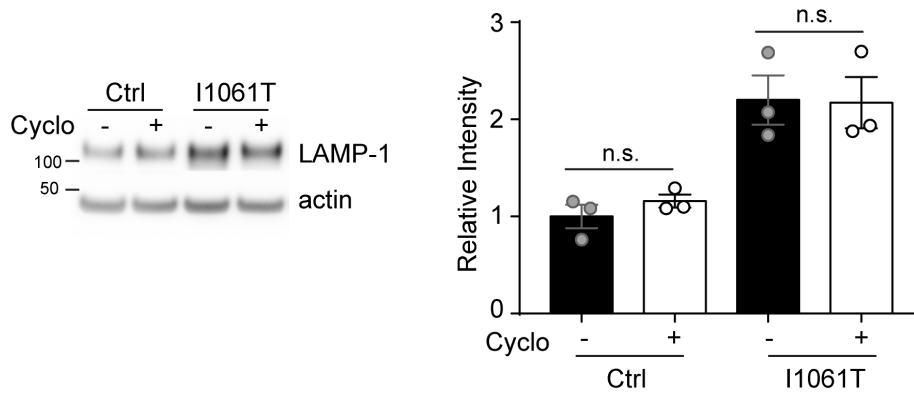
Figure 3.5 LAMP-1 levels do not change after cyclodextrin treatment. CTRL and I1061T patient fibroblasts were treated with Veh or 1mM cyclodextrin (Cyclo) for 48 hrs, then treated with 2mM LLOMe for 1 hr. LAMP-1 levels were analyzed by western blot. Data are shown as mean ± s.e.m. from 3 independent experiments. n.s., not significant

3.3.3 Increased lysosomal damage is not due to impaired clearance

Our prior time course experiments demonstrated clearance of Gal3 puncta in I1061T patient fibroblasts (Figure 3.2A, Figure 3.3) suggesting functioning lysophagy. To examine the rate at which damaged lysosomes were cleared from cells, we utilized a cycloheximide (CHX) chase assay [10] (Figure 3.6A). Cells were treated with LLOMe and CHX for 1 hr. Following LLOMe washout, CHX treatment was continued for various times to assess degradation rates of LAMP-1 or Gal3 as indicators of lysosomal clearance. We first corroborated the use of this assay as a readout of lysophagy. Without lysosomal damage, LAMP-1 and Gal3 levels remained constant for the duration of the CHX chase (Figure 3.7). After lysosomal damage, LAMP-1 levels diminished with time in WT mouse embryonic fibroblasts (WT MEFs), but this effect was prevented in Atg5-/- MEFs, which are autophagy deficient [45] (Figure 3.6B). We next performed this analysis on Ctrl and I1061T patient fibroblasts, and consistent with prior time course experiments (Figure 3.2), found that Gal3 was cleared in both Ctrl and I1061T patient fibroblasts at equivalent rates (Figure 3.6C); similarly, LAMP-1 was efficiently cleared from I1061T patient fibroblasts (Figure 3.8). We conclude that Niemann-Pick C cells exhibit enhanced sensitivity to lysosomal damage but clear damaged lysosomes at a similar rate to controls.
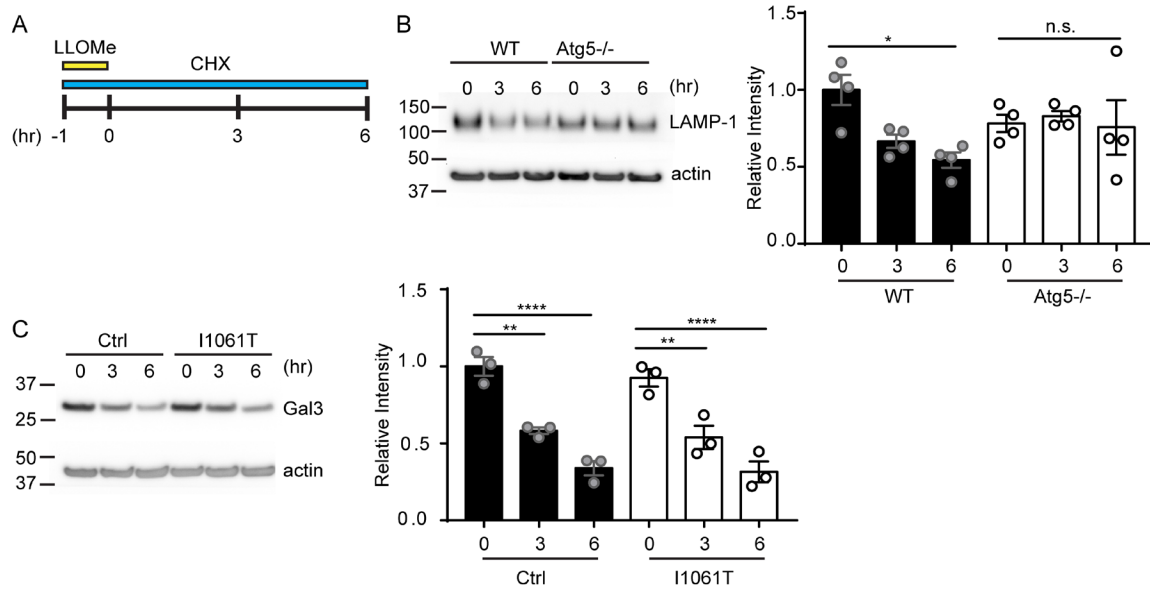
Figure 3.6 Increased lysosomal damage is not due to impaired clearance. **(A)** To examine lysophagy progression, cells were treated with 30μg/mL CHX and 2mM LLOMe for 1 hr and CHX treatment continued for indicated times before lysates were collected. **(B)** WT and Atg5-/- MEFs were treated as in **(A)**. LAMP-1 levels were analyzed and quantified at the right. **(C)** Ctrl and I1061T patient fibroblasts were treated as in **(A)**. Gal3 levels were analyzed and quantified at the right. Data are shown as mean ± s.e.m. from **(B)** 4 or **(C)** 3 independent experiments. n.s., not significant, *P ≤ 0.05, **P ≤ 0.01, ****P ≤ 0.0001 by one-way ANOVA with Tukey's multiple comparisons (**(B)** F=2.862, **(C)** F=25.49)
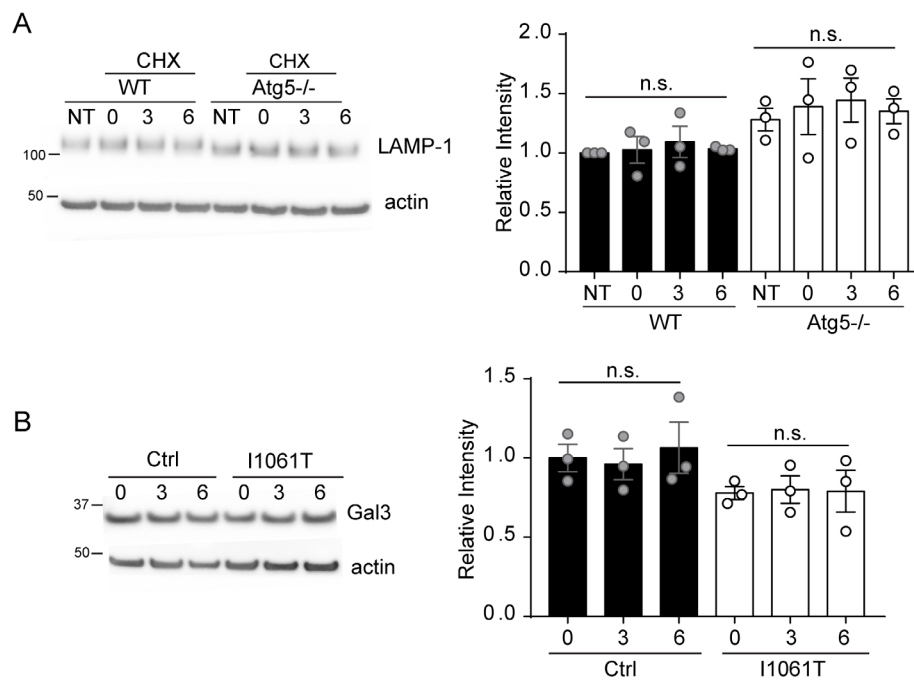

Figure 3.7 LAMP-1 and Gal3 levels are not changed in the absence of LLOMe treatment. **(A)** WT and Atg5-/- MEFs were treated with 30μg/mL CHX for the indicated times and LAMP-1 levels were analyzed by western blot. **(B)** CTRL and I1061T patient fibroblasts were treated with CHX for the indicated times and Gal3 levels were analyzed by western blot. Data are shown as mean ± s.e.m. from 3 independent experiments. n.s., not significant
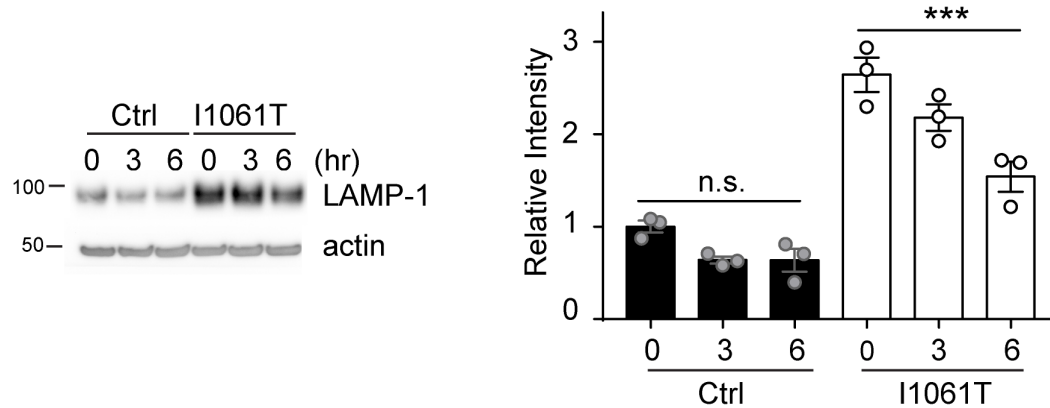
Figure 3.8 LAMP-1 levels are decreased after LLOME treatment. CTRL and I1061T patient fibroblasts were treated with 30μg/mL CHX and 2mM LLOMe for 1hr. CHX treatment continued for the indicated time points. LAMP-1 levels were analyzed and quantified at the right. This blot was derived from the same gel as in Figure 3.6C and has the same loading control. Data are shown as mean ± s.e.m. from 3 independent experiments. n.s., not significant, ***P ≤ 0.001 by one-way ANOVA F=40.7

3.3.4 Fbxo2 is the most highly expressed glycan binding F-box protein in the brain

With evidence that Niemann-Pick C fibroblasts are more susceptible to lysosomal damage, we sought to further elucidate mechanisms of lysophagy, a critical cellular response to lysosomal damage. LMP exposes N-glycan-modified proteins of the limiting membrane of the lysosome to the cytosol, making them accessible to lectin binding. A recent study showed that following lysosomal damage, Fbxo27, a glycan binding F-box protein, ubiquitinates lysosomal proteins and targets damaged lysosomes for degradation by autophagy [10]. F-box proteins function within the S phase kinase-associated protein 1 (SKP1)-cullin 1 (CUL1)-F-box protein (SCF) ubiquitin ligase complex, one of the largest classes of E3 ubiquitin protein ligases. There are ~70 different F-box proteins in humans, and the variable F-box protein determines substrate specificity [46]. Confirming the importance of ubiquitination in lysophagy, inhibiting E1 ubiquitin-activating enzymes with MLN7423 [47] delayed clearance of damaged lysosomes (Figure 3.9A).
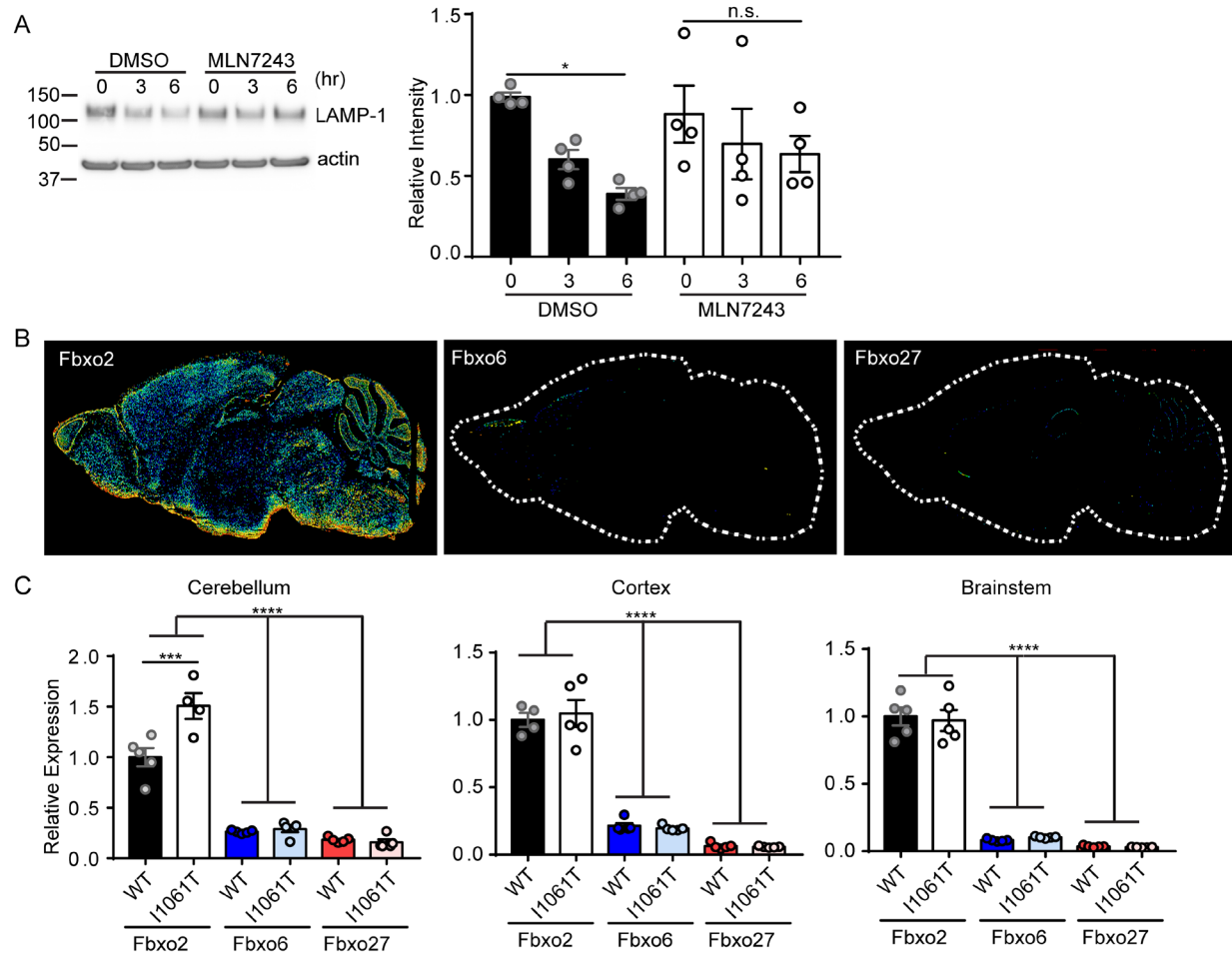
Figure 3.9 Fbxo2 is the most highly expressed glycan binding F-box protein in the brain. **(A)** Ctrl patient fibroblasts were pre-treated with DMSO or 1μM MLN7243 for 4 hrs and then treated as indicated with 30μg/mL CHX and 2mM LLOMe. LAMP-1 levels quantified at the right. **(B)** Allen Brain Atlas expression data of Fbxo2, Fbxo6 and Fbxo27 in mouse brain. **(C)** Relative expression of Fbxo2, Fbxo6 and Fbxo27 was determined in the cerebellum, cortex and brainstem of WT and I1061T mice at 12 wks by qPCR. N=4-5 mice per genotype. Data are shown as mean ± s.e.m from **(A)** 4 independent experiments. n.s., not significant, *P ≤ 0.05, ***P ≤ 0.001, ****P ≤ 0.0001 by **(A, C)** one-way ANOVA with Tukey's multiple comparisons (**(A)** F=2.803, **(C)** F=78.88 (CB), F=95.66 (CX) F=128.7 (BS)). Fbxo2, F-box protein 2; Ctrl, control; CHX, cycloheximide; LLOMe, L-leucyl-L-leucine methyl ester; CB, cerebellum; CX, cortex; BS, brainstem

Prior studies have provided evidence of LMP in the Niemann-Pick C brain [19] and established neurons as a critical cell type for disease pathogenesis [48]. Therefore, we were curious as to the function of Fbxo27 in the brain. Utilizing the Allen Brain Atlas, we found, however, that Fbxo27 exhibits very low expression in the brain (Figure 3.9B). As the importance of ubiquitination in lysophagy has been described [2], we wondered whether other glycan binding F-box proteins might play a more significant role in the brain. Fbxo2, Fbxo6 and Fbxo27 are in the

F-box associated (FBA) family of F-box proteins, which is the only family of ubiquitin ligase subunits thought to target glycoproteins [49]. Utilizing the Allen Brain Atlas, we found that both Fbxo27 and Fbxo6 exhibit low brain expression; in contrast, Fbxo2 is highly expressed throughout the brain (Figure 3.9B). Indeed, Fbxo2 was originally identified as a brain enriched F-box protein [50], with expression annotated in neurons, astrocytes, oligodendrocytes and microglia [51]. We confirmed by qPCR that Fbxo2 is the most highly expressed glycan binding F-box protein in multiple brain regions, with no significant change in expression in WT compared to Npc1-I1061T knock-in mice [36], except for a slight increase in the cerebellum (Figure 3.9C). Similarly, protein levels of Fbxo2 were not significantly different between WT and Npc1-I1061T mice (Figure 3.10).
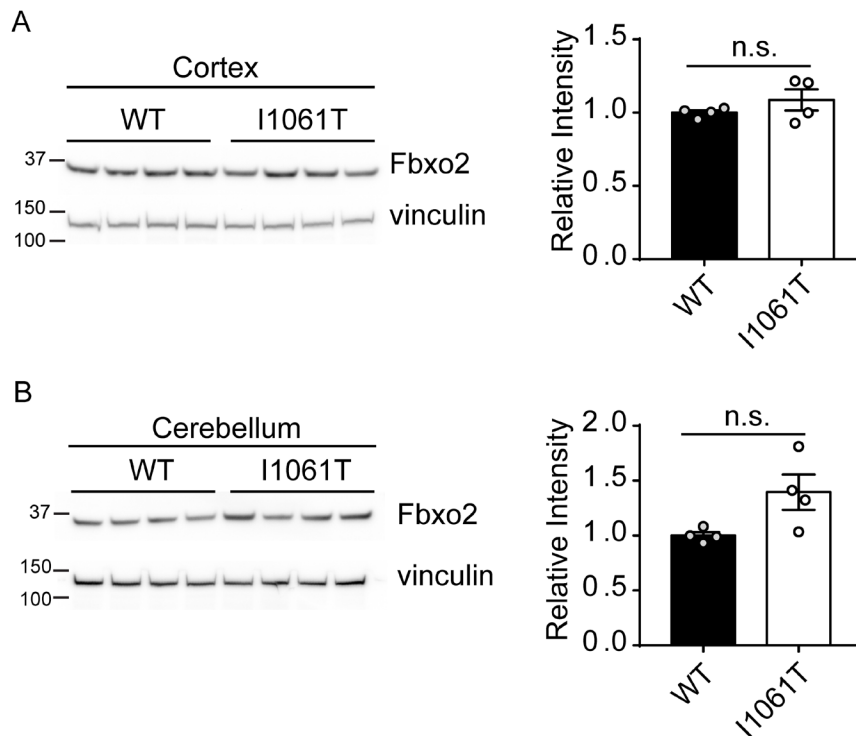

Figure 3.10 WT and Npc1-I1061T mice have similar levels of Fbxo2. Cortex and cerebellum lysates were collected from 12wk WT and Npc1-I1061T mice. Fbxo2 levels are quantified at the right. N=4 mice per genotype. Data are shown as mean ± s.e.m. n.s., not significant by t-test.

3.3.5 Fbxo2 localizes to damaged lysosomes

Fbxo2 has been shown to play roles in glycoprotein quality control through ER-associated degradation [52]. To our knowledge, it has not been shown to play a role in lysophagy, though prior work has demonstrated interaction with LAMP-1 and LAMP-2 after lysosomal damage [10]. To begin to investigate whether Fbxo2 contributes to lysophagy, we overexpressed HA-FBXO2 in Ctrl and I1061T patient fibroblasts. As anticipated, this manipulation did not affect cholesterol accumulation in I1061T fibroblasts (Figure 3.11). Notably, we found a strikingly altered distribution of HA-FBXO2 following lysosomal damage. Prior to LLOMe treatment, HA-FBXO2 exhibited diffuse, cytoplasmic staining, similar to Gal3 (Figure 3.12A). After lysosomal damage, HA-FBXO2 became punctate and partially co-localized with Gal3, indicating recruitment to damaged lysosomes (Mander's coefficient = 0.80 (Ctrl), 0.81 (I1061T)) (Figure 3.12A).

Figure 3.11 Overexpression of HA FBXO2 does not affect cholesterol storage. I1061T patient fibroblasts were electroporated with HA FBXO2 and stained for filipin. Data are shown as mean ± s.e.m. from 3 independent experiments. Data are shown as mean ± s.e.m. n.s., not significant by t-test.

This recruitment of HA-FBXO2 to damaged lysosomes suggested that it may function in their clearance. Overexpressed FBXO6 and FBXO27 showed similar recruitment to Gal3 puncta after lysosomal damage (Figure 3.13), raising the possibility that functional differences among the FBA family of F-box proteins is determined, in part, by expression patterns, with Fbxo2 expression in the CNS being most prominent. Co-immunoprecipitation experiments after LLOMe treatment confirmed that HA-FBXO2 interacts with LAMP-2 and Skp1, demonstrating its interaction with damaged lysosomes in the SCF complex (Figure 3.12B). We also observed
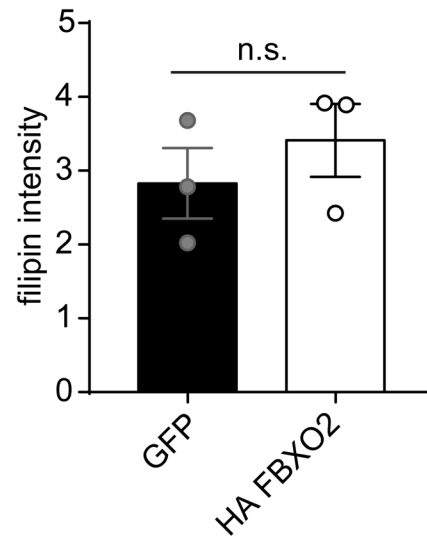
interaction of HA-FBXO2 with LAMP-2 and Skp1 following vehicle treatment (Figure 3.14),

consistent with prior co-immunoprecipitation experiments with FBXO2, FBXO6 and FBXO27

before and after lysosomal damage [10] and suggesting their recruitment to damaged lysosomes

even in the absence of treatment with a lysosomal damaging agent. With evidence that HA-

FBXO2 is recruited to damaged lysosomes in patient fibroblasts, we asked whether Fbxo2 plays

a role in lysophagy in the CNS. In primary cortical cultures transfected with HA-FBXO2, we

saw a similar transition from diffuse cytoplasmic to punctate staining in neurons after lysosomal

damage (Figure 3.12C) and partial co-localization with LAMP-1 (Figure 3.15), indicating

recruitment to damaged lysosomes.
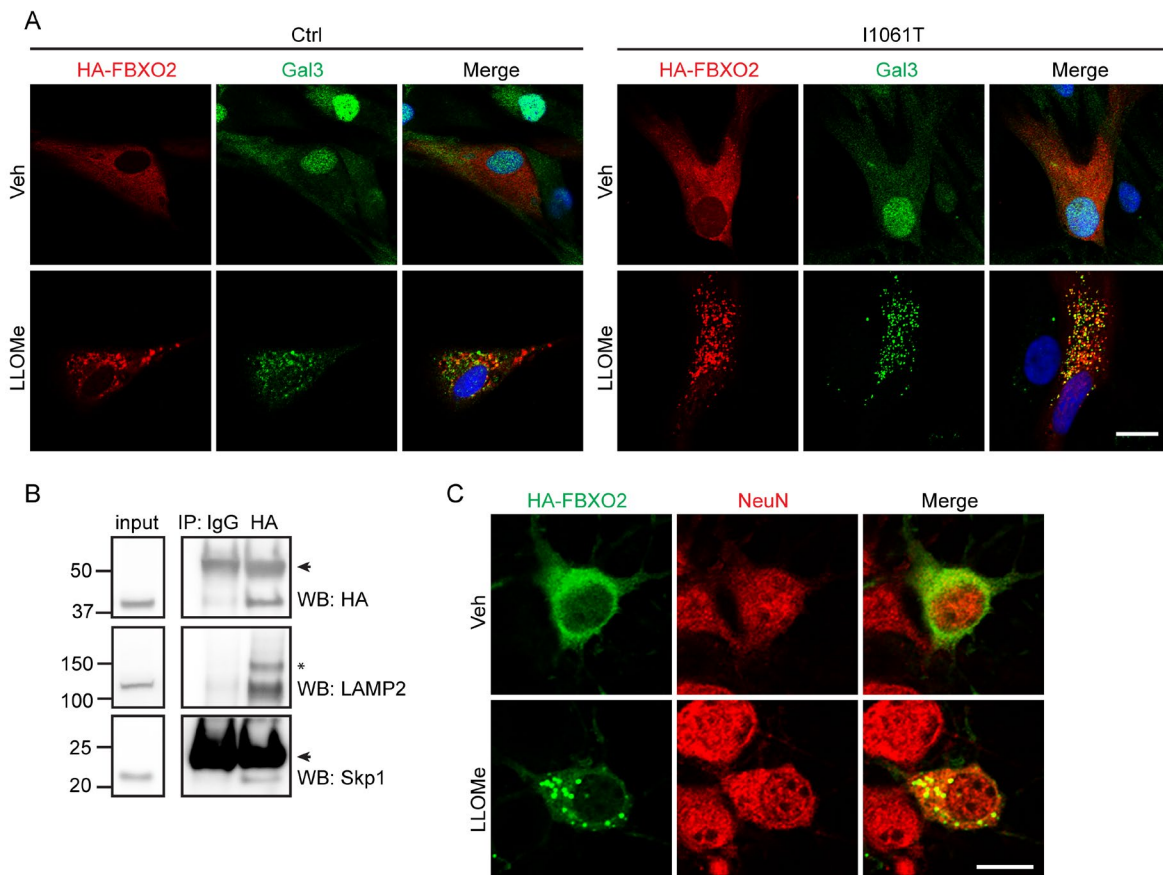

Figure 3.12 Fbxo2 localizes to damaged lysosomes. **(A)** Ctrl and I1061T patient fibroblasts were transfected with HA-FBXO2 and then treated with Veh or 1mM LLOMe for 1 hr and stained for HA and Gal3. Co-localization is indicated by yellow staining in merged image. Mander's coefficients: 0.80 (Ctrl) and 0.81 (I1061T) **(B)** I1061T patient fibroblasts were electroporated with

HA-FBXO2, and after 48hr treated with 2mM LLOMe for 2hr. Lysates were immunoprecipitated with either HA antibody or control IgG. Arrowheads at ~50kD and ~25kD indicate immunoglobulin heavy and light chains, respectively. Asterisk denotes a non-specific band detected by the LAMP2 antibody. **(C)** WT primary cortical cultures were transfected with HA-FBXO2 and treated with Veh or 2mM LLOMe for 1 hr on D9IV. Cell were stained for HA and NeuN, a neuronal marker.
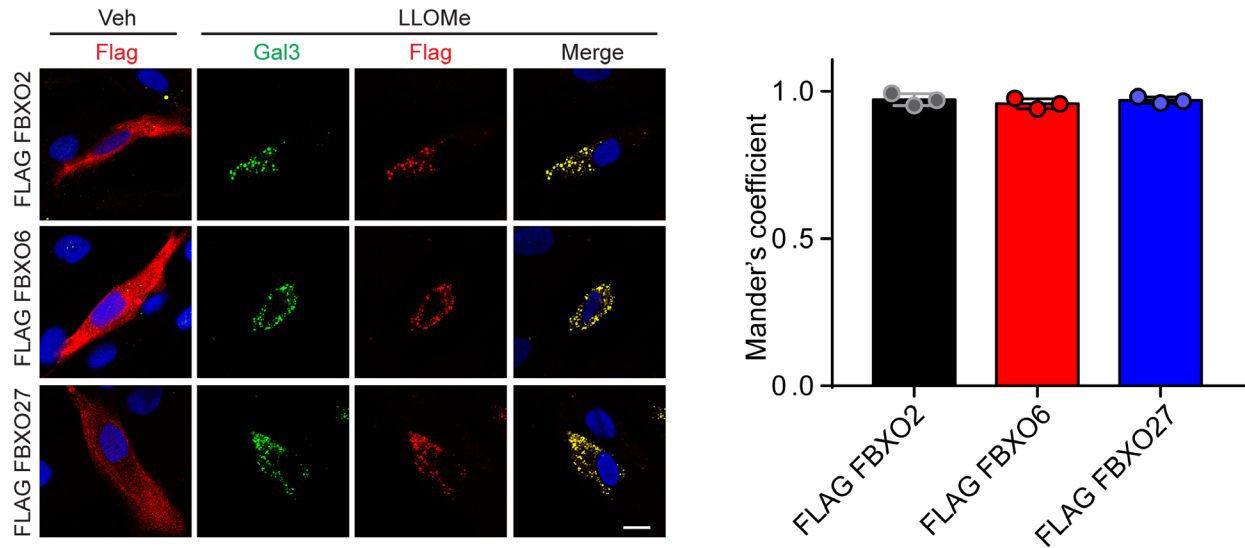

Figure 3.13 FLAG FBXO2, FBXO6 and FBXO27 show similar levels of recruitment to damaged lysosomes. I1061T patient fibroblasts were transfected with FLAG constructs, treated with 2mM LLOMe for 1hr and stained 2hrs after washout. Mander's coefficients for co-localization of Gal3 and Flag are shown at the right. Data are shown as mean ± s.e.m. from 3 independent experiments. Scale bar: 25μm

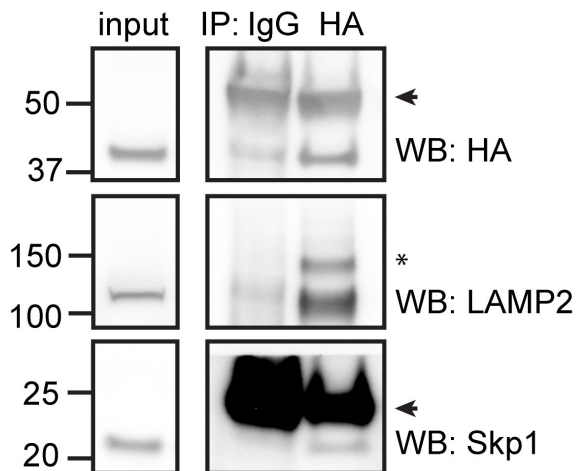***Figure 3.14 Co-immunoprecipitation shows interaction of HA-FBXO2 with Skp1 and LAMP2.*** I1061T patient fibroblasts were electroporated with HA-FBXO2, and after 48hr treated with vehicle for 2hr. Lysates were immunoprecipitated with either HA antibody or control IgG. Arrowheads at ~50kD and ~25kD indicate immunoglobulin heavy and light chains, respectively. Asterisk denotes a non-specific band detected by the LAMP2 antibody.
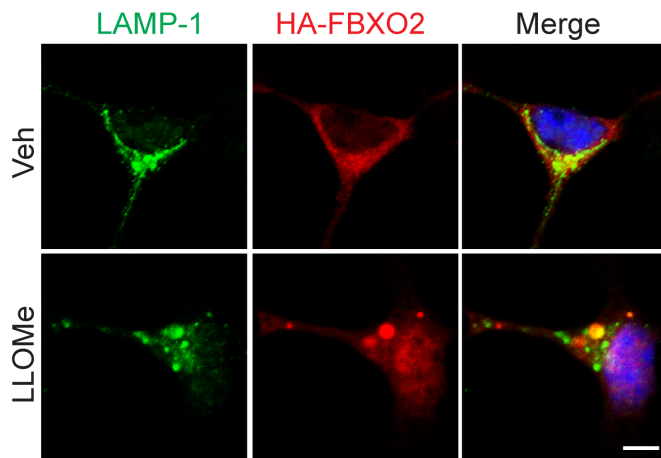
| LAMP-1 | HA-FBXO2 | Merge |

Figure 3.15 FBXO2 is recruited to damaged lysosome in primary cortical neurons. WT primary cortical cultures were transfected with HA-FBXO2 and treated with vehicle (Veh) or 2mM LLOMe for 1hr and stained after 2hrs. Scale bar:10μm

3.3.6 Fbxo2 plays a role in CNS lysophagy

To investigate a role for Fbxo2 in lysophagy in the brain, we established primary cortical cultures from WT and Fbxo2 deficient (Fbxo2-/-) mice [53]. qPCR demonstrated that Fbxo2 was the most highly expressed glycan binding F-box protein in WT primary cortical cultures and that there was no compensatory upregulation of Fbxo6 or Fbxo27 in response to Fbxo2 deficiency (Figure 3.16A). Notably, clearance of damaged lysosomes was significantly delayed in Fbox2-/- cultures. When we overexpressed Gal3 in WT and Fbxo2-/- primary cortical cultures, we found significantly slower clearance of Gal3 puncta in Fbxo2-/- cultures (Figure 3.16B). Further, by CHX chase assay (Figure 3.6A), the half-life of Gal3 was extended from ~30 min in WT cultures to ~105 min in Fbxo2-/- primary cortical cultures (Figure 3.16C). These data demonstrate delayed lysophagy progression and support a role for Fbxo2 in the clearance of damaged lysosomes. As lysosomal membrane damage releases luminal enzymes and can lead to cell death [2], we next compared cell viability in WT and Fbxo2-/- primary cortical cultures after lysosomal damage. When assessing toxicity 4 hrs after LLOMe treatment, we observed significantly decreased viability in Fbxo2-/- cultures compared to WT (Figure 3.16D), indicating increased cell death following lysosomal damage. Supporting on-target effects of LLOMe, this toxicity was rescued by preventing lysosomal damage with the cathepsin inhibitor E64D [54] (Figure 3.16E, Figure 3.17).
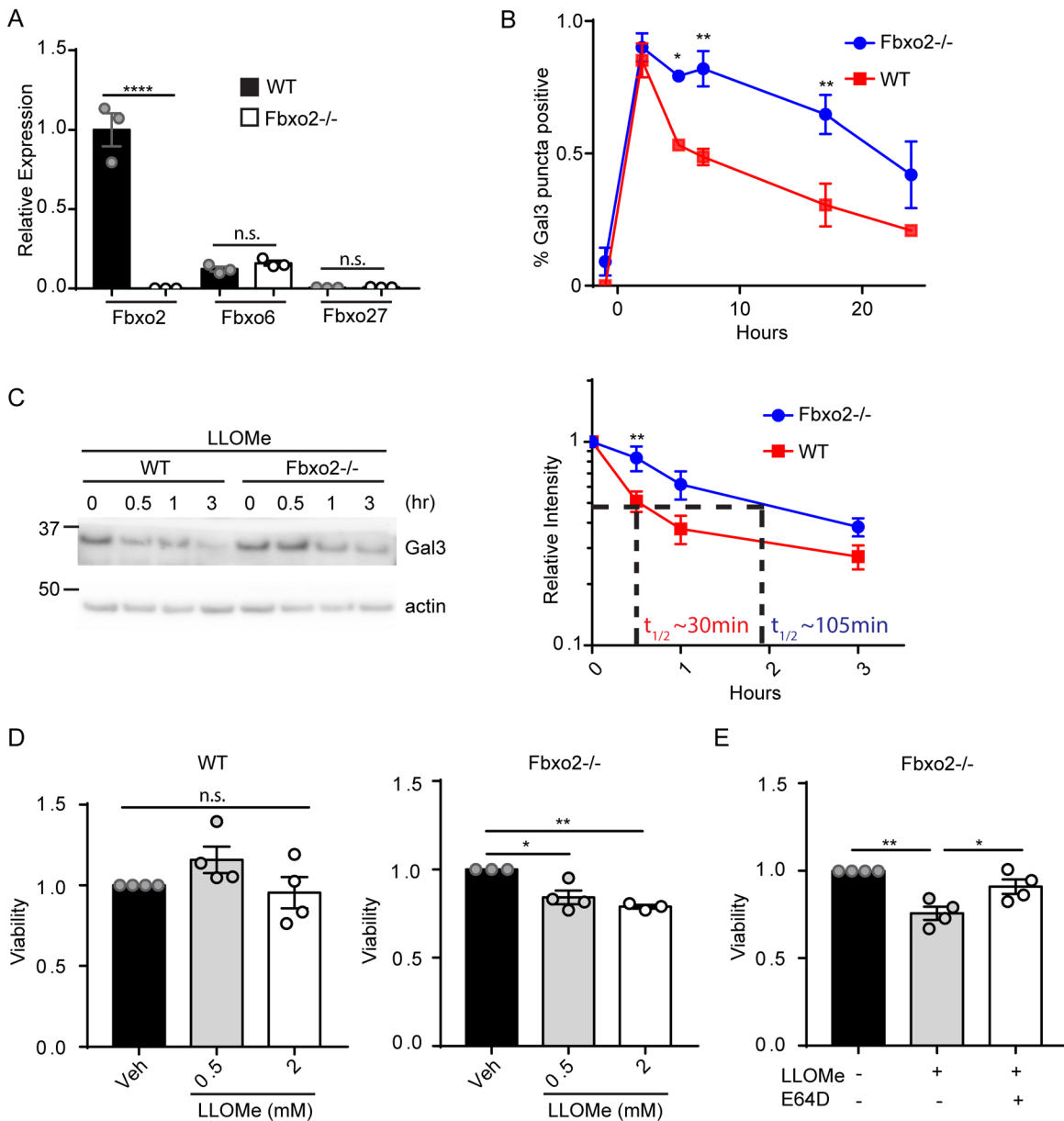
Figure 3.16 Fbxo2 mediates CNS lysophagy. **(A)** Relative expression of Fbxo2, Fbxo6 and Fbxo27 was determined in WT and Fbxo2-/- primary cortical cultures at D9IV by qPCR. **(B)** WT and Fbxo2-/- primary cortical cultures were transfected with EGFP-hGal3 on D4IV, treated with Veh or 2mM LLOMe for 1hr, and stained at various times after washout. Percentage of cells with Gal3+ puncta was quantified. **(C)** WT and Fbxo2-/- primary cortical cultures were treated on D9IV with 30µg/mL CHX and 2mM LLOMe for 1 hr and CHX treatment continued for indicated times before lysates were collected. Gal3 levels quantified at the right. **(D)** WT and Fbxo2-/- primary cortical cultures were treated with Veh or LLOMe (0.5 or 2 mM) for 1 hr and cell viability was determined by XTT assay 4 hrs after LLOMe washout. **(E)** Fbxo2-/- primary cortical cultures were pre-treated with Veh (-) or 100µM E64D for 30min, then treated with 2mM LLOMe for 1 hr and viability determined by XTT assay 4 hrs after LLOMe washout. Data are shown as mean ± s.e.m. from **(A, B, D)** 3, **(C)** 5 or **(E)** 4 independent experiments. n.s., not significant, *$P \leq 0.05$, **$P \leq 0.01$, ****$P \leq 0.0001$ by **(A, D-E)** one-way ANOVA with Tukey's multiple comparisons or **(B-C)** two-way ANOVA with Sidak's test. (**(A)** F=81.08, **(D)** F=23.2, **(E)** F=14.55).
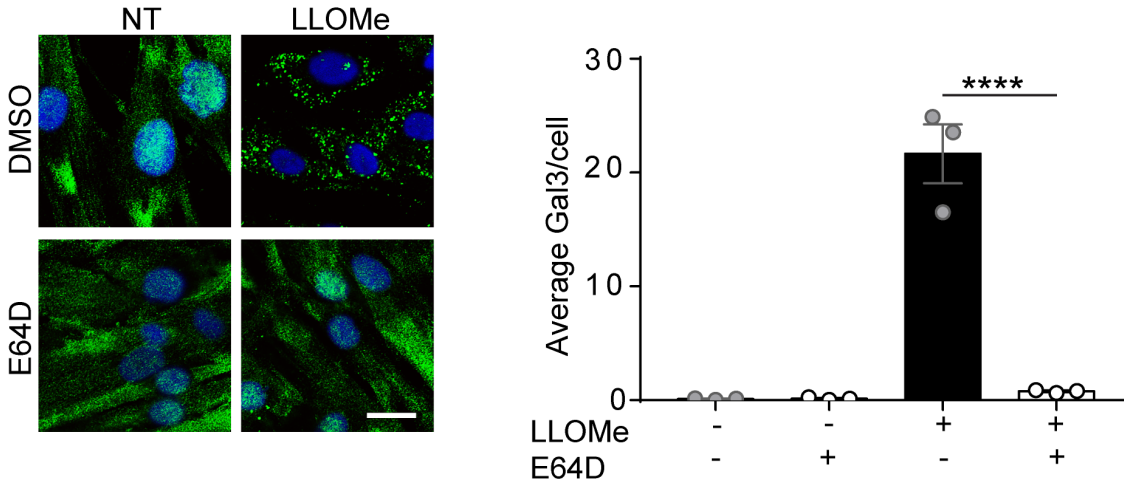
Figure 3.17 Pre-treatment with E64D prevents lysosomal damage. I1061T patient fibroblasts were treated with 100µM E64D for 30min, then treated with 2mM LLOMe for 1 hr and stained for Gal3. Gal3 puncta per cell quantified at the right. Data are shown as mean ± s.e.m. from 3 independent experiments. ****P≤0.0001 by one-way ANOVA with Tukey's multiple comparisons. F=67.39 Scale bar: 25µm

3.3.7 Loss of Fbxo2 exacerbates the Niemann-Pick C disease phenotype

As our analyses indicated the occurrence of increased susceptibility to lysosomal damage in NPC1 or NPC2 deficient cells, we sought to determine whether loss of Fbxo2 modified the disease phenotype in a mouse model of NPC disease. To accomplish this, we generated Npc1-I1061T mutant mice deficient in Fbxo2. Fbxo2 deficiency is well tolerated in mice, except for the occurrence of hearing loss [53]. Similarly, Fbxo2-/- mice were indistinguishable from WT littermates in our analyses (Figure 3.18). However, loss of Fbxo2 in Npc1-I1061T mice exacerbated deficits in motor function as quantified by performance on the balance beam (Figure 3.18A) and rotarod (Figure 3.18B) and significantly decreased survival (Figure 3.18C). Consistent with expression analysis in primary cortical cultures, loss of Fbxo2 did not lead to compensatory upregulation of Fbxo6 or Fbxo27 in the mouse brain (Figure 3.18D). Fbxo2 deficient mice also had similar expression levels of the SCF component Cul1 and a slight increase in expression of Rbx1 (Figure 3.19).
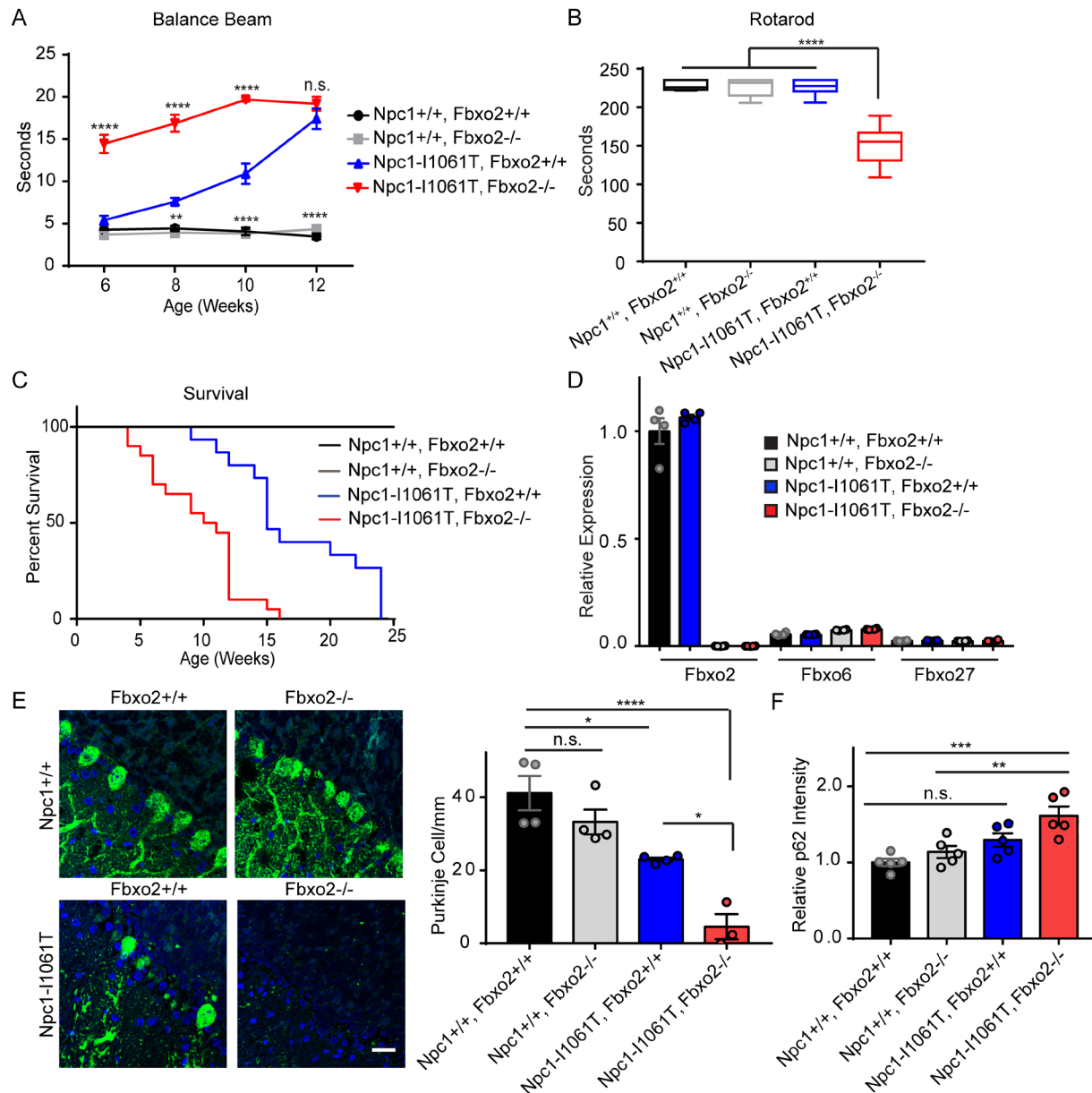
Figure 3.18 Loss of Fbxo2 exacerbates the Niemann-Pick C disease phenotype. **(A)** Age-dependent performance on balance beam. Mice were trained at 5 wks and run every other week starting at 6 wks. The average of 3 trials was taken and max time was set at 20 s. N=5 males and 5 females per genotype. **(B)** Performance on accelerating rotarod from 4-40 rpm at 9 wks. N=5 males and 5 females per genotype. **(C)** Kaplan-Meyer survival curves. N=6-10 males and 6-10 females per genotype. **(D)** Relative expression of Fbxo2, Fbxo6 and Fbxo27 was determined by qPCR in 8 wk brainstem. N=4 mice per genotype. **(E)** Quantification of Purkinje cell density in lobules IV and V of midline cerebellar sections. N=3-4 mice per genotype. **(F)** The relative abundance of p62 in brainstem from 8 wk mice was determined by western blot. N=5 mice per genotype. Data are shown as mean ± s.e.m. n.s., not significant, *P ≤ 0.05, **P ≤ 0.01, ***P ≤ 0.001, ****P ≤ 0.0001 by **(A)** two-way ANOVA, **(B,E,F)** one-way ANOVA or **(C)** Log-rank (Mantal-Cox) test and Gehan-Breslow-Wilcoxon test with **(A,E)** Bonferroni or **(B, F)** Tukey's multiple comparisons (**(A)** F=26.88, **(B)** F=63.59, **(E)** F=19.49, **(F)** F=11.64). Scale bar: 25μm

Exacerbation of motor phenotypes prompted us to examine changes in neuropathology.

We focused our analysis on Purkinje neurons, the major output neurons of the cerebellar folia,

71

which degenerate in Niemann-Pick C brain [19,55] and whose loss is sufficient to trigger motor impairment [56]. Npc1-I1061T mice deficient in Fbxo2 exhibited significantly increased Purkinje cell loss, correlating with their exacerbated motor phenotypes (Figure 3.18E). In contrast, Fbxo2 deficiency alone did not alter Purkinje cell density. Furthermore, brain tissue from Npc1-I1061T, Fbxo2-/- mice showed enhanced accumulation of p62 protein (Figure 3.18F, Figure 3.20A) without upregulation of p62 mRNA (Figure 3.20B), similar to findings in cell culture after lysosomal damage [14]. Taken together, these data indicate that loss of Fbxo2 in Niemann-Pick C mice exacerbates behavioral phenotypes and neurodegeneration while altering markers of autophagy.

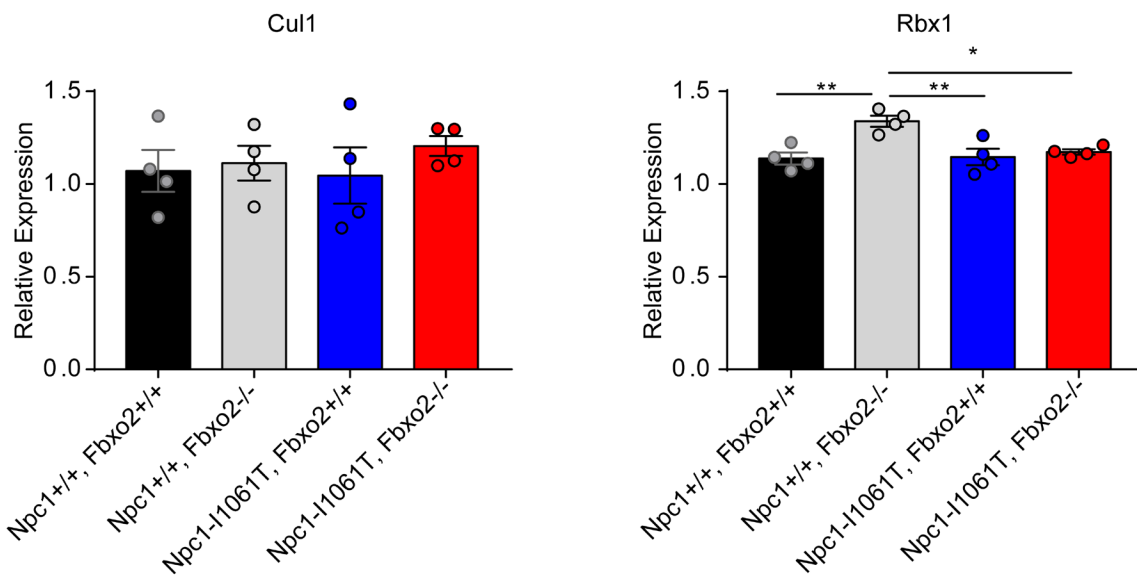

Figure 3.19 Expression of SCF components in Fbxo2-/- mice. Relative expression of Cul1 and Rbx1 was determined by qPCR in 8wk brainstem. N=4 mice per genotype. Data are shown as mean ± s.e.m. *P ≤ 0.05, **P ≤ 0.01 by one-way ANOVA
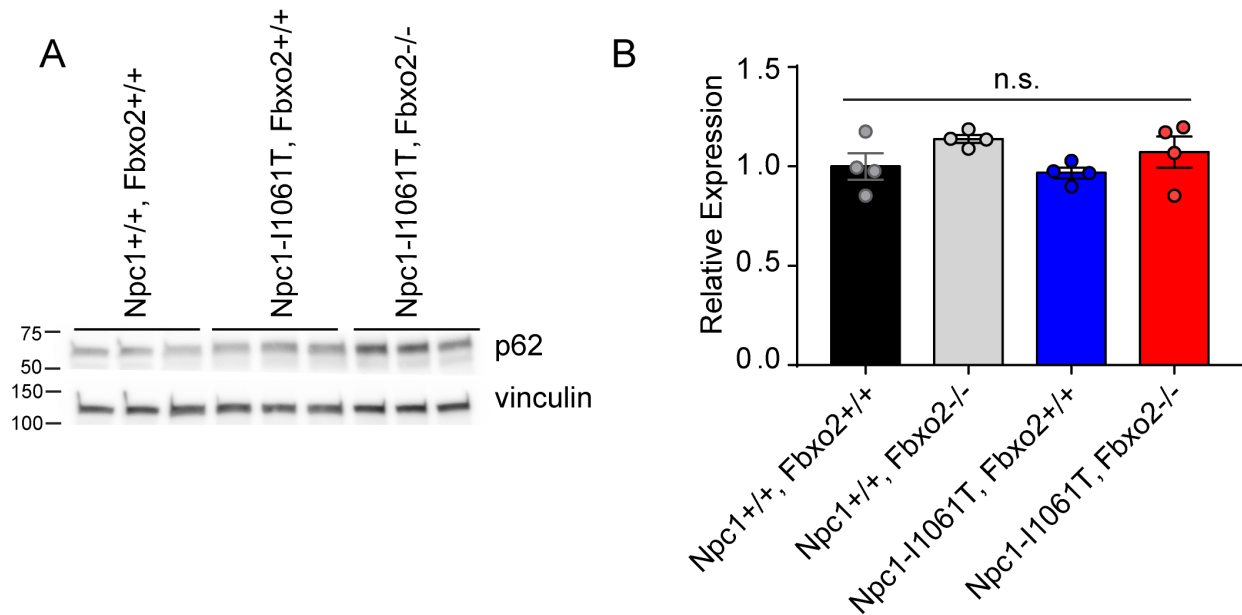
Figure 3.20 p62 protein levels are increased in Npc1-I1061T, Fbxo2-/- mice without changes in gene expression. Brainstem was collected from 8 wk mice and p62 levels were analyzed by **(A)** western blot or **(B)** qPCR. N=4 mic per genotype. Data are shown as mean ± s.e.m. n.s., not significant by one-way ANOVA.

3.4 Discussion

In this study, we describe a novel role for Fbxo2 in CNS lysophagy and demonstrate the importance of lysophagy as a key compensatory pathway in Niemann-Pick C knock-in mice. We show that Niemann-Pick C patient fibroblasts are more sensitive to lysosomal damage by LLOMe and that this occurs in the context of functioning lysophagy (Figures 3.1, 3.2, 3.4, 3.6). Our data suggest that the primary driver of increased sensitivity to lysosomal damage is a factor intrinsic to the lysosome that affects membrane stability. Increased oxidative stress has been posited as a contributor to LMP in Niemann-Pick C [19], but it is likely that additional factors also function in this context. We now show that lipid storage, independent of loss of the NPC1 protein, contributes to increased sensitivity to lysosomal damage (Figure 3.4). Consistent with this finding, studies have demonstrated that lipids including accumulated sphingomyelin [16,17,41] and cholesterol [39,40] induce lysosomal damage. As diverse storage materials in Gaucher disease [13]

and late-infantile neuronal ceroid lipofuscinosis [14] also contribute to lysosomal damage, LMP is likely the consequence of aberrant accumulations within lysosomes. In contrast, studies have also described the importance of lipids in membrane rigidity and lysosomal membrane stability [57-59]. Notably, the absence of functional NPC1 protein is expected to impair the movement of luminal cholesterol into the limiting membrane of the lysosome. Defining the role of altered luminal versus lysosomal membrane lipid composition and their effects on lysosomal membrane stability will be important in furthering our understanding of lysosomal dysfunction in Niemann-Pick C. Additionally, as some of our studies were conducted in patient fibroblasts, we acknowledge that these cells may not fully mirror events in neurons in a complex disorder like Niemann-Pick C disease, and further work on LMP in NPC neurons will be of importance.

Lysophagy is a critical response to LMP, and we show that of the FBA family of glycoprotein binding F-box proteins, Fbxo2 is most highly expressed in the brain (Figure 3.9) and is recruited to damaged lysosomes (Figure 3.12). Supporting its function in lysophagy, loss of Fbxo2 in primary cortical cultures delays clearance of damaged lysosomes and leads to decreased viability after lysosomal damage (Figure 3.16). This finding is consistent with work on the glycan binding F-box protein Fbxo27, where Fbxo27 deficiency slows but does not abolish lysophagy [10]. Likely, additional pathways function to mediate lysophagy in the brain. TRIM16, a RING-type ubiquitin ligase, has also been shown to mediate lysophagy progression [5] and may function redundantly with Fbxo2.

Supporting the function of Fbxo2 in lysophagy, Niemann-Pick C mice deficient in Fbxo2 exhibit exacerbated disease phenotypes, with significantly worse impairments in motor function and decreased survival (Figure 3.18). This correlates with increased loss of Purkinje cells and an increase in the autophagic adapter protein p62 (Figure 3.18). These findings support a model

74

wherein impairing lysophagy in a background of increased lysosomal damage exacerbates the disease phenotype. The characterization of Fbxo2 as a component of the machinery that regulates efficient lysophagy in the CNS is intriguing, as it demonstrates specificity of the mediators of this process. Among CNS cell types, RNA-seq datasets demonstrate broad expression of Fbxo2 in neurons and glia [51]. Loss of functional Npc1 in mouse neurons and oligodendrocytes, but not astrocytes, has been shown to contribute to Niemann-Pick C neuropathology [30,48,56,60]. As such, it is possible the Fbxo2 functions in multiple cell types to maintain efficient lysophagy and promote CNS homeostasis.

Collectively, our data describe a novel function for Fbxo2 in lysophagy and establish its proof-of-concept disease relevance in compensating for Niemann-Pick C pathophysiology. Our findings suggest that strategies aimed at targeting the lysosomal cell death pathway and enhancing lysophagy function may be protective against neurodegeneration in Niemann-Pick C. Furthermore, additional studies to probe the function of Fbxo2 will continue to advance our understanding of mechanisms involved in protein and organellar quality control pathways that likely contribute to the neuropathology in a diverse array of lysosomal diseases.

3.5 Methods

Antibodies

Primary antibodies (antigen, dilution, vendor): galectin-3, 1:100 (IF), 1:500 (WB), Santa Cruz Biotechnology Inc. sc-20157 (discontinued); galectin-3, 1:100, Santa Cruz Biotechnology Inc. sc-23938; LAMP-1, 1:100 (IF), DSHB at the University of Iowa H4A3; LAMP-2, 1:10 (IF), DSHB at the University of Iowa ABL-93; LC3B, 1:500 (IF), 1:1000 (WB) Novus Biologicals NB600-1384; LAMP-1, 1:1000, abcam ab24170; Calbindin-D-28K, 1:500, Sigma-Aldrich

C2724; HA.11, 1:500, BioLegend 901501; NeuN, 1:500, Sigma-Aldrich ABN90; β-Actin, 1:2000, Sigma-Aldrich A5441; Vinculin, 1:2000, Sigma-Aldrich V9131, p62, 1:1000, Sigma-Aldrich P0067; Skp1, 1:1000, BD 610530; LAMP2, 1:100 (WB), abcam ab25631; FBXO2, 1:100, Santa Cruz Biotechnology Inc. sc-393873; FLAG, 1:500, Sigma-Aldrich F1804

The following secondary antibodies (dilution, antibody, and vendor) were used: Alexa Fluor 488 goat anti–rabbit IgG (H+L) (1:500, A11008, Invitrogen); Alexa Fluor 495 Fab'2 fragment of goat anti–mouse IgG (H+L) (1:500, A11020, Invitrogen); Alexa Fluor 488 goat anti–mouse IgG (H+L) (1:500, A11029, Invitrogen); Alexa Fluor 594 goat anti–guinea pig IgG (H+L) (1:500, A11076, Invitrogen); Goat anti–mouse IgG (H+L)-HRP conjugate (1:2000, Bio-Rad 170-6516); Alexa Fluor 488 goat anti–rat IgG (H+L) (1:500, A11006, Invitrogen); and goat anti–rabbit IgG (H+L)-HRP conjugate (1:2000, Bio-Rad 170-6515).

Reagents

The following drugs and small molecules were used: MLN7243 (CT-M7243, Chemietek); Leu-Leu methyl ester hydrobromide (L7393, Sigma-Aldrich); Cycloheximide (C7698, Sigma-Aldrich); E-64d (13533, Cayman); 2-hydroxypropyl-beta-cyclodextrin (H-107, Sigma-Aldrich); vinblastine sulfate salt (cat. V1377, Sigma); filipin (F9765, Sigma). Plasmid encoding HA-FBXO2 was from Dr. Henry Paulson (University of Michigan, Ann Arbor). Plasmids encoding FLAG-FBXO2, FLAG-FBXO6 and FLAG-FBXO27 were from Dr. Yukiko Yoshida (Tokyo Metropolitan Institute of Medical Science, Tokyo, Japan). Plasmid encoding EGFP-hGal3 was from addgene (#73080).

Cells

The following cell lines were obtained from the NIGMS Human Genetic Cell Repository at the Coriell Institute for Medical Research: GM08399 (Ctrl), GM18453 (I1061T/I1061T), and GM18429 (NPC2-1), GM18455 (NPC2-2). Fibroblasts were cultured in MEM (Gibco 10370), PSG (Gibco), and 20% premium FBS (Atlanta Biologicals). WT and Atg5-/- MEF cell lines RCB2710 and RCB2711 were obtained from the RIKEN BRC Cell Bank and were cultured in MEM (Gibco 10370), PSG (Gibco), and 20% premium FBS (Atlanta Biologicals).

Mice

Npc1-I1061T mice [36] were a gift from Daniel Ory (Washington University in St Louis) and backcrossed to C57BL/6 (≥10 generations). Fbxo2-/- mice [53] were a gift from Henry Paulson (University of Michigan, Ann Arbor) and on the C57BL/6 background.

Western blot

Cell culture media was aspirated, cells were washed 1x with ice cold PBS, then cells were removed with a cell scraper and centrifuged at 1000xg for 5 min at 4°C. The cell pellet was resuspended in RIPA (Teknova) with complete protease inhibitor (Thermo Scientific 11836153001) and 0.625mg/ml N-ethylmaleimide (Sigma E3876) and sonicated. For primary cortical cultures, lysates were centrifuged at 12,000xg for 10min at 4°C and the supernatant was collected. For tissue preparation, mice were perfused with saline before tissue was collected and flash frozen in liquid nitrogen. Tissue was homogenized and sonicated in RIPA buffer. Protein concentrations were determined by DC™-protein assay (Bio-Rad) and normalized. Proteins were separated on NuPAGE™ 4-12% Bis-Tris Protein Gels (Thermo Scientific NP0336BOX) and

transferred to Immobilon-P 0.45um PVDF (Merck Millipore). Immunoreactivity was detected with ECL (Thermo Scientific) or SuperSignal™ West Pico PLUS Chemiluminscent Substrate (Thermo Scientific) and an iBright (Thermo Fisher Scientific). Quantification was performed using Image Studio. Band intensity was normalized to the indicated loading control.

RT-qPCR

RNA was collected using TRIzol® (Thermo Fisher) according to manufacturer's instructions and converted to cDNA using the High Capacity Reverse Transcription kit (Applied Biosystems 4368814). Quantitative real-time PCR was performed using 10ng cDNA, FastStart Taqman Probe Master Mix (Roche), and gene-specific FAM-labeled TaqMan probes (Thermo Scientific) for mouse Fbxo2 (Mm00805188), Fbxo6 (Mm01257500), Fbxo27 (Mm01179110), Sqstm1 (Mm0044809), Rbx1 (Mm01705487), and Cul1 (Mm00516318). Gene expression was normalized to mouse Cpsf2-Vic (Mm00489754) multiplexed within the same well. RT-qPCR was performed using an ABI 7900HT Sequence Detection System and relative expression calculated by the $2^{(-\Delta\Delta Ct)}$ method.

Transfection

Human patient fibroblasts: Cells were transfected with Lipofectamine® LTX with Plus™ Reagent (Invitrogen). Briefly, 320ng of endotoxin-free plasmid was incubated in 43uL opti-MEM (Gibco) and .425uL PLUS reagent for 5 min. Separately, 43uL opti-MEM was incubated with 1.28uL LTX reagent for 5 min. Then, the LTX mixture was added to the plasmid mixture and incubated for 30 min before adding dropwise to cells.

Mouse primary cortical cultures: Cells were transfected on D2-4IV with Lipofectamine 2000 (Invitrogen). Briefly, cells were washed 2x with Neurobasal™-A Medium (Gibco). 200ng of endotoxin-free plasmid was incubated with 50uL opti-MEM (Gibco) for 5min. Separately, 50uL opti-MEM and 1uL Lipofectamine 2000 was incubated for 5min. After 5min, the Lipofectamine mixture was added to the plasmid mixture and incubated 20 min before adding dropwise to cells. Transfection mixture was kept on cells for 20 min before removing, and cells were washed 2x in Neurobasal™-A Medium (Gibco).

Immunofluorescence staining

Cells were washed 3x with HBSS and fixed with ice cold 100% methanol for 20min at -20°C. Cells were washed 3x with PBS and placed in 2.5mg/ml glycine for 10 min at room temperature. Cells were washed 3X with PBS, permeabilized with 0.1% Triton in PBS for 20min, then placed in blocking solution (10% goat serum, 1% BSA in PBS) for 1 hr. Cells were incubated with primary antibodies diluted in blocking solution overnight at 4°C. The next day, slides were washed 3x with PBS and incubated with secondary antibody diluted in blocking solution for 1 hr at room temperature. Slides were washed 3x with PBS and mounted with Vectashield + DAPI (Vector Laboratories). For LAMP-1 staining, after glycine incubation, cells were placed in saponin blocking solution (0.02% saponin, 5% NGS, 1% BSA) for 1 hr and then incubated with primary antibody diluted in saponin blocking solution overnight at 4°C. Slides were washed with PBS + 0.02% saponin and incubated with secondary antibody diluted in saponin blocking solution, washed and mounted.

For tissue preparation, mice were perfused with saline and 4% PFA and tissue was removed and post-fixed in 4% PFA overnight at 4°C prior to paraffin embedding. Paraffin-embedded tissues were cut on a Reichert-Jung 2030 microtome into 5μm sections and placed on Fisher Scientific Superfrost Plus microscope slides. Sections were adhered onto slides in an oven at 55-60°C for 1 hr. Samples were deparaffinized and antigen retrieval was performed by boiling in 10mM sodium citrate (pH 6.0) for 10 min and incubating in hot citrate solution for an additional 20 min, then washed 3x in deionized water. For staining, slides were incubated in a solution with 0.1% Triton, 10% goat serum and 1% BSA in PBS for 20 min. Then, slides were placed in blocking solution (10% goat serum, 1% BSA in PBS) before incubating in primary antibody diluted in blocking solution overnight at 4°C. Slides were washed 3x in PBS and incubated for 1 hr with secondary antibody diluted in blocking solution. Slides were then washed 3x in PBS and mounted with Vectashield + DAPI (Vector Laboratories).

Filipin staining

Cells were stained following the immunofluorescence protocol described above, with the exception of being fixed in 4% PFA. After the secondary antibody incubation, cells were washed and incubated with 1mL filipin staining solution (5% FBS + 40uL filipin solution (1mg filipin + 40uL DMSO) in PBS) for 2 hr at room temperature. Cells were washed 3x in PBS and slides were mounted with ProLong® Gold (Thermo Fisher).

Primary cortical cultures

Cortices were dissected using the Papain Dissociation System (Worthington) from P0-P1 WT or Fbxo2-/- pups. Briefly, cortices were dissected free of meninges, placed in papain solution and

incubated at 37°C for 20 min. Cortices were triturated 15x with a 10mL pipette tip and spun at 30.9 xg for 5 min. Cells were resuspended and spun over a discontinuous density gradient at 22 xg for 5 min. Cells were then resuspended in Neurobasal™-A Medium (Gibco) with B-27™ Supplement (Gibco), GlutaMAX™ (Gibco) and Pen Strep, counted and plated. Media was changed every 3 days.

Cell Survival

The XTT assay (ATCC) was used to assess cell survival according to manufacturer's protocol. Briefly, 50μL of XTT solution was added to 100μL of cell culture media for 4 hrs in a CO_2 incubator at 37°C. Plates were read on a Synergy HTX multimode plate reader (BioTek) at 475 and 660nm.

Neon^{TM} Transfection System

Cells were transfected by Neon^{TM} Transfection System (Thermo Fisher) according to manufacturer's protocol. Briefly, cells were counted and resuspended in DPBS (Gibco) along with plasmid DNA. Cell culture plates were pre-incubated with culture medium without antibiotics. Neon® Tube was set up with 3mL Electrolytic Buffer E2 and the 100μL Neon® Tip was used at 1200V, 40ms, 1 pulse.

Co-Immunoprecipitation

Cells were washed in PBS and cross-linked with DSP (Thermo 22585) for 30 min at RT. Tris-HCl pH 7.5 was added to a final concentration of 20mM and cells were incubated on a rotator for 15 min at 4°C. Cells were centrifuged for 5 min at 1000g and resuspended in lysis buffer (.025M

Tris, 0.15M NaCl, 0.001M EDTA, 1% NP-40, 5% glycerol; pH 7.4) with complete protease inhibitor (Thermo Scientific 11836153001). Lysates were pre-cleared with protein A/G beads for 30 min at 4°C. Beads were pelleted at 1000g for 1 min and lysates were incubated with HA (BioLegend) antibody or control IgG on a rotator overnight at 4°C. Protein A/G beads were then added and lysates tumbled at 4°C for 1 hr. Beads were placed into spin columns (Pierce) and washed 6 times in lysis buffer. Finally, beads were boiled at 95°C for 5 min in 6X loading buffer and loaded on NuPAGE 4-12% 10 well gels (Invitrogen).

Microscopy

Confocal images were collected using a Nikon A-1 confocal with diode-based laser system. Co-localization and puncta quantification were determined using CellProfiler Analyst Software. For Gal3 puncta quantification, 100-200 cells per experiment were examined.

Phenotype analysis

Balance beam: The balance beam consists of a 5mm wide square beam suspended at 50cm. Mice were trained at 5 wks of age to cross the beam and then tested every other week starting at 6 wks. For testing, mice were run 3 times across the beam, and the average time was taken. Maximum time was set at 20 sec and falls were scored as 20 sec.

Rotarod: After acclimating to the testing room for 30 min, mice were gently placed on a moving (4 RPM) rotarod for 30 sec. Then, over a period of 235 sec, rotarod speed was increased to 40 RPM. The trial ended if mice stopped walking for two revolutions or dropped onto the paddle. Mice were trained three times per day with a 30 min interval between each training session over

a period of 3 days. The following week, mice were tested on a single day using the training protocol.

Survival: All deaths were recorded. Mice that lost >20% maximal body weight were euthanized and recorded as deaths.

Purkinje Cell Quantification

Quantification of Purkinje cells was performed as described previously [19]. Briefly, midline sagittal sections were stained with calbindin to identify Purkinje cells. The number of cells was normalized to the length of the Purkinje layer as measured by NIH ImageJ software.

Vinblastine treatment

Mice were injected with vinblastine (0.04mg/g) I.P. at 7 weeks of age as previously described [37]. Liver was collected 2 hr post-injection and processed for immunofluorescence staining.

Statistics

Graphpad Prism 7.0 was used to determine significance (P<0.05), F (F-statistic) and t (T-statistic) values. Unpaired Student's t-test (two-tailed) and one-way or two-way ANOVA were used as indicated in the figure legends. A P value less than 0.05 was considered significant. All error bars are s.e.m.

Study Approval

All procedures involving mice were approved by the University of Michigan Committee on Use and Care of Animals (PRO00008133) and conducted in accordance with institutional and federal guidelines.

Author Contributions

EAL and APL conceptualized the study. EAL and MS provided methodology. EAL, MS, CM, and CC provided investigation. HP obtained resources. EAL and APL wrote the original draft. MS, CM, CC, and HP wrote, reviewed, and edited the manuscript. EAL, MS, and APL visualized data. APL supervised the study and acquired funding.

3.6 Acknowledgements

References

1   Settembre, C., Fraldi, A., Medina, D. L. & Ballabio, A. Signals from the lysosome: a control centre for cellular clearance and energy metabolism. *Nat Rev Mol Cell Biol* **14**, 283-296, doi:10.1038/nrm3565 (2013).

2   Papadopoulos, C. & Meyer, H. Detection and Clearance of Damaged Lysosomes by the Endo-Lysosomal Damage Response and Lysophagy. *Curr Biol* **27**, R1330-R1341, doi:10.1016/j.cub.2017.11.012 (2017).

3   Serrano-Puebla, A. & Boya, P. Lysosomal membrane permeabilization in cell death: new evidence and implications for health and disease. *Ann N Y Acad Sci* **1371**, 30-44, doi:10.1111/nyas.12966 (2016).

4   Aits, S. *et al.* Sensitive detection of lysosomal membrane permeabilization by lysosomal galectin puncta assay. *Autophagy* **11**, 1408-1424, doi:10.1080/15548627.2015.1063871 (2015).

5   Chauhan, S. *et al.* TRIMs and Galectins Globally Cooperate and TRIM16 and Galectin-3 Co-direct Autophagy in Endomembrane Damage Homeostasis. *Dev Cell* **39**, 13-27, doi:10.1016/j.devcel.2016.08.003 (2016).

6   Paz, I. *et al.* Galectin-3, a marker for vacuole lysis by invasive pathogens. *Cell Microbiol* **12**, 530-544, doi:10.1111/j.1462-5822.2009.01415.x (2010).

7   Thurston, T. L., Wandel, M. P., von Muhlinen, N., Foeglein, A. & Randow, F. Galectin 8 targets damaged vesicles for autophagy to defend cells against bacterial invasion. *Nature* **482**, 414-418, doi:10.1038/nature10744 (2012).

8   Hung, Y. H., Chen, L. M., Yang, J. Y. & Yang, W. Y. Spatiotemporally controlled induction of autophagy-mediated lysosome turnover. *Nat Commun* **4**, 2111, doi:10.1038/ncomms3111 (2013).

9   Huett, A. *et al.* The LRR and RING domain protein LRSAM1 is an E3 ligase crucial for ubiquitin-dependent autophagy of intracellular Salmonella Typhimurium. *Cell Host Microbe* **12**, 778-790, doi:10.1016/j.chom.2012.10.019 (2012).

10   Yoshida, Y. *et al.* Ubiquitination of exposed glycoproteins by SCF(FBXO27) directs damaged lysosomes for autophagy. *Proc Natl Acad Sci U S A* **114**, 8574-8579, doi:10.1073/pnas.1702615114 (2017).

11   Pentchev, P. G. *et al.* A defect in cholesterol esterification in Niemann-Pick disease (type C) patients. *Proc Natl Acad Sci U S A* **82**, 8247-8251, doi:10.1073/pnas.82.23.8247 (1985).

12   Platt, F. M., d'Azzo, A., Davidson, B. L., Neufeld, E. F. & Tifft, C. J. Lysosomal storage diseases. *Nat Rev Dis Primers* **4**, 27, doi:10.1038/s41572-018-0025-4 (2018).

13   Vitner, E. B. *et al.* Altered expression and distribution of cathepsins in neuronopathic forms of Gaucher disease and in other sphingolipidoses. *Hum Mol Genet* **19**, 3583-3590, doi:10.1093/hmg/ddq273 (2010).

14   Micsenyi, M. C., Sikora, J., Stephney, G., Dobrenis, K. & Walkley, S. U. Lysosomal membrane permeability stimulates protein aggregate formation in neurons of a lysosomal disease. *J Neurosci* **33**, 10815-10827, doi:10.1523/JNEUROSCI.0987-13.2013 (2013).

15   Gabande-Rodriguez, E., Boya, P., Labrador, V., Dotti, C. G. & Ledesma, M. D. High sphingomyelin levels induce lysosomal damage and autophagy dysfunction in Niemann Pick disease type A. *Cell Death Differ* **21**, 864-875, doi:10.1038/cdd.2014.4 (2014).

16   Gabande-Rodriguez, E. *et al.* Lipid-induced lysosomal damage after demyelination corrupts microglia protective function in lysosomal storage disorders. *EMBO J* **38**, doi:10.15252/embj.201899553 (2019).

17   Kirkegaard, T. *et al.* Hsp70 stabilizes lysosomes and reverts Niemann-Pick disease-associated lysosomal pathology. *Nature* **463**, 549-553, doi:10.1038/nature08710 (2010).

18   Amritraj, A. *et al.* Increased activity and altered subcellular distribution of lysosomal enzymes determine neuronal vulnerability in Niemann-Pick type C1-deficient mice. *Am J Pathol* **175**, 2540-2556, doi:10.2353/ajpath.2009.081096 (2009).

19   Chung, C., Puthanveetil, P., Ory, D. S. & Lieberman, A. P. Genetic and pharmacological evidence implicates cathepsins in Niemann-Pick C cerebellar degeneration. *Hum Mol Genet* **25**, 1434-1446, doi:10.1093/hmg/ddw025 (2016).

20   Vanier, M. T. & Millat, G. Niemann-Pick disease type C. *Clin Genet* **64**, 269-281 (2003).

21   Carstea, E. D. *et al.* Niemann-Pick C1 disease gene: homology to mediators of cholesterol homeostasis. *Science* **277**, 228-231 (1997).

22 Naureckiene, S. *et al.* Identification of HE1 as the second gene of Niemann-Pick C disease. *Science* **290**, 2298-2301, doi:10.1126/science.290.5500.2298 (2000).

23 Infante, R. E. *et al.* NPC2 facilitates bidirectional transfer of cholesterol between NPC1 and lipid bilayers, a step in cholesterol egress from lysosomes. *Proc Natl Acad Sci U S A* **105**, 15287-15292, doi:10.1073/pnas.0807328105 (2008).

24 Vanier, M. T. Niemann-Pick disease type C. *Orphanet J Rare Dis* **5**, 16, doi:10.1186/1750-1172-5-16 (2010).

25 Maejima, I. *et al.* Autophagy sequesters damaged lysosomes to control lysosomal biogenesis and kidney injury. *EMBO J* **32**, 2336-2347, doi:10.1038/emboj.2013.171 (2013).

26 Thiele, D. L. & Lipsky, P. E. Mechanism of L-leucyl-L-leucine methyl ester-mediated killing of cytotoxic lymphocytes: dependence on a lysosomal thiol protease, dipeptidyl peptidase I, that is enriched in these cells. *Proc Natl Acad Sci U S A* **87**, 83-87 (1990).

27 Platt, F. M. & Lachmann, R. H. Treating lysosomal storage disorders: current practice and future prospects. *Biochim Biophys Acta* **1793**, 737-745, doi:10.1016/j.bbamcr.2008.08.009 (2009).

28 Papadopoulos, C. *et al.* VCP/p97 cooperates with YOD1, UBXD1 and PLAA to drive clearance of ruptured lysosomes by autophagy. *EMBO J* **36**, 135-150, doi:10.15252/embj.201695148 (2017).

29 Sarkar, S. *et al.* Impaired autophagy in the lipid-storage disorder Niemann-Pick type C1 disease. *Cell Rep* **5**, 1302-1315, doi:10.1016/j.celrep.2013.10.042 (2013).

30 Ko, D. C. *et al.* Cell-autonomous death of cerebellar purkinje neurons with autophagy in Niemann-Pick type C disease. *PLoS Genet* **1**, 81-95, doi:10.1371/journal.pgen.0010007 (2005).

31 Liao, G. *et al.* Cholesterol accumulation is associated with lysosomal dysfunction and autophagic stress in Npc1 -/- mouse brain. *Am J Pathol* **171**, 962-975, doi:10.2353/ajpath.2007.070052 (2007).

32 Pacheco, C. D., Kunkel, R. & Lieberman, A. P. Autophagy in Niemann-Pick C disease is dependent upon Beclin-1 and responsive to lipid trafficking defects. *Hum Mol Genet* **16**, 1495-1503, doi:10.1093/hmg/ddm100 (2007).

33 Elrick, M. J., Yu, T., Chung, C. & Lieberman, A. P. Impaired proteolysis underlies autophagic dysfunction in Niemann-Pick type C disease. *Hum Mol Genet* **21**, 4876-4887, doi:10.1093/hmg/dds324 (2012).

34 Ordonez, M. P. *et al.* Disruption and therapeutic rescue of autophagy in a human neuronal model of Niemann Pick type C1. *Hum Mol Genet* **21**, 2651-2662, doi:10.1093/hmg/dds090 (2012).

35 Maetzel, D. *et al.* Genetic and chemical correction of cholesterol accumulation and impaired autophagy in hepatic and neural cells derived from Niemann-Pick Type C patient-specific iPS cells. *Stem Cell Reports* **2**, 866-880, doi:10.1016/j.stemcr.2014.03.014 (2014).

36 Praggastis, M. *et al.* A murine Niemann-Pick C1 I1061T knock-in model recapitulates the pathological features of the most prevalent human disease allele. *J Neurosci* **35**, 8091-8106, doi:10.1523/JNEUROSCI.4173-14.2015 (2015).

37 Schultz, M. L. *et al.* Coordinate regulation of mutant NPC1 degradation by selective ER autophagy and MARCH6-dependent ERAD. *Nat Commun* **9**, 3671, doi:10.1038/s41467-018-06115-2 (2018).

38   Magtanong, L., Ko, P. J. & Dixon, S. J. Emerging roles for lipids in non-apoptotic cell death. *Cell Death Differ* **23**, 1099-1109, doi:10.1038/cdd.2016.25 (2016).

39   Rajamaki, K. *et al.* Cholesterol crystals activate the NLRP3 inflammasome in human macrophages: a novel link between cholesterol metabolism and inflammation. *PLoS One* **5**, e11765, doi:10.1371/journal.pone.0011765 (2010).

40   Cantuti-Castelvetri, L. *et al.* Defective cholesterol clearance limits remyelination in the aged central nervous system. *Science* **359**, 684-688, doi:10.1126/science.aan4183 (2018).

41   Gelsthorpe, M. E. *et al.* Niemann-Pick type C1 I1061T mutant encodes a functional protein that is selected for endoplasmic reticulum-associated degradation due to protein misfolding. *J Biol Chem* **283**, 8229-8236, doi:10.1074/jbc.M708735200 (2008).

42   Wichit, S. *et al.* Imipramine Inhibits Chikungunya Virus Replication in Human Skin Fibroblasts through Interference with Intracellular Cholesterol Trafficking. *Sci Rep* **7**, 3145, doi:10.1038/s41598-017-03316-5 (2017).

43   Rosenbaum, A. I., Zhang, G., Warren, J. D. & Maxfield, F. R. Endocytosis of beta-cyclodextrins is responsible for cholesterol reduction in Niemann-Pick type C mutant cells. *Proc Natl Acad Sci U S A* **107**, 5477-5482, doi:10.1073/pnas.0914309107 (2010).

44   McCauliff, L. A. *et al.* Multiple Surface Regions on the Niemann-Pick C2 Protein Facilitate Intracellular Cholesterol Transport. *J Biol Chem* **290**, 27321-27331, doi:10.1074/jbc.M115.667469 (2015).

45   Kuma, A. *et al.* The role of autophagy during the early neonatal starvation period. *Nature* **432**, 1032-1036, doi:10.1038/nature03029 (2004).

46   Skaar, J. R., Pagan, J. K. & Pagano, M. Mechanisms and function of substrate recruitment by F-box proteins. *Nat Rev Mol Cell Biol* **14**, 369-381, doi:10.1038/nrm3582 (2013).

47   Kuo, C. L. & Goldberg, A. L. Ubiquitinated proteins promote the association of proteasomes with the deubiquitinating enzyme Usp14 and the ubiquitin ligase Ube3c. *Proc Natl Acad Sci U S A* **114**, E3404-E3413, doi:10.1073/pnas.1701734114 (2017).

48   Yu, T., Shakkottai, V. G., Chung, C. & Lieberman, A. P. Temporal and cell-specific deletion establishes that neuronal Npc1 deficiency is sufficient to mediate neurodegeneration. *Hum Mol Genet* **20**, 4440-4451, doi:10.1093/hmg/ddr372 (2011).

49   Glenn, K. A., Nelson, R. F., Wen, H. M., Mallinger, A. J. & Paulson, H. L. Diversity in tissue expression, substrate binding, and SCF complex formation for a lectin family of ubiquitin ligases. *J Biol Chem* **283**, 12717-12729, doi:10.1074/jbc.M709508200 (2008).

50   Erhardt, J. A. *et al.* A novel F box protein, NFB42, is highly enriched in neurons and induces growth arrest. *J Biol Chem* **273**, 35222-35227 (1998).

51   Zhang, Y. *et al.* An RNA-sequencing transcriptome and splicing database of glia, neurons, and vascular cells of the cerebral cortex. *J Neurosci* **34**, 11929-11947, doi:10.1523/JNEUROSCI.1860-14.2014 (2014).

52   Nelson, R. F., Glenn, K. A., Miller, V. M., Wen, H. & Paulson, H. L. A novel route for F-box protein-mediated ubiquitination links CHIP to glycoprotein quality control. *J Biol Chem* **281**, 20242-20251, doi:10.1074/jbc.M602423200 (2006).

53   Nelson, R. F. *et al.* Selective cochlear degeneration in mice lacking the F-box protein, Fbx2, a glycoprotein-specific ubiquitin ligase subunit. *J Neurosci* **27**, 5163-5171, doi:10.1523/JNEUROSCI.0206-07.2007 (2007).

54   Skowyra, M. L., Schlesinger, P. H., Naismith, T. V. & Hanson, P. I. Triggered recruitment of ESCRT machinery promotes endolysosomal repair. *Science* **360**, doi:10.1126/science.aar5078 (2018).

55   Chung, C. *et al.* Heat Shock Protein Beta-1 Modifies Anterior to Posterior Purkinje Cell Vulnerability in a Mouse Model of Niemann-Pick Type C Disease. *PLoS Genet* **12**, e1006042, doi:10.1371/journal.pgen.1006042 (2016).

56   Elrick, M. J. *et al.* Conditional Niemann-Pick C mice demonstrate cell autonomous Purkinje cell neurodegeneration. *Hum Mol Genet* **19**, 837-847, doi:10.1093/hmg/ddp552 (2010).

57   Appelqvist, H. *et al.* Attenuation of the lysosomal death pathway by lysosomal cholesterol accumulation. *Am J Pathol* **178**, 629-639, doi:10.1016/j.ajpath.2010.10.030 (2011).

58   Appelqvist, H. *et al.* Sensitivity to lysosome-dependent cell death is directly regulated by lysosomal cholesterol content. *PLoS One* **7**, e50262, doi:10.1371/journal.pone.0050262 (2012).

59   Repnik, U., Hafner Cesen, M. & Turk, B. Lysosomal membrane permeabilization in cell death: concepts and challenges. *Mitochondrion* **19 Pt A**, 49-57, doi:10.1016/j.mito.2014.06.006 (2014).

60   Yu, T. & Lieberman, A. P. Npc1 acting in neurons and glia is essential for the formation and maintenance of CNS myelin. *PLoS Genet* **9**, e1003462, doi:10.1371/journal.pgen.1003462 (2013).

This work has been published in *JCI Insight* (2020):

Chapter 4

TDP-43 Proteinopathy Occurs Independently of Autophagic Substrate Accumulation and Underlies Nuclear Defects in Niemann-Pick C Disease

4.1 Abstract

Neuronal cytoplasmic inclusions of TDP-43 are a pathological hallmark of amyotrophic lateral sclerosis (ALS) and frontotemporal degeneration (FTD), but the processes that mediate their formation and their functional significance remain incompletely understood. Dysfunction in autophagy has been linked to TDP-43 mislocalization, as mutations in autophagy genes cause ALS/FTD, and autophagy induction rescues neuron survival in ALS models. Here, we investigate TDP-43 proteinopathy in Niemann-Pick type C disease (NPC), an autosomal recessive lysosomal storage disease (LSD) distinguished by the accumulation of unesterified cholesterol within late endosomes and lysosomes. NPC is characterized by neurodegeneration, early death, and multifocal disruption of the autophagy pathway. Unexpectedly, we found that cytoplasmic TDP-43 mislocalization in $Npc1^{-/-}$ neurons was independent of autophagic substrate accumulation. These pathologies occurred in distinct neuronal subtypes, as brainstem cholinergic neurons were more susceptible to TDP-43 mislocalization while glutamatergic neurons exhibited hallmarks of autophagic dysfunction. Furthermore, TDP-43 mislocalization did not co-localize with markers of stress granules or progress to ubiquitinated aggregates over months in vivo,

indicating an early stage in the aggregation process. Neither microgliosis nor neuroinflammation, also implicated in TDP-43 pathology, were sufficient to drive TDP-43 proteinopathy in the NPC brain. Notably, cytoplasmic TDP-43 co-localized with the nuclear import factor importin α, and TDP-43 mislocalized neurons demonstrated nuclear membrane abnormalities and disruption of nucleocytoplasmic transport. Collectively, our findings reinforce the relationship between LSDs and TDP-43 proteinopathy, define its functional importance in NPC, and expand the spectrum of TDP-43 pathology in the diseased brain.

4.2 Introduction

A pathological hallmark of amyotrophic lateral sclerosis (ALS) and frontotemporal degeneration (FTD) is nuclear depletion and neuronal cytoplasmic inclusions of TAR-DNA binding protein of 43 kDa (TDP-43) [1,2]. Although ALS and FTD are biochemically, genetically, and clinically heterogeneous, pathological TDP-43 cytoplasmic inclusions are observed in over 90% of ALS and over 50% of FTD patients, highlighting its role in disease pathogenesis [3]. TDP-43 is a nuclear RNA-binding protein that functions in RNA processing, including splicing, translation and degradation, and its expression levels and localization are critical for normal cellular function. TDP-43 knockout and overexpression cause neurodegeneration [4-7], and cytoplasmic mislocalization of TDP-43 is sufficient to drive neuron death [8]. Despite increased understanding of both gain- and loss-of-function pathological mechanisms of TDP-43 mislocalization [9], the processes that mediate the formation of these pathological aggregates remain incompletely understood.

TDP-43 contains a C-terminal low-complexity domain which renders it aggregation prone [10]. Nearly all ALS-associated TDP-43 mutations are concentrated in this region, but

contribute to only 2%-5% of ALS cases [9,10]. Increasingly, dysfunction in the clearance of TDP-43 aggregates by autophagy has been linked to disease pathogenesis [11-13], and autophagy induction enhances neuronal survival in ALS models [14]. Consistent with this idea, multiple ALS- and FTD-associated genes are linked to autophagy and the lysosomal pathway [15], including *C9ORF72*, *TBK1*, *UBQLN2*, *VCP*, *SQSTM1*, and *OPTN*, and mutations in these genes result in TDP-43 pathology [16-21]. Furthermore, a link between lysosomal dysfunction and TDP-43 proteinopathy has been described. Mouse and patient brains with progranulin mutations accumulate TDP-43 inclusions and exhibit pathologic hallmarks of the lysosomal storage disease (LSD) neuronal ceroid lipofuscinosis [22].

Here, we investigate TDP-43 proteinopathy in Niemann-Pick type C disease (NPC), an autosomal recessive LSD characterized by the accumulation of unesterified cholesterol in lysosomes and late endosomes [23]. Most cases of NPC (~95%) are due to mutations in the *NPC1* gene [24], although a small subset (~5%) is due to mutations in *NPC2*. NPC1 and NPC2 function in concert to export cholesterol from lysosomes [25-28]. Loss-of-function mutations in either of these proteins lead to cholesterol accumulation, liver disease, severe neurodegeneration, and early death, often in childhood [29]. Several general principles have emerged that guide our understanding of NPC pathogenesis. The importance of lipid storage in the disease phenotype is apparent, as reduction of cholesterol storage by hydroxypropyl-beta-cyclodextrin dampens neurodegeneration and prolongs lifespan in *Npc1* mutant mice and cats [30-32]; similarly, peripheral administration of synthetic HDL nanoparticles to NPC mice mobilizes cholesterol and rescues liver dysfunction and body weight [33]. Lipid storage has also been linked to lysosomal membrane permeabilization in NPC [34-36], highlighting the importance of functional lysophagy to mitigate cytotoxicity [36]. Furthermore, the significance of neurons in disease has been established.

Conditional deletion of *Npc1* in neurons leads to age-dependent, cell autonomous neuron loss without evidence of a critical window for neuronal vulnerability [37] as well as dysmyelination [38]. Conversely, transgenic over-expression of *Npc1* in neurons of null mice ameliorates neurodegeneration [39]. Notably, as lysosomal function is essential for autophagy, LSDs can also be viewed primarily as "autophagy disorders" [40], and NPC models exhibit multifocal disruption of macroautophagy [41-48].

With the association between dysregulated autophagy and TDP-43 proteinopathy, we sought to characterize neuronal TDP-43 pathology in NPC, examine mechanisms that drive TDP-43 mislocalization, and explore functional consequences in the NPC brain. We show that *Npc1*$^{-/-}$ neurons accumulate cytoplasmic mislocalized TDP-43. Unexpectedly, this TDP-43 pathology occurs independently of autophagic substrate accumulation and does not progress to ubiquitinated protein aggregates over months in vivo. Moreover, we find that alternative factors implicated in TDP-43 pathology, including microgliosis and neuroinflammation are insufficient to drive TDP-43 mislocalization in the NPC brain. We also present evidence of nuclear pathology and disruption in nucleocytoplasmic transport in *Npc1*$^{-/-}$ neurons with mislocalized TDP-43. Our findings highlight the relationship between TDP-43 pathology and LSDs, expand the spectrum of TDP-43 pathology in the diseased brain, and provide evidence of nuclear dysfunction in an LSD.

4.3 Materials and Methods

Antibodies

Primary antibodies (antigen, dilution, vendor)

Neurofilament, 1:200, Millipore MAB5266; Neurofilament, 1:1000, Abcam ab8135; NeuN, 1:500, Millipore ABN78; NeuN, 1:500, Millipore ABN90; Synapsin-1, 1:200, Cell Signaling D12G5; GFAP, 1:500, Dako Z0334; Tom20, 1:500, Santa Cruz Biotechnology Inc. sc-11415; Ubiquitin, 1:400, Cell Signaling 3933S; phospho-Ubiquitin (Ser65), 1:100, Millipore ABS1513-I; SQSTM1, 1:500, Abnova H00008878-MO1; LC3B, 1:500, Novus NB100-2220; TDP-43, 1:500, Proteintech 10782-2-AP; karyopherin α2, 1:150, Santa Cruz Biotechnology Inc. sc-55538; TDP43 Phospho (Ser409/410), 1:100 Biolegend 829901; TIA-1, 1:200, Abcam ab40693; G3BP1, 1:500 Proteintech 103057-2-AP; Nup62, 1:500 BD 610497; Lamin B1, 1:1000, abcam ab16048; LMP2, 1:1000, abcam ab3328; Iba1, 1:500, Wako 019-19741; Iba1, 1:100 abcam ab5076, LMP7, 1:500, abcam ab3329; PSMB10, 1:1000, abcam ab183506; β-Actin, 1:2000, Sigma-Aldrich A5441; Vinculin, 1:2000, Sigma-Aldrich V9131; p62/SQSTM1, 1:1000, Sigma-Aldrich P0067; VDAC1, 1:500, abcam ab14734; VGLUT1, 1:500, Synaptic Systems 135303; VGAT *cytoplasmic domain*, 1:100, Synaptic Systems 131008; Choline Acetyltransferase, 1:100, Sigma-Aldrich AB144P

Secondary antibodies

Alexa Fluor™ 594 donkey anti-goat IgG (H+L), 1:500, Invitrogen A11058; Alexa Fluor™ 594 Fab'2 fragment of goat anti-rabbit IgG (H+L), 1:500, Invitrogen A11072; Alexa Fluor™ 594 Fab'2 fragment of goat anti-mouse IgG (H+L), 1:500, Invitrogen A11020; Alexa Fluor™ 488 goat anti-rabbit IgG (H+L), 1:500, Invitrogen A11008; Alexa Fluor™ 594 goat anti guinea pig IgG (H+L), Invitrogen A1076; Alexa Fluor™ 488 goat anti-mouse IgG (H+L), Invitrogen A11029; Alexa Fluor™ 488 rabbit anti mouse IgG (H+L), 1:500, Invitrogen A11059; Goat anti-mouse IgG (H+L)-HRP conjugate, 1:2000, Bio-Rad 170-6516; Goat anti-rabbit IgG (H+L)-HRP conjugate, 1:2000, Bio-Rad 170-6515

Reagents

Filipin was from Sigma (F9765).

Mice

$Npc1^{nih}$ Balb/cJ mice were obtained from Jackson Laboratories (#003092) and backcrossed to C57BL6/J (≥10 generations). $Npc1^{-/-}$ mice were F1 hybrids between $Npc1^{+/-}$ mice on the C57BL6/J and Balb/cJ backgrounds, respectively, to restore the Mendelian frequency of the $Npc1^{-/-}$ genotype [41]. $Npc1^{flox/flox}$ were generated as previously described [49]. *Syn1-Cre* mice were obtained from Jackson Laboratories (#003474) and backcrossed to C57BL6/J (≥10 generations). *Npc1-I1061T* mice [50] were a gift from Daniel Ory (Washington University in St Louis) and backcrossed to C57BL/6 (≥10 generations).

Western blot

For tissue preparation, mice were perfused with saline before tissue was collected and flash frozen in liquid nitrogen. Tissue was homogenized and sonicated in RIPA buffer (Teknova) with complete protease inhibitor (Thermo Scientific 11836153001) and 0.625mg/ml N-ethylmaleimide (Sigma E3876). Protein concentrations were determined by DC™-protein assay (Bio-Rad) and normalized. Proteins were separated on NuPAGE™ 4-12% Bis-Tris Protein Gels (Thermo Scientific NP0336BOX) and transferred to Immobilon-P 0.45um PVDF (Merck Millipore). Immunoreactivity was detected with ECL (Thermo Scientific) or SuperSignal™ West Pico PLUS Chemiluminscent Substrate (Thermo Scientific) and an iBright (Thermo Fisher Scientific). Quantification was performed using Image Studio. Band intensity was normalized to the indicated loading control.

RT-qPCR

RNA was collected using TRIzol® (Thermo Fisher) according to manufacturer's instructions and converted to cDNA using the High Capacity Reverse Transcription kit (Applied Biosystems 4368814). Quantitative real-time PCR was performed using 10ng cDNA, FastStart Taqman Probe Master Mix (Roche), and gene-specific FAM-labeled TaqMan probes (Thermo Scientific) for mouse C3 (Mm01232779_m1), C1qa (Mm07295529_m1), PSMB8 (Mm00440207_m1), PSMB9 (Mm00479004_m1), PSMB10 (Mm00479052_g1), PSME1 (Mm00650858_g1), PSME2 (Mm01702832_g1), PSMB5 (Mm01615821_g1), and PSMB7 (Mm01327044_m1). Gene expression was normalized to mouse Cpsf2-Vic (Mm00489754) multiplexed within the same well. RT-qPCR was performed using an ABI 7900HT Sequence Detection System and relative expression calculated by the $2^{\wedge}(-\Delta\Delta Ct)$ method.

Immunofluorescence staining

For tissue preparation, mice were perfused with saline and 4% PFA. Then, tissue was removed and post-fixed in 4% PFA overnight at 4°C. Brains were bisected; one hemisphere processed for paraffin embedding, and the other half was incubated in 30% sucrose for 48hr at 4°C and frozen in O.C.T. (Tissue-Tek). Paraffin-embedded tissues were cut on a Reichert-Jung 2030 microtome into 5µm sections and placed on Fisher Scientific Superfrost Plus microscope slides. Sections were adhered onto slides in an oven at 55-60°C for 1 hr. Frozen sections were prepared at 16µm in a cryostat.

For staining of paraffin embedded sections: Samples were deparaffinized and antigen retrieval was performed by boiling in 10mM sodium citrate (pH 6.0) for 10 min and incubating

in hot citrate solution for an additional 20 min, then washed 3x in deionized water. For staining, slides were incubated in a solution with 0.1% Triton, 10% goat or donkey serum and 1% BSA in PBS for 20 min. Then, slides were placed in blocking solution (10% goat or donkey serum, 1% BSA in PBS) before incubating in primary antibody diluted in blocking solution overnight at 4°C. Slides were washed 3x in PBS and incubated for 1 hr with secondary antibody diluted in blocking solution. Slides were then washed 3x in PBS and mounted with Vectashield + DAPI (Vector Laboratories).

Filipin staining

For filipin staining of tissue, frozen sections were stained for immunofluorescence as described above (without deparaffinization). Following the washes after secondary antibody incubation, sections were incubated in filipin staining solution (4mL FBS + 40uL filipin solution (1mg filipin + 40uL DMSO) + 16mL PBS) for 2 hrs at room temperature. Slides were washed 3x in PBS and mounted with Vectashield (Vector Laboratories).

RNA Fluorescence In Situ Hybridization with Immunofluorescence

Immunofluorescence staining was performed on paraffin embedded tissue sections as described above. Following the washes after secondary antibody incubation, slides were washed in Stellaris® RNA FISH Wash Buffer A (Biosearch Technologies) with 10% formamide for 2-5 min. Then, slides were incubated with a solution containing 125 nM oligo-d(T) probes conjugated to CAL Fluor Red 610 (Biosearch Technologies) in Stellaris® RNA FISH Hybridization Buffer (Biosearch Technologies) with 10% formamide for 4 hrs at 37°C. Slides were then washed in Stellaris® RNA FISH Wash Buffer A (Biosearch Technologies) for 30 min

at 37°C, Stellaris® RNA FISH Wash Buffer B (Biosearch Technologies) for 2-5 min, then 3x in

PBS. Finally, slides were mounted with Vectashield + DAPI (Vector Laboratories).

Proteasome activity

To measure the activity of immunoproteasome subunits, $Me_4BodipyFL-Ahx_3Leu_3VS$ was

used as previously described [51]. Briefly, tissue was homogenized and sonicated in HR buffer

(50mM Tris-HCl [pH 7.4], 5mM $MgCl_2$, 250mM sucrose, 1mM DTT, 2mM ATP). Protein

concentrations were determined by DC™-protein assay (Bio-Rad) and incubated with 1μM

$Me_4BodipyFL-Ahx_3Leu_3VS$ for 1 hr at 37°C. Samples were run on NuPAGE™ 12% Bis-Tris

Protein Gels (Thermo Scientific) at 140V for 2 hrs and imaged using a Typhoon Trio Plus

Scanner (Amersham Bioscience).

Electron Microscopy

Mice were perfused with 0.9% normal saline followed by 3% paraformaldehyde and

2.5% glutaraldehyde in 0.1 M Sorensen's buffer. The brainstem was removed and post-fixed in

perfusion solution overnight, followed by fixation in 1% osmium tetroxide solution for 1 h at

room temperature. After dehydration, tissues were embedded in epoxy resin. For transmission

electron microscopy, ultrathin sections were cut, and images were captured on a Philips CM-100

imaging system.

Microscopy

Confocal images were collected using a Nikon A-1 confocal microscope with diode-

based laser system. Filipin images were captured on a Zeiss Axioplan 2 imaging system. For

quantification of the nuclear-to-cytoplasmic (N:C) ratio of poly(A) RNA, the pixel intensity in the nucleus and cytoplasm was measured by ImageJ. Quantification of circularity of Lamin B1 staining was performed by ImageJ. Co-localization was determined using CellProfiler Analyst Software.

Phenotype analysis

Balance beam: The balance beam consists of a 12mm diameter circular beam (thick beam) and a 5mm wide square beam (thin beam) suspended at 50cm. Mice were trained at 4 weeks of age to cross the beam and then tested every other week starting at 5 weeks. For testing, mice were run 3 times across the beam, and the average time was taken. Maximum time was set at 20 sec and falls were scored as 20 sec.

Rotarod: After acclimating to the testing room for 30 min, mice were gently placed on a moving (4 RPM) rotarod for 30 sec. Then, over a period of 235 sec, rotarod speed was increased to 40 RPM. The trial ended if mice stopped walking for two revolutions or dropped onto the paddle. Mice were trained three times per day with a 30 min interval between each training session over a period of 3 days. The following week, mice were tested on a single day using the training protocol.

Statistics

Graphpad Prism 7.0 was used to determine significance ($P<0.05$), F (F-statistic) and t (T-statistic) values. Unpaired Student's t-test (two-tailed) and one-way or two-way ANOVA were used as indicated in the figure legends. A P value less than 0.05 was considered significant. All error bars are s.e.m.

4.4 Results

4.4.1 *Npc1* deficiency triggers age-dependent accumulation of swollen axons containing autophagic cargo

As NPC1 deficiency causes autophagic impairment, we sought to characterize the accumulation of autophagic substrates in mutant mouse brain, initially focusing on swollen axons (so-called spheroids) that are a prominent neuropathologic feature in the brainstem of diseased mice. Axonal spheroids, as identified by neurofilament staining, appeared as NPC1 deficient mice aged (Figure 4.1). In 4-week *Npc1*^{-/-} mice, before the onset of behavioral phenotypes (Figure 4.2), axonal spheroids were sparse; as mice progressed in the disease course to 11 weeks, the numbers of axonal spheroids significantly increased (Figure 4.3a, Figure 4.1a). Similar pathology occurs in the brainstem of mice deficient for *Npc1* only in neurons [37]. To further characterize the cell autonomous development of axonal spheroids, we utilized *Npc1*[flox], *Syn1-Cre*[+] mice, which harbor a conditional null allele of the *Npc1* gene (*Npc1*[flox]) [49] and express Cre recombinase as a transgene under the control of the *Synapsin1* promoter (*Syn1-Cre*[+]). In these mice, *Npc1* is deleted in neurons throughout the brain during late embryonic development [52]. As with global *Npc1*^{-/-} mice, axonal spheroids increased in an age-dependent manner in *Npc1*[flox/-], *Syn1-Cre*[+] mice from 7 to 16 weeks (Figure 4.3a, Figure 4.1b).
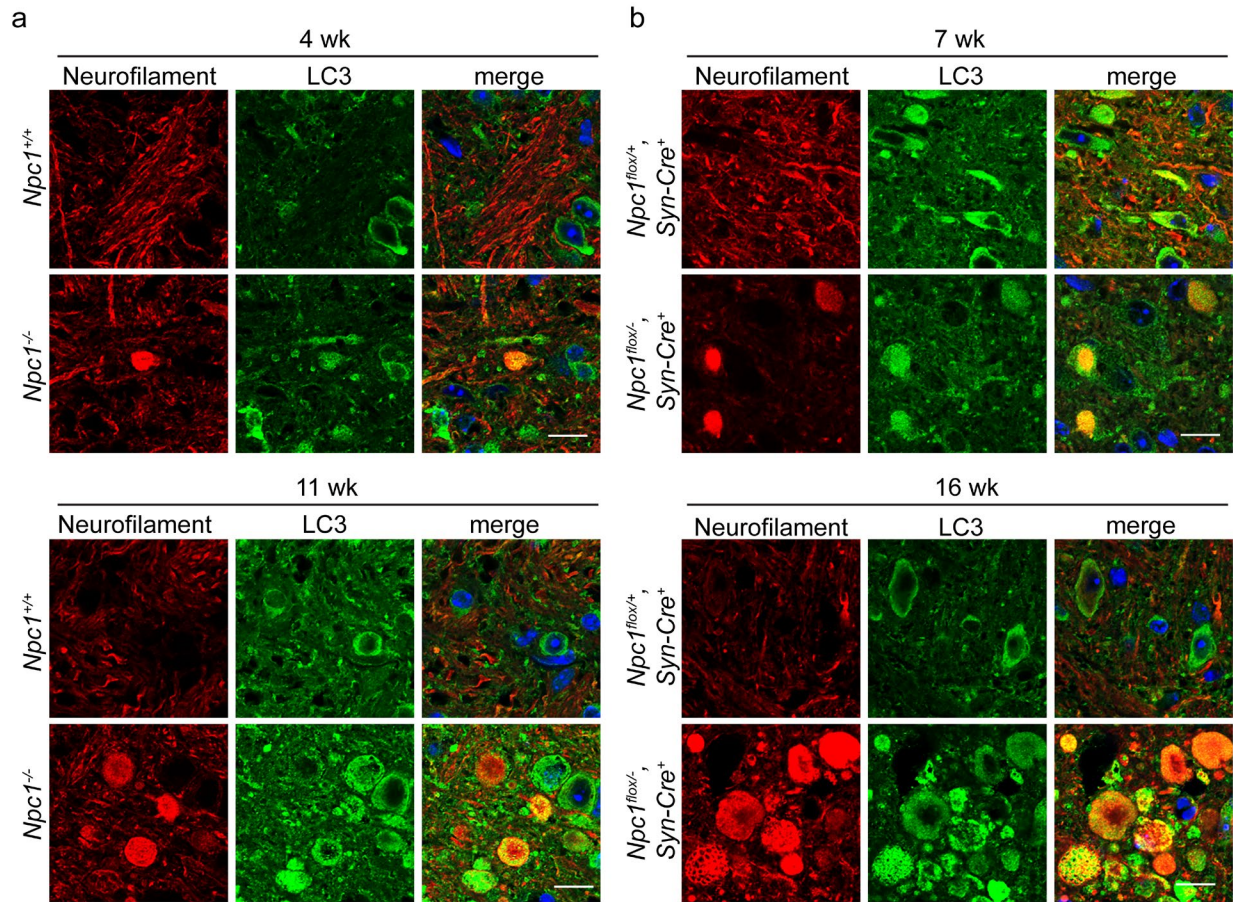
Figure 4.1 Age dependent accumulation of axonal spheroids. (a-b) Brain sections were stained with neurofilament and LC3 to identify axonal spheroids in the brainstem. Sections were imaged by confocal microscopy. Scale bar: 10 μm.
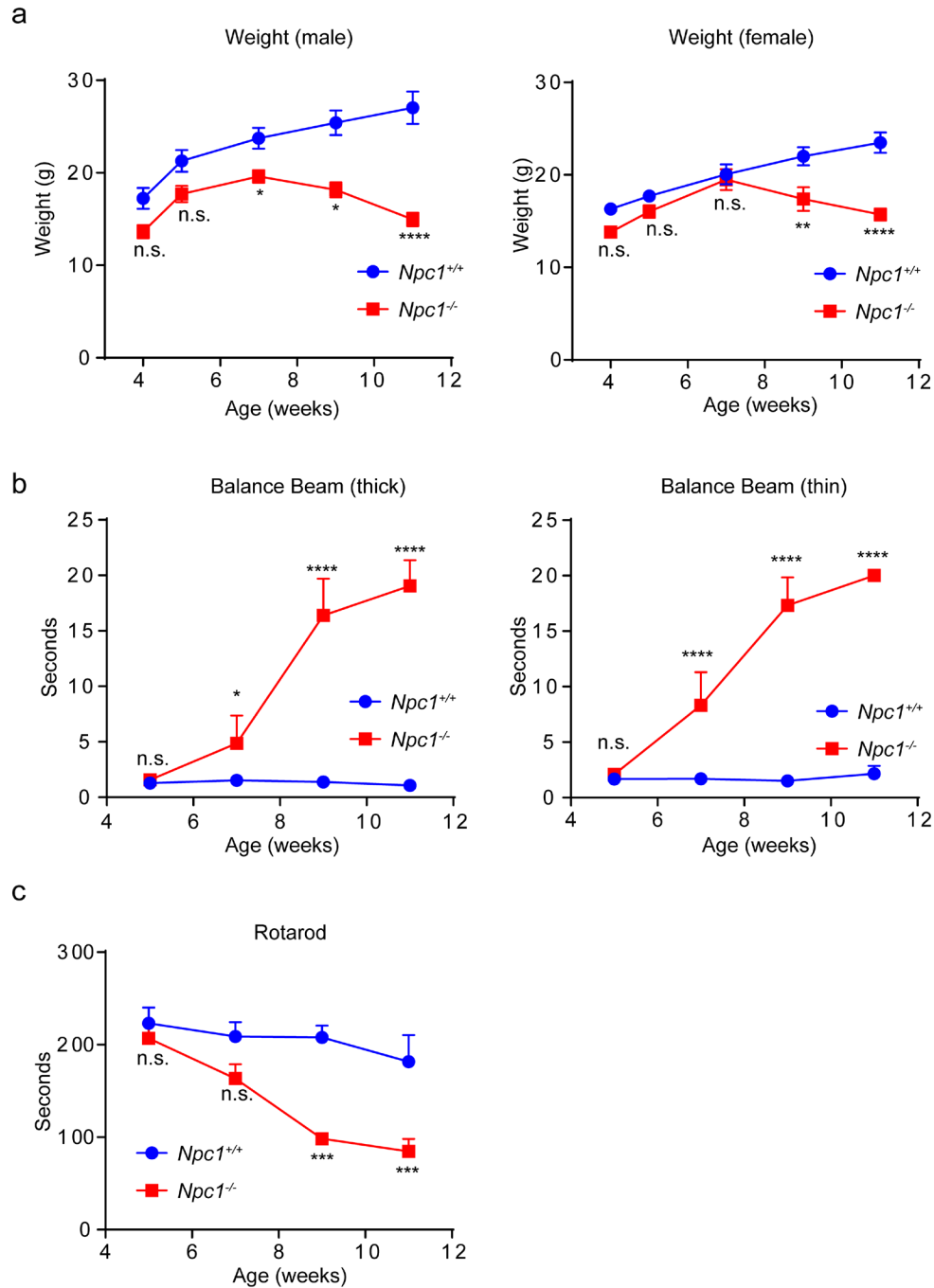
Figure 4.2 Age-dependent progression of weight loss and motor deficits of Npc1$^{-/-}$ mice. **(a)** Body weight of male and female *Npc1*$^{+/+}$ and *Npc1*$^{-/-}$ mice. N=4-5 mice per sex and genotype. **(b)** Age-dependent performance on balance beam using thick or thin beams. N=4-6 mice per genotype. **(c)** Age-dependent performance on accelerating rotarod. N=4-6 mice per genotype. Data are shown as mean ± s.e.m. n.s., not significant, *P ≤ 0.05, **P ≤ 0.01, ***P ≤ 0.001, ****P ≤ 0.0001 by **(a-c)** two-way ANOVA with Sidak's multiple comparisons test.
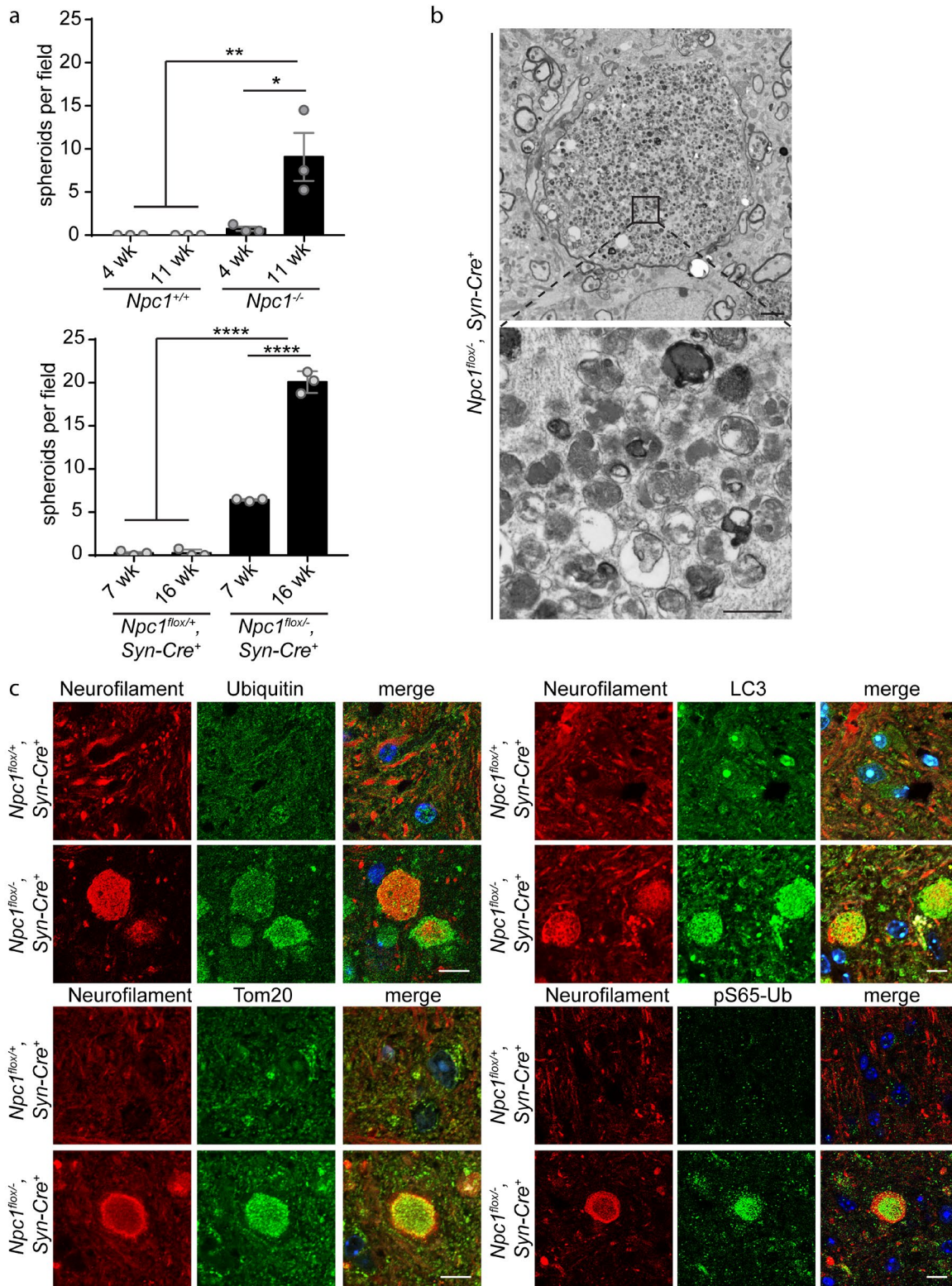
Figure 4.3 Npc1 deficiency triggers age-dependent accumulation of swollen axons containing autophagic cargo. **(a)** Axonal spheroids in brainstem, quantified from 4-5 fields, N=3 mice per genotype and age. **(b)** Electron micrographs of brainstem taken from 16-week *Npc1^flox/-, Syn-Cre^+* mice. *Top*: An axonal spheroid surrounded by normal sized axons. Scale bar: 2 µm. *Bottom*: Higher magnification shows accumulation of vesicular cargo. Scale bar: 500 nm. **(c)** Brain sections from 16-week *Npc1^flox/+, Syn-*

Axonal spheroids may reflect impaired autophagy, as autophagosomes are formed at the distal ends of axons and must be transported in a retrograde manner towards the cell soma for autolysosome formation and degradation; disruption of this process can cause accumulation of cargo and dysfunctional organelles within swollen axons [53-55]. Accordingly, deleting essential autophagy genes in Purkinje cells causes axonal swellings [56,57], and swollen axons in mouse models of Alzheimer's disease contain autophagic cargo [58-60]. In agreement with these
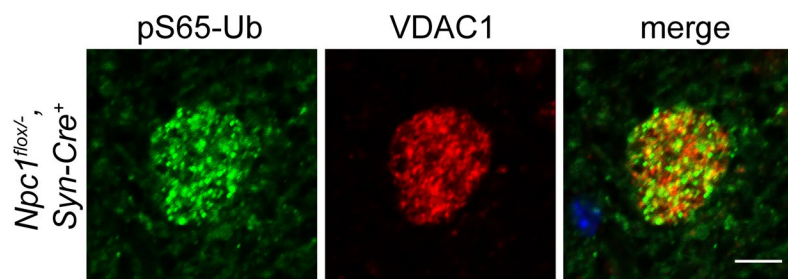

Figure 4.4 pS65-Ub co-localizes with mitochondrial marker VDAC1. Brainstem from 16-week *Npc1^{flox/-}, Syn-Cre⁺* mice were stained with pS65-Ub and VDAC1 and imaged by confocal microscopy. Mander's coefficient = 0.84. Scale bar: 5 μm.

observations, electron micrographs of 16-week *Npc1^{flox/-}, Syn1-Cre⁺* mice revealed striking enlargement of axons in the brainstem with the accumulation of polymorphous vesicular structures, including

vesicles consistent with double-membraned autophagosomes and mitochondria (Figure 4.3b). To confirm the presence of autophagic and organellar cargo, we performed immunofluorescence staining in the brainstem of *Npc1^{flox/-}, Syn1-Cre⁺* mice. Both ubiquitinated cargo and autophagosomes were visualized within axonal spheroids (Figure 4.3c). Furthermore, Tom20 staining identified mitochondria (Figure 4.3c). As impaired neuronal autophagy leads to accumulation of dysfunctional mitochondria [61] and mitochondrial abnormalities occur in NPC [46,62,63], we wondered if damaged mitochondria accumulated within swollen axons. Indeed, staining for pS65-Ub, a marker of damaged mitochondria [64], indicated the presence of

mitochondria targeted for degradation by autophagy (Figure 4.3c). Supporting this conclusion,

staining for pS65-Ub co-localized with VDAC1 (Mander's coefficient = 0.84) (Figure 4.4).

Altogether, these findings demonstrated an accumulation of autophagic and organellar cargo

within the swollen axons of *Npc1*-deficient mice.

4.4.2 Independent accumulation of autophagic cargo and cytoplasmic TDP-43

mislocalization

Defective autophagy is linked to the development of ALS/FTD and to the cytoplasmic

mislocalization and aggregation of TDP-43 [11,13-15,65]. As autophagic impairment is prominent in

NPC [41-48] and manifests with the accumulation of autophagic cargo (Figure 4.3), we sought to

determine whether TDP-43 proteinopathy was present in *Npc1*-deficient mice. Interestingly, in

4-week *Npc1*^{-/-} mice, we observed cytoplasmic mislocalization of TDP-43 primarily within

brainstem neurons (Figure 4.5a). This occurred at an early age, before the onset of behavioral

phenotypes (Figure 4.2). With the described connection between deficient autophagy and TDP-

43 mislocalization, we determined whether TDP-43 mislocalized neurons also accumulated

autophagic cargo. As a marker of autophagic substrate accumulation, we stained for p62,

showing accumulation in neuronal cell bodies, stained by NeuN, of *Npc1*-deficient mice, but not

at synapses or in astrocytes (Figure 4.6). Unexpectedly, we observed that neurons accumulating

p62 did not accumulate cytoplasmic TDP-43 and vice versa (Figure 4.5b, 4.5d). This indicated

that *Npc1*^{-/-} mice harbor distinct subpopulations of neurons: those that accumulate autophagic

cargo and those that accumulate mislocalized TDP-43. Notably, filipin staining showed that both

subpopulations of neurons accumulated unesterified cholesterol (Figure 4.7), suggesting

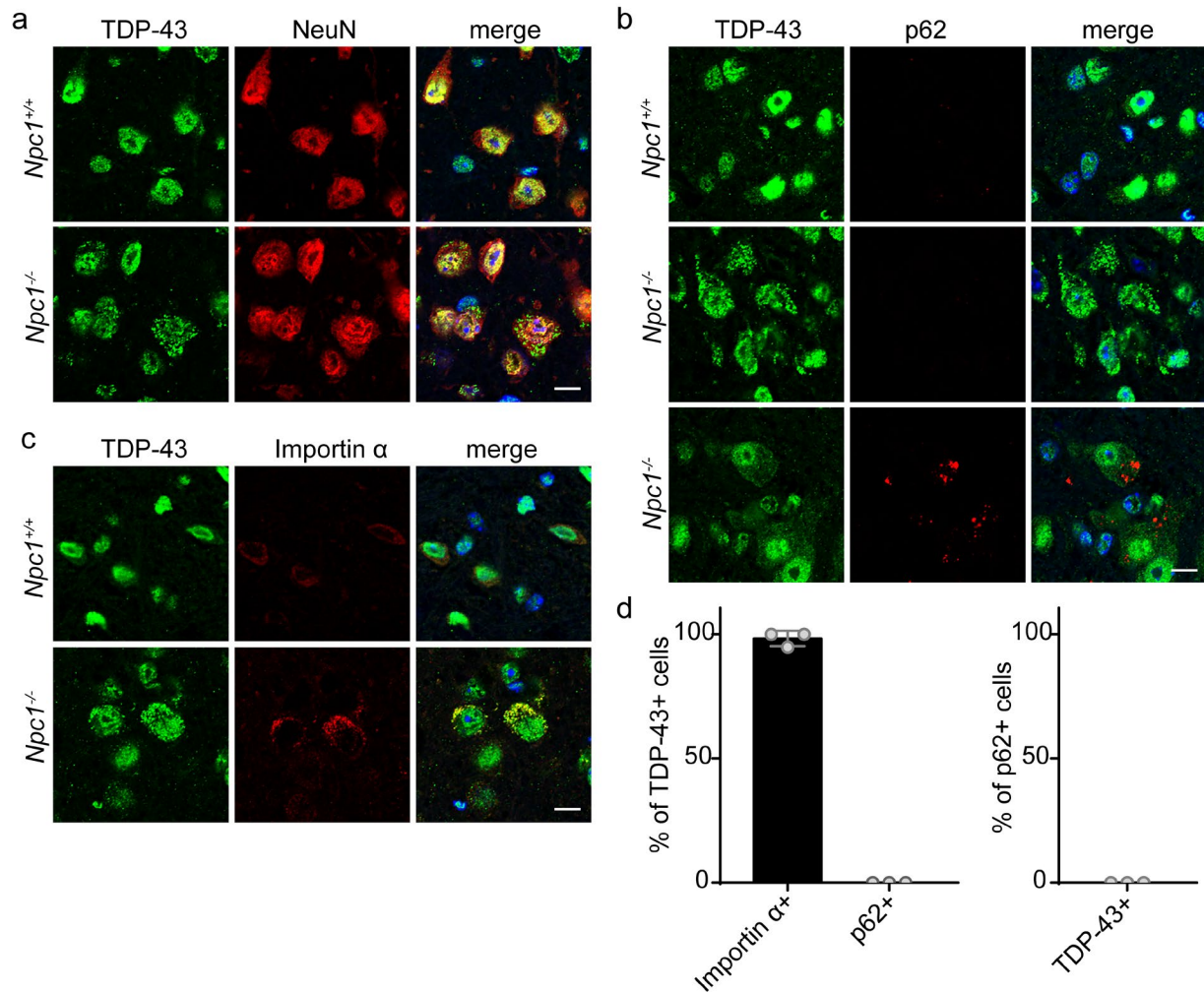divergent pathologic responses following lipid storage.

Figure 4.5 Independent accumulation of autophagic cargo and cytoplasmic TDP-43 mislocalization. **(a-c)** Brainstem from 4-week *Npc1*^{+/+} and *Npc1*^{-/-} mice was stained for the indicated markers and imaged by confocal microscopy. Scale bar: 10 μm. **(d)** *Left:* The percentage of TDP-43 mislocalized cells co-localized with importin α or p62. *Right:* The percentage of p62+ cells co-localized with cytoplasmic TDP-43. Twenty to thirty TDP-43+ or p62+ cells were quantified per mouse, N=3 mice. Data are shown as mean ± s.e.m.

Lack of p62 co-localization indicated that cytoplasmic TDP-43 was not present in ubiquitinated aggregates, but instead resembled TDP-43 de-mixing (the formation of cytoplasmic liquid droplets) that has been reported to occur in cell culture at an early stage of progressive TDP-43 aggregation [66]. We wondered if this cytoplasmic TDP-43 co-localized with
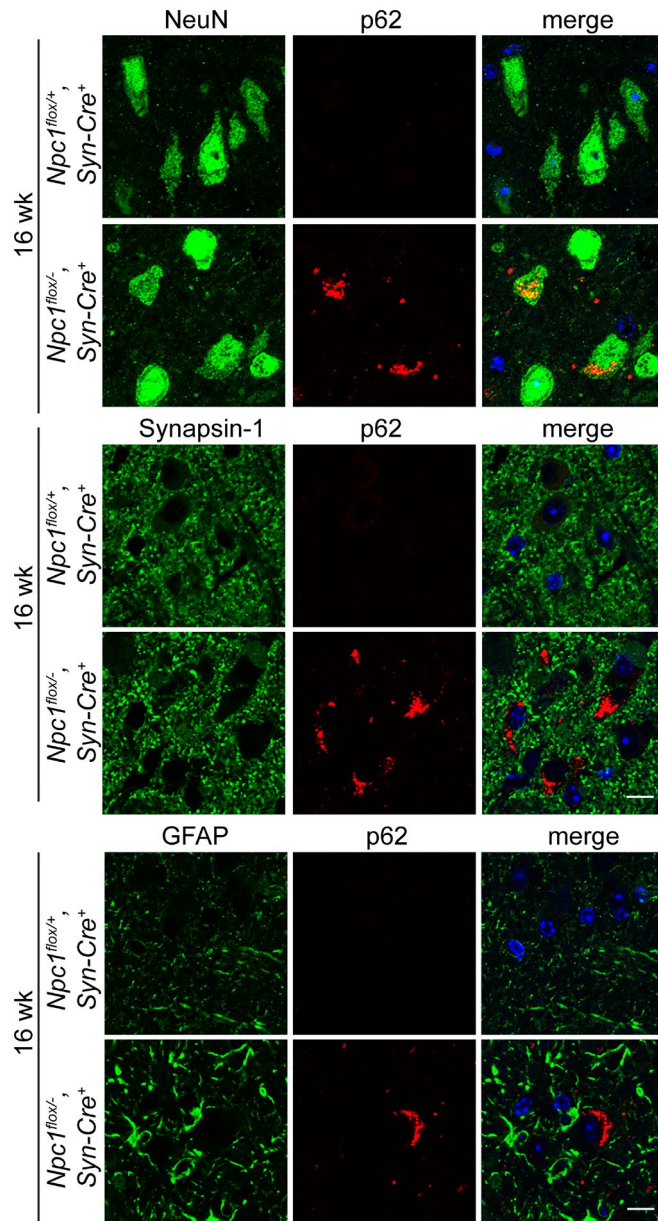
Figure 4.6 p62 accumulates in neuron cell bodies and not in presynaptic terminals or astrocytes. Brain sections from 16-week $Npc1^{flox/+}$, Syn-Cre^+ and $Npc1^{flox/-}$, Syn-Cre^+ mice were stained with the indicated markers and imaged by confocal microscopy. Scale bar: 10 μm.

other proteins shown to de-mix with it in vitro, including nuclear transport factors [66]. Indeed, the nuclear import factor importin α co-localized with TDP-43 in affected neurons (Figure 4.5c-d), suggesting the occurrence of impaired nucleocytoplasmic transport with TDP-43 mislocalization. Unlike ALS/FTD, we did not observe coincident nuclear clearance of TDP-43 (Figure 4.5a), a hallmark of TDP-43 aggregation [2] that has been shown to promote neurodegeneration [67]. Our findings support an early stage of TDP-43 proteinopathy in 4-week $Npc1^{-/-}$ mice.
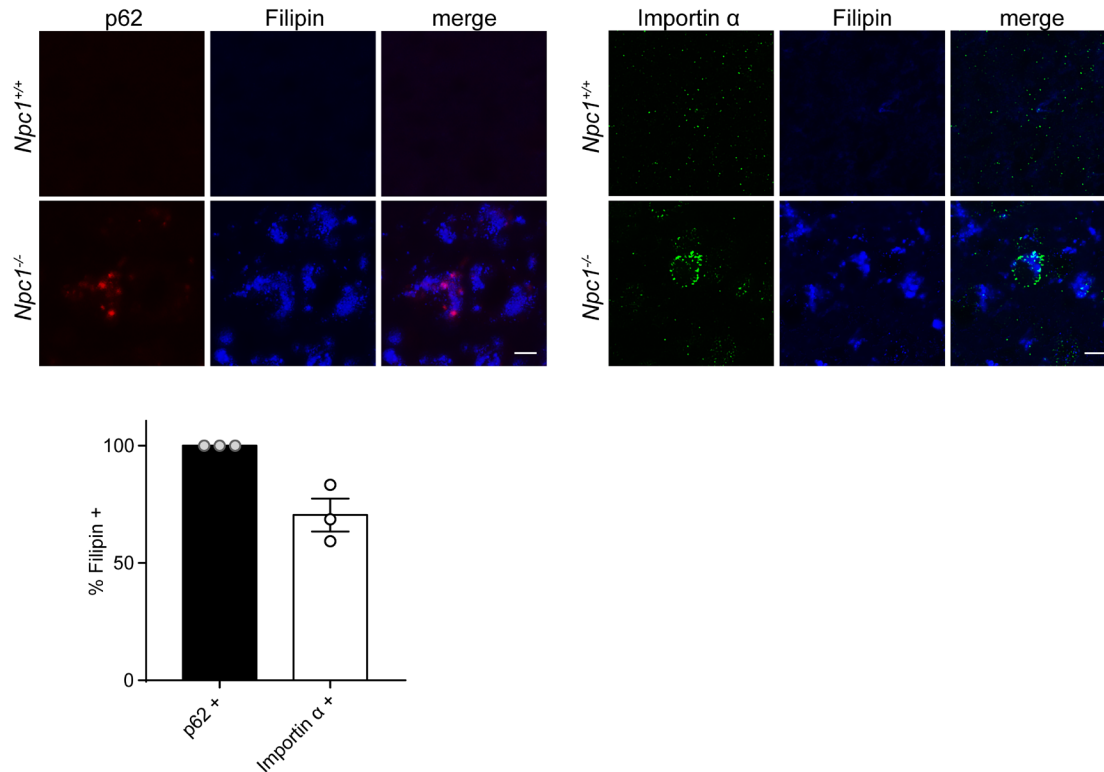
Figure 4.7 Cholesterol accumulates in both p62+ and importin α+ neurons. Brain sections from 11-week *Npc1*^{+/+} and *Npc1*^{-/-} mice were stained with the indicated markers and imaged by fluorescent microscopy. Scale bar: 10 μm. The percentage of p62+ or importin α+ cells that stain for filipin is shown below. Data are shown as mean ± s.e.m.

4.4.3 TDP-43 cytoplasmic mislocalization persists in vivo for months, up to end-stage in *Npc1*^{-/-} mice

With prolonged stress, cytoplasmic TDP-43 droplets progress to aggregates and clear TDP-43 from the nucleus in cell culture [66]. As aberrant phase transitions are suggested to drive the formation of pathological inclusions of RNA-binding proteins [10,68,69], we wondered if cytoplasmic mislocalized TDP-43 in 4-week *Npc1*^{-/-} mice progressed to aggregates at end-stage. Thus, we examined 11-week *Npc1*^{-/-} mice, which have developed significant weight loss and motor impairment (Figure 4.2). Unexpectedly, TDP-43 pathology at this stage was indistinguishable from that present at 4-weeks of age (Figure 4.5). TDP-43 mislocalized to the cytoplasm of 11-week *Npc1*^{-/-} neurons, with continued localization in the nucleus (Figure 4.8a).
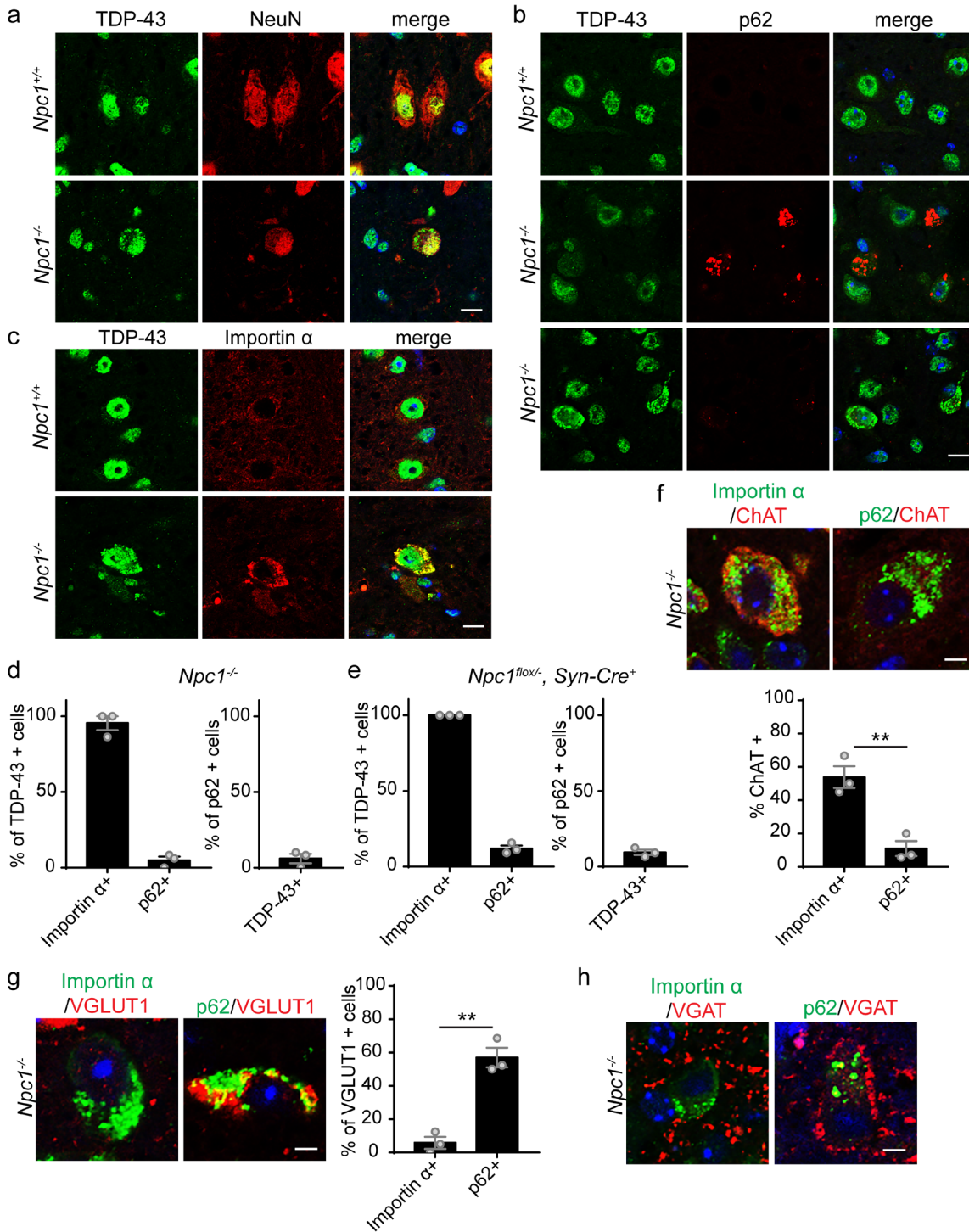
Figure 4.8 TDP-43 cytoplasmic mislocalization persists in vivo for months, up to end-stage in Npc1⁻/⁻ mice. **(a-c)** Brainstem from 11-week *Npc1⁺/⁺* and *Npc1⁻/⁻* mice was stained with the indicated markers and imaged by confocal microscopy. Scale bar: 10 μm. **(d-e)** *Left:* The percentage of TDP-43 mislocalized cells co-localized with importin α or p62. *Right:* The percentage of p62+ cells co-localized with cytoplasmic TDP-43. Twenty to thirty TDP-43+ or p62+ cells were quantified per mouse, N=3 mice per genotype. **(f)** *Top*: Brainstem from 11-week *Npc1⁻/⁻* mice was stained with the indicated markers and imaged by confocal microscopy. Scale bar: 5 μm. *Bottom*: The percentage of importin α+ or p62+ that were ChAT+. Fifteen to twenty-five cells were quantified per mouse, N=3 mice per genotype. **(g)** *Left:* Brainstem from 11-week *Npc1⁻/⁻* mice was stained with the indicated markers and imaged by confocal microscopy. Scale bar: 5 μm. *Right*: The percentage of VGLUT1+ cells that were p62+ or

importin α+. Fifteen to twenty-five cells were quantified per mouse, N=3 mice per genotype. **(h)** Brainstem from 11-week *Npc1*^{-/-} mice was stained with the indicated markers and imaged by confocal microscopy. Scale bar: 5 μm. Data are shown as mean ± s.e.m. **P ≤ 0.01 by **(f-g)** Student's t-test **(f)** t=5.388 **(g)** t=7.429

Furthermore, neurons that accumulated mislocalized TDP-43 did not accumulate p62, but co-localized with importin α (Figure 4.8b-d). Similar findings were observed in 16-week *Npc1*[flox], *Syn1-Cre*[+] mice following conditional deletion of *Npc1* in neurons (Figure 4.8e, Figure 4.9). Therefore, cytoplasmic mislocalized TDP-43 in *Npc1*-deficient neurons persisted in vivo for months without progression to ubiquitinated aggregates or nuclear depletion and remained independent of autophagic substrate accumulation. Moreover, as TDP-43 can be recruited to stress granules, which may increase its propensity to form pathological aggregates [70-72], we stained for stress granule markers G3BP1 and TIA-1 but found no co-localization (Figure 4.10a-b). We conclude that TDP-43 mislocalization occurred independently of stress granule formation, in agreement with prior observations of TDP-43 de-mixing [66,73].
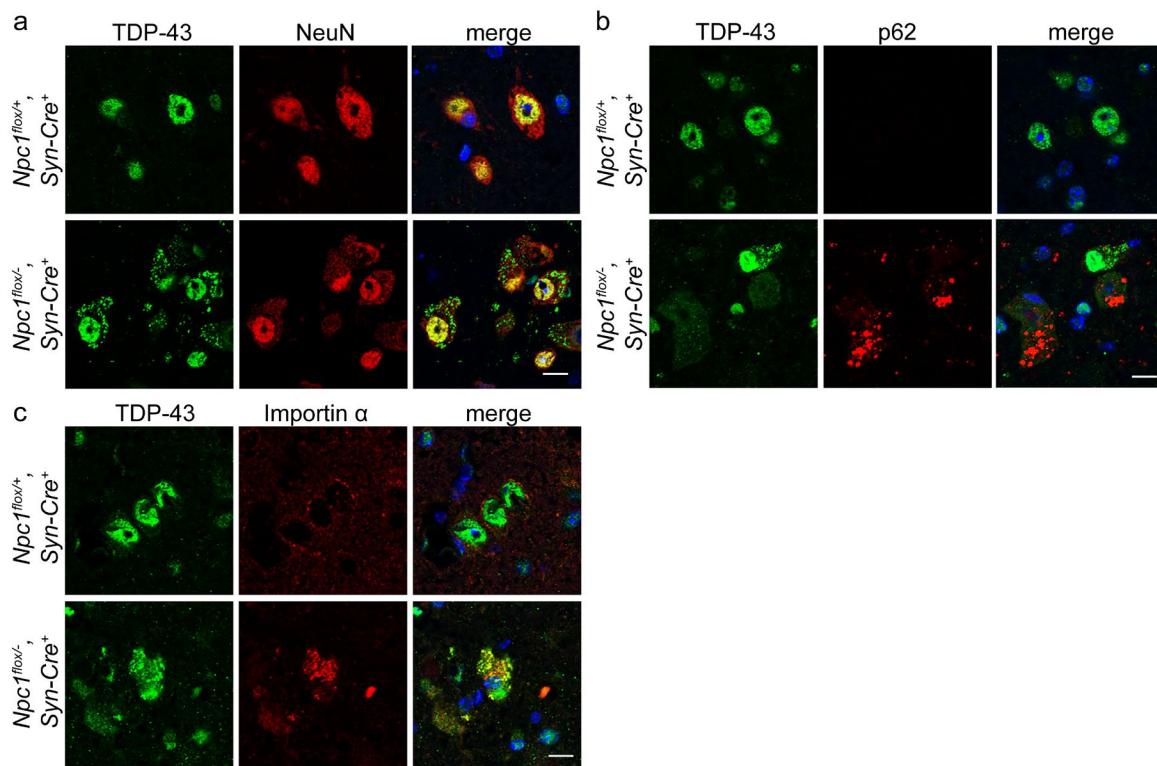

Figure 4.9 TDP-43 mislocalization in neurons occurs cell autonomously. **(a-c)** Brainstem from 16-week *Npc1*[flox/+], *Syn-Cre*[+] and *Npc1*[flox/-], *Syn-Cre*[+] mice was stained with the indicated markers and imaged by confocal microscopy. Scale bar: 10 μm.

We sought to determine whether other hallmarks of TDP-43 proteinopathy were present in *Npc1*-deficient neurons, including phosphorylated TDP-43 and the accumulation of C-terminal fragments [2]. Immunofluorescence and western blot analysis were negative for these pathologies, and TDP-43 protein levels were unchanged in brain lysates (Figure 4.10c, Figure 4.11). Furthermore, despite co-localization with importin α (Figure 4.5c, Figure 4.8c), we did not observe mislocalization of the nucleoporin Nup62 (Figure 4.10d), which has been associated with TDP-43 pathology in vitro [66,74].
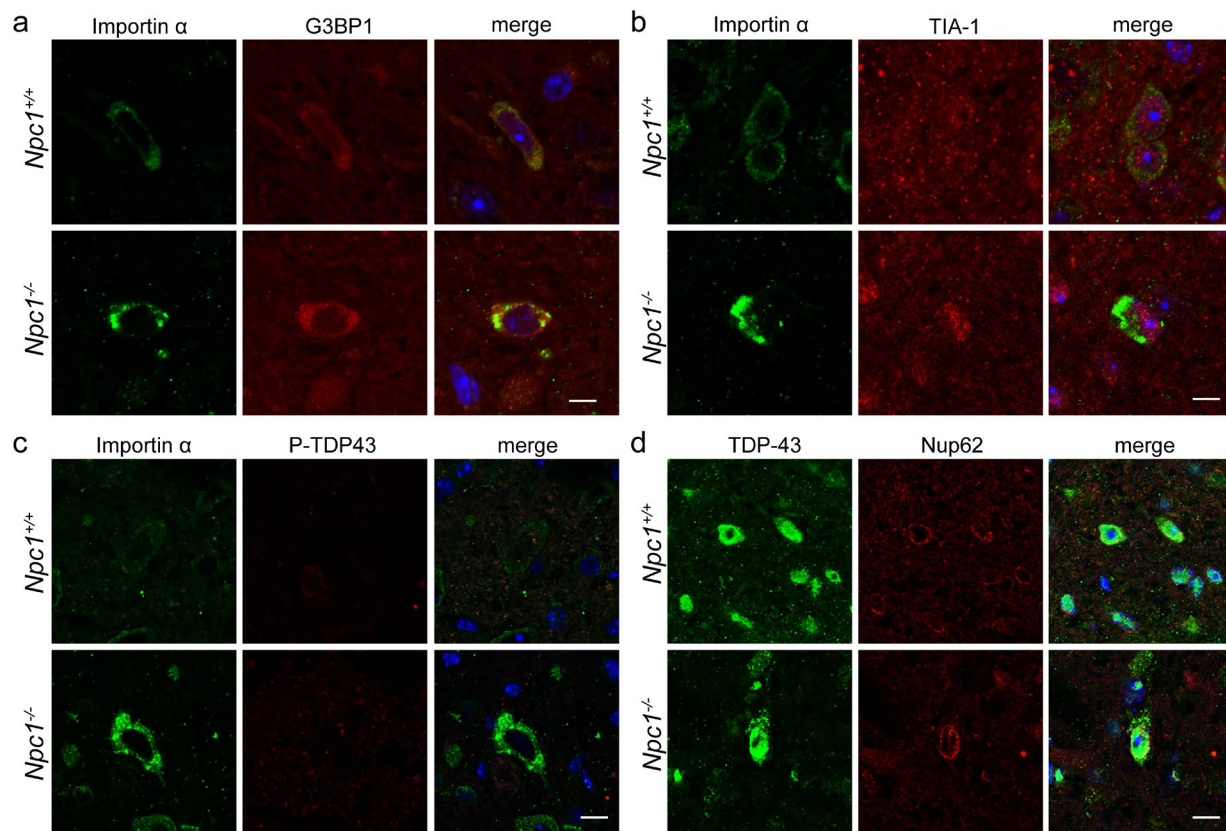
Figure 4.10 Npc1^{-/-} mice do not accumulate stress granules, P-TDP43 or mislocalized Nup62. **(a-d)** Brainstem from 11-week *Npc1^{+/+}* and *Npc1^{-/-}* mice was stained with the indicated markers and imaged by confocal microscopy. Scale bar: 10 μm.

To examine neuron subtypes involved by these pathologies, we first co-stained for choline acetyltransferase (ChAT) to identify brainstem cholinergic neurons. Interestingly, almost

50% of neurons that were importin α+, but not p62+, co-stained with ChAT (Figure 4.8f),

indicating a preferential susceptibility to TDP-43 pathology among brainstem cholinergic

neurons. Conversely, p62 but not importin α accumulated in VGLUT1+ cells (Figure 4.8g),

indicating that brainstem glutamatergic neurons preferentially accumulated autophagic substrates

over mislocalized TDP-43. VGAT expressing neurons have been shown to form inhibitory

synapses on excitatory neurons [75]. Correspondingly, we found VGAT+ synapses surrounding the

soma of p62+ but not importin α+ neurons (Figure 4.8h), revealing differential inhibitory

signaling and connectivity between these neuron populations.

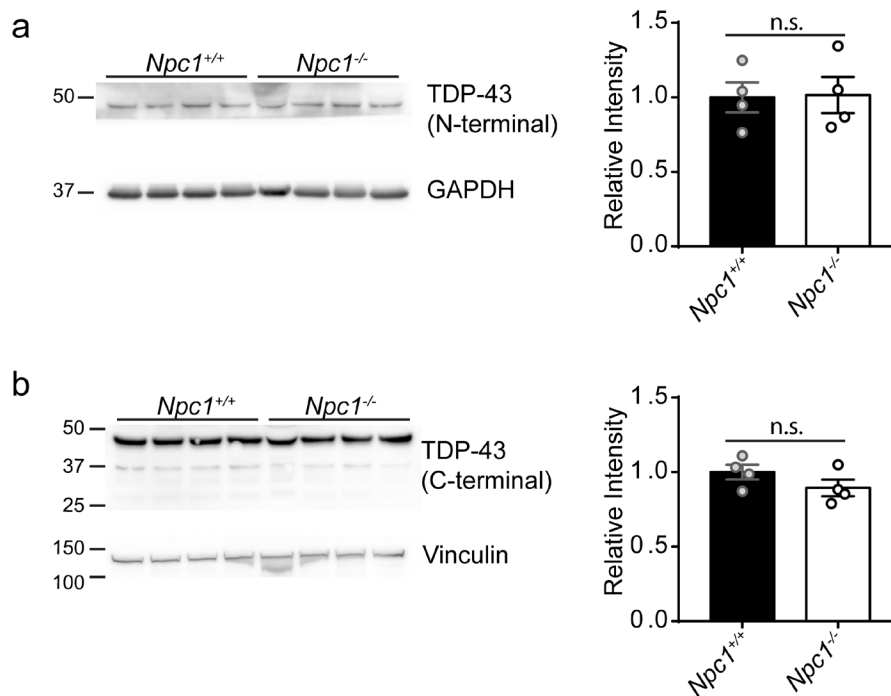***Figure 4.11 TDP-43 protein levels are unchanged, and C-terminal fragments do not accumulate in Npc1^{-/-} mice.*** **(a-b)** The relative abundance of TDP-43 was determined in the brainstem of 11-week *Npc1*^{+/+} and *Npc1*^{-/-} mice using an N-terminal **(a)** or C-terminal **(b)** TDP-43 antibody. Quantified at right. N=3 mice per genotype. Data are shown as mean ± s.e.m. n.s., not significant.

4.4.4 Progressive accumulation of autophagic cargo without TDP-43 cytoplasmic mislocalization in *Npc1-I1061T* mice

To further characterize the relationship between autophagic dysfunction and TDP-43 pathology we studied *Npc1-I1061T* knock-in mice [50], which harbor the most common disease-causing allele in patients of Western European ancestry [76]. In contrast to null models, *Npc1-I1061T* mice express mutant NPC1 protein that misfolds in the ER and is largely degraded, while a small fraction of protein that escapes degradation can traffic to the lysosome and function in cholesterol efflux [77,78]. Therefore, *Npc1-I1061T* mice exhibit a similar although milder phenotype than *Npc1$^{-/-}$* mice. We first assessed autophagic impairment in this model. *Npc1-I1061T* mice developed stored cholesterol as early as 3.7 weeks of age and showed progressive accumulation of ubiquitinated substrates, axonal spheroids and p62 by 7 weeks of age (Figure 4.12, Figure 4.13). However, despite the progressive accumulation of autophagic cargo, *Npc1-I1061T* mice did not accumulate either cytoplasmic TDP-43 or importin α in neurons (Figure 4.12e). This observation further supported the conclusion that autophagic impairment is not sufficient to drive TDP-43 mislocalization, and provided a model system in which to test the contribution of alternative factors that have been implicated as underlying TDP-43 pathology.
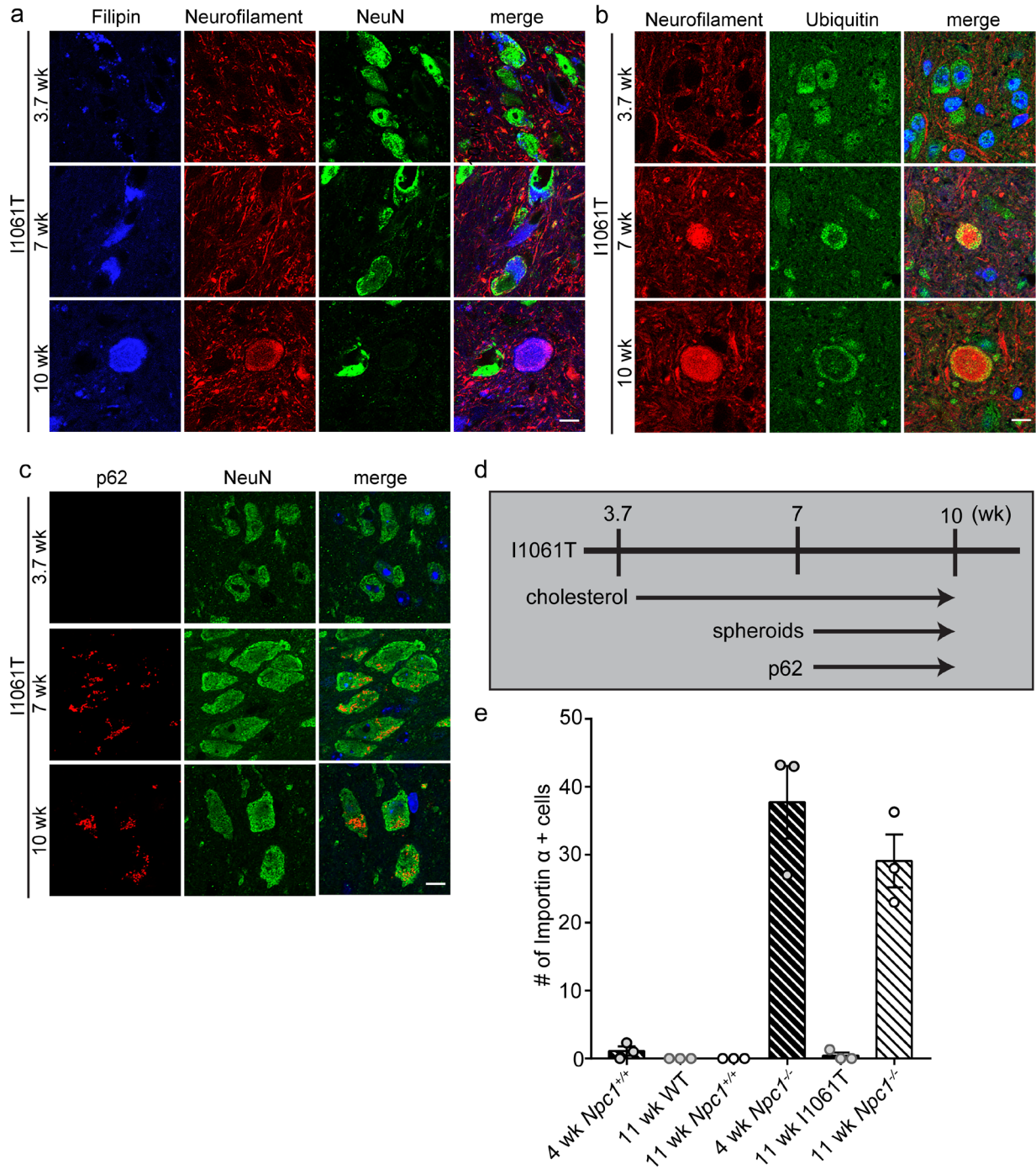
Figure 4.12 Progressive accumulation of autophagic cargo without TDP-43 cytoplasmic mislocalization in Npc1-I1061T mice. **(a-c)** Brainstem from *Npc1-I1061T* mice at 3.7, 7, and 10-weeks of age was stained with the indicated markers and imaged by confocal microscopy. Scale bar: 10 μm. **(d)** Timeline summarizes the age dependent accumulation of cholesterol and autophagic substrates in I1061T mice. **(e)** Importin α+ cells in the brainstem, quantified from N=3 mice per genotype. Data are shown as mean ± s.e.m.
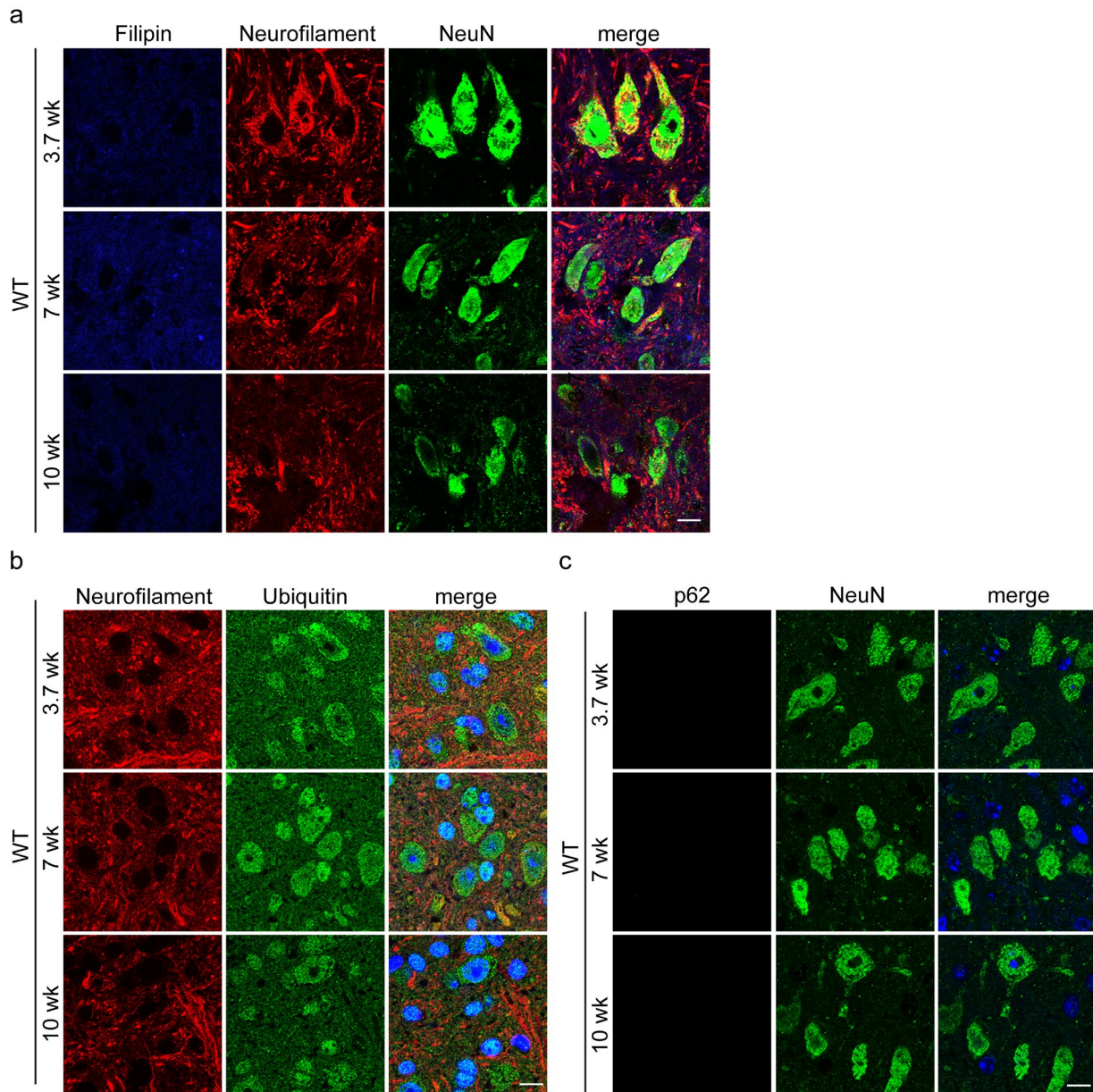
Figure 4.13 WT mice do not accumulate cholesterol or autophagic substrates. **(a-c)** Brainstem from 3.7, 7 and 10-week WT mice was stained with the indicated markers and imaged by confocal microscopy. Scale bar: 10μm.

Recent studies have focused on the role of microglia in neurodegenerative disease [79,80] because of their production of pro-inflammatory cytokines and other factors that underlie neuroinflammation [81]. Neurotoxic microglia and complement activation promote TDP-43 proteinopathy in progranulin deficient neurons [82]. Thus, we quantified the number of Iba1+ microglia in the brainstem of 4-week and 11-week $Npc1^{+/+}$ and $Npc1^{-/-}$ mice and compared them

with 11-week WT and *Npc1-I1061T* mice. We found that 11-week *Npc1-I1061T* mice exhibited intermediate levels of microgliosis compared to 4- and 11-week *Npc1⁻/⁻* mice (Figure 4.14a). Despite microgliosis at greater levels than that of 4-week *Npc1⁻/⁻* mice, TDP-43 was not mislocalized in *Npc1-I1061T* neurons (Figure 4.12e). Similarly, expression of genes encoding complement factors C1qa and C3 in 11-week *Npc1-I1061T* mice was intermediate to that of 4- and 11-week *Npc1⁻/⁻* mice (Figure 4.14b). Thus, induction of microgliosis and expression of complement components were not sufficient to account for TDP-43 mislocalization in NPC1 deficient neurons.

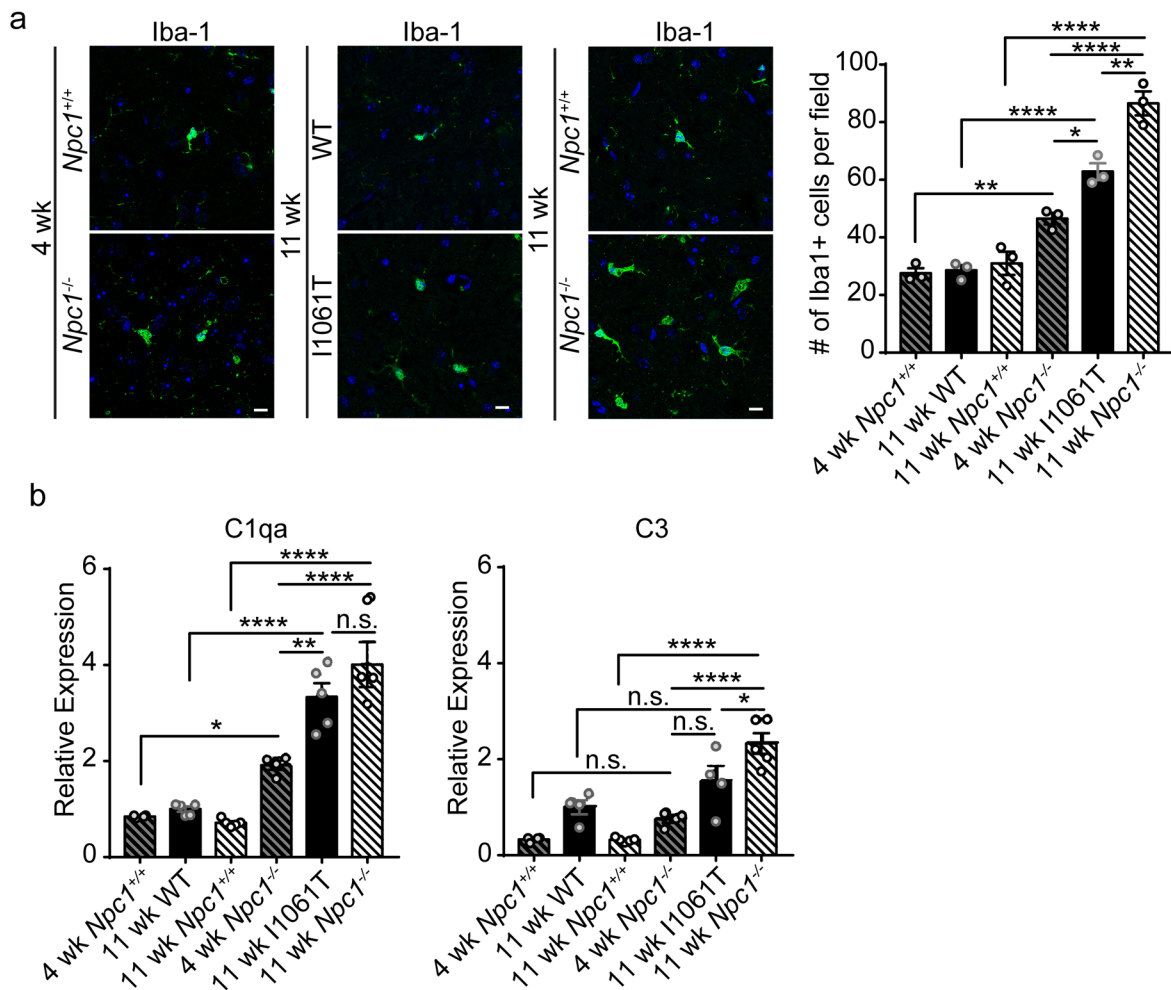***Figure 4.14 11-week Npc1-I1061T mice exhibit intermediate levels of microgliosis and complement activation compared to 4- and 11-week Npc1⁻/⁻ mice.. (a)*** Brainstem from 4-week *Npc1⁺/⁺* and *Npc1⁻/⁻* mice, 11-week WT and *Npc1-I1061T* mice, and 11-week *Npc1⁺/⁺* and *Npc1⁻/⁻* mice was stained with Iba-1 and imaged by confocal microscopy. Scale bar: 10 µm. *Right:* Iba1+ cells

per field, quantified from 4-5 fields, N=3 mice per genotype. **(b)** Relative expression of C1qa and C3 mRNA in brainstem by qPCR. N=4-5 mice per genotype. Data are shown as mean ± s.e.m. *$P \le 0.05$, **$P \le 0.01$, ****$P \le 0.0001$ by **(a-b)** one-way ANOVA with Tukey's multiple comparisons **(a)** F=64.48; **(b)** F=40.57 (C1qa) and F=22.51 (C3)

To more broadly assess neuroinflammation in the NPC brain, we examined induction of the immunoproteasome [83]. While the constitutive proteasome is a key effector of proteolysis, the immunoproteasome plays an important role in antigen processing and is induced in response to oxidative stress and proinflammatory cytokines in neurodegenerative diseases [84,85]. The constitutive proteasome is composed of a 20S cylindrical core containing four stacked α and β rings, with the β rings containing three catalytic β subunits (PSMB5-7). In contrast, the immunoproteasome incorporates three alternative β subunits (PSMB8-10) that replace the constitutive catalytic subunits as well as distinct 11S lid components (PSME1-2) [86]. In *Npc1-I1061T* mice, expression of these immunoproteasome subunits was increased in the cerebellum and brainstem in an age-dependent manner (Figure 4.15a-b, Figure 4.16a-b). This induction was specific to immunoproteasome subunits as expression of constitutive proteasome β subunits was unchanged (Figure 4.16c). Correspondingly, protein levels (Figure 4.15c) and activity (Figure 4.16d) of immunoproteasome subunits were increased, and immunofluorescence localized the immunoproteasome to both microglia and axonal spheroids (Figure 4.16e). Notably, immunoproteasome subunit expression was increased to comparable levels in the brainstem of 11-week *Npc1*^{-/-} mice (Figure 4.15d). Thus, robust neuroinflammation as reflected by microgliosis, complement expression, and immunoproteasome induction occured similarly in *Npc1*^{-/-} and *I1061T* mice. Our analyses suggest a role for alterative stressors in the occurrence of TDP-43 pathology in *Npc1*^{-/-} neurons.
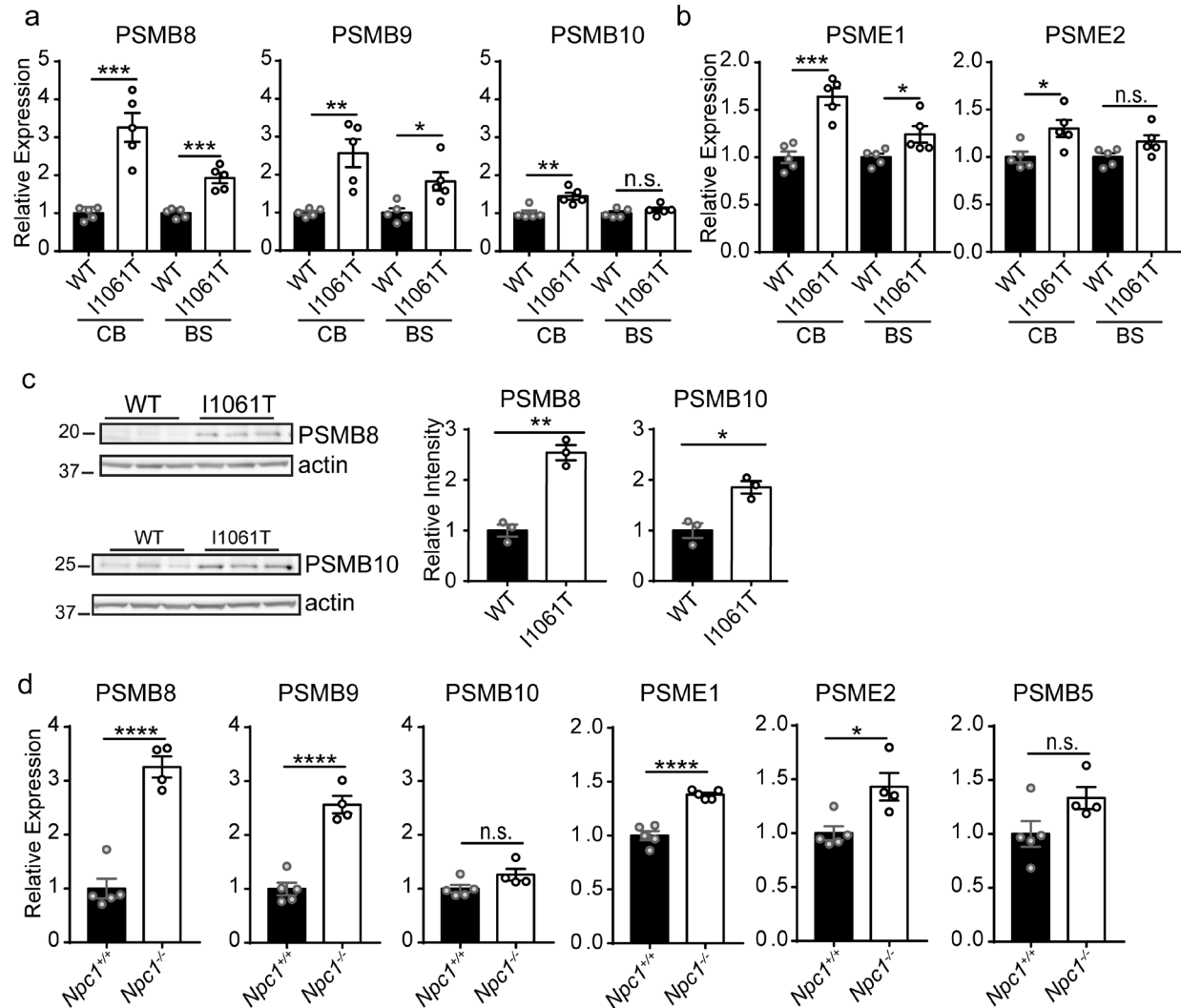
Figure 4.15 The immunoproteasome is induced in Npc1-I1061T and Npc1^{-/-} mice. **(a-b)** Relative expression of immunoproteasome 20S core subunits **(a)** and alternative lid **(b)** was determined in the cerebellum (CB) and brainstem (BS) of 12-week WT and *Npc1-I1061T* mice by qPCR. N=5 mice per genotype. **(c)** The relative abundance of immunoproteasome subunits in the cerebellum of 12-week WT and *Npc1-I1061T* mice was determined by western blot. N=3 mice per genotype. Quantified at right. **(d)** Relative expression of immunoproteasome, alternative lid and constitutive proteasome subunits was determined by qPCR in the brainstem of 11-week *Npc1^{+/+}* and *Npc1^{-/-}* mice. Data are shown as mean ± s.e.m. *P ≤ 0.05, **P ≤ 0.01, ***P ≤ 0.001, **** P ≤ 0.0001 by **(a-d)** Student's t-test **(a)** t=5.833 (CB PSMB8); t=6.27 (BS PSMB8); t=4.23 (CB PSMB9); t=3.088 (BS PSMB9); t=3.864 (CB PSMB10); t=1.083 (BS PSMB10) **(b)** t=5.893 (CB PSME1); t=2.556 (BS PSME1); t=2.853 (CB PSME2); t=2.077 (BS PSME2) **(c)** t=8.039 (PSMB8); t=4.454 (PSMB10) **(d)** t=8.351 (PSMB8); t=8.067 (PSMB9); t=2.077 (PSMB10); t=8.281 (PSME1); t=3.216 (PSME2); t=2.05 (PSMB5)
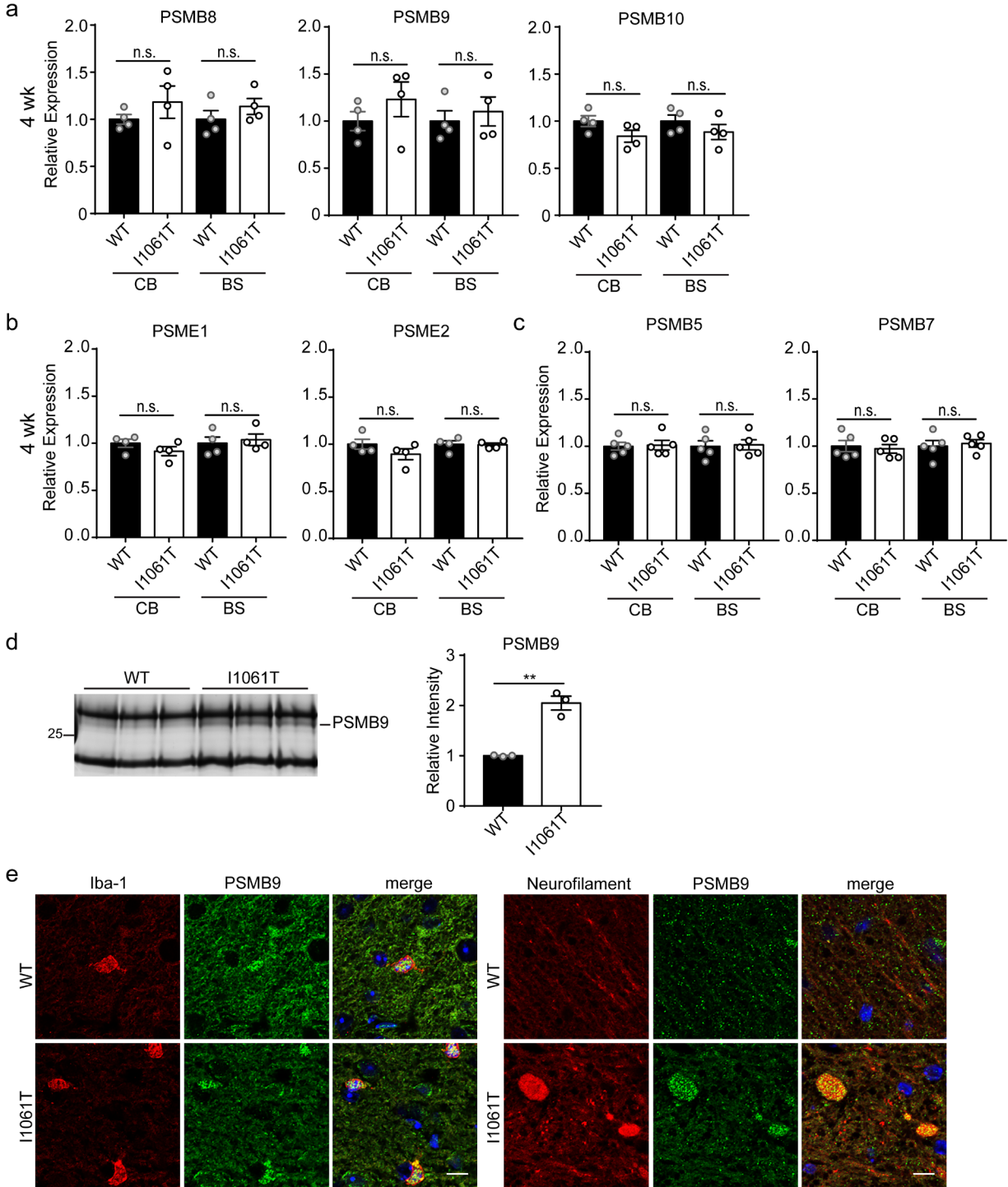
Figure 4.16 Age dependent induction of the immunoproteasome in Npc1-I1061T mice. **(a-c)** Relative expression of immunoproteasome 20S core **(a)**, alternative lid **(b)** and constitutive proteasome **(c)** subunits was determined by qPCR in the cerebellum (CB) and brainstem (BS) of 4-week **(a-b)** and 12-week **(c)** WT and *Npc1-I1061T* mice. N=4-5 mice per genotype. **(d)** Lysates from 8-week brainstem were incubated with a BODIPY-labeled activity-based probe, then resolved by SDS-PAGE. Quantification at right, N=3 mice per genotype. **(e)** Brainstem from 11-week WT and *Npc1-I1061T* mice was stained with the indicated markers and imaged by confocal microscopy. Scale bar: 10 μm. Data are shown as mean ± s.e.m. n.s., not significant, **P ≤ 0.005 by **(a-d)** Student's t-test **(a)** t=1.023 (CB PSMB8); t=1.088 (BS PSMB8); t=1.11 (CB PSMB9); t=0.5413 (BS PSMB9); t=1.873 (CB PSMB10); t=1.126 (BS PSMB10) **(b)** t=1.307 (CB PSME1); t=0.4092 (BS PSME1); t=1.353 (CB

118

PSME2); t=0.1487 (BS PSME2) **(c)** t=0.1711 (CB PSMB5); t=0.1898 (BS PSMB5); t=0.3676 (CB PSMB7); t=0.4048 (BS PSMB7) **(d)** t=7.489

4.4.5 Importin α mislocalization marks neurons with disrupted poly(A) RNA export and nuclear membrane morphology

With persistent cytoplasmic TDP-43 mislocalization in *Npc1*^{-/-} mice, we sought to characterize the functional consequences of this pathology. As TDP-43 proteinopathy has been associated with mislocalization or aggregation of nucleocytoplasmic transport factors and disruption of the nuclear membrane and nuclear pore complexes [66,74,87,88], we hypothesized that nucleocytoplasmic transport was disrupted in TDP-43 mislocalized neurons. To assess this hypothesis, we performed RNA fluorescence in situ hybridization (FISH) to quantify the N:C ratio of poly(A) RNA in *Npc1*^{-/-} neurons. We focused on the subpopulations of neurons that accumulated p62 versus those that accumulated importin α. We detected a significantly increased N:C ratio in importin α+ neurons (Figure 4.17a), indicating nuclear retention and a defect in poly(A) RNA export. Similar findings have been observed in models of TDP-43 proteinopathy [74,87,89]. Further indication of nuclear pathology in TDP-43 mislocalized neurons came from our observation of altered nuclear membrane morphology. Lamin B1 staining demonstrated significantly decreased circularity of the nuclear membrane in importin α+ neurons compared to p62+ neurons (Figure 4.17b). These results indicated that TDP-43 mislocalization in *Npc1*^{-/-} neurons compromises nucleocytoplasmic transport and nuclear membrane integrity, providing the first evidence of nuclear pathology in an LSD.
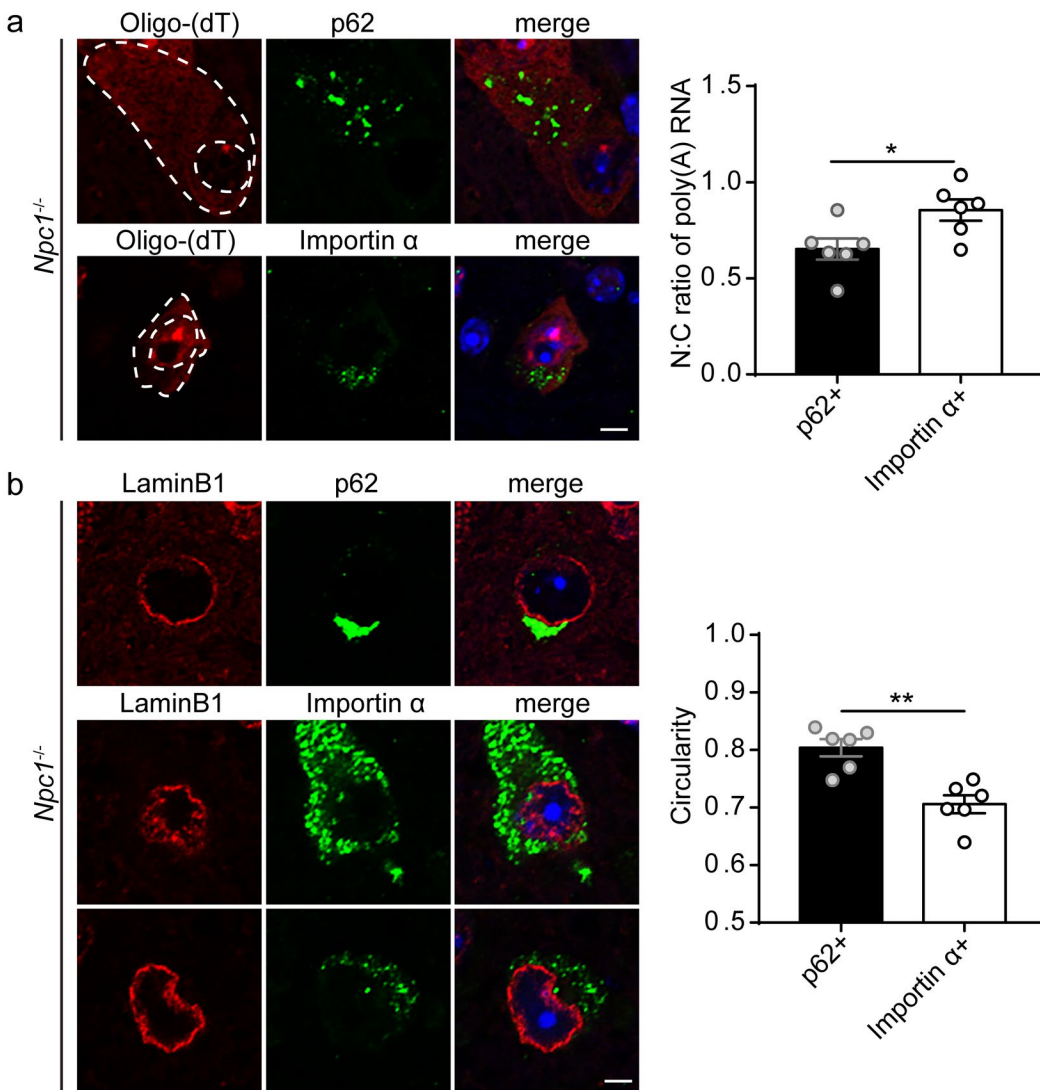
Figure 4.17 Importin α mislocalization marks neurons with disrupted poly(A) RNA export and nuclear membrane morphology. **(a)** Brainstem from 11-week Npc1^{-/-} mice was stained with p62 or importin α. Poly(A) RNA was detected by RNA fluorescence in situ hybridization (FISH) with an oligo(dT) probe and imaged by confocal microscopy. Scale bar: 5 µm. Poly(A) RNA N:C ratio quantified from 20-30 p62+ or importin α+ cells per mouse, with N=6 mice. **(b)** Brainstem from 11-week Npc1^{-/-} mice was stained with the indicated markers and imaged by confocal microscopy. Scale bar: 5 µm. Circularity of Lamin B1 staining was quantified from 20-30 p62+ or importin α+ cells per mouse, with N=6 mice. Data are shown as mean ± s.e.m. *P ≤ 0.05, **P ≤ 0.01, by **(a-b)** Student's t-test **(a)** t=2.603 **(b)** t=4.53

4.5 Discussion

We demonstrate novel aspects of degeneration in the NPC brain that are mediated by

TDP-43 proteinopathy, which we integrate into a model (Figure 4.18). NPC1-deficient neurons

exhibit mislocalization of TDP-43 that is characterized by hallmarks of cytoplasmic de-mixing,

an early stage in the aggregation process that was recently described in stressed neurons in cell culture [66]. Cytoplasmic TDP-43 in *Npc1*^{-/-} neurons co-localizes with the nuclear import factor importin α, but not with markers of stress granules or ubiquitinated protein aggregates, nor is it associated with loss of nuclear TDP-43 or the generation of C-terminal cleavage fragments. This pathology is remarkably stable in the brainstem of *Npc1* null mice, appearing as early as 4 weeks of age, before the onset of behavioral phenotypes, and remaining constant through end stage disease, almost two months later. Similarly long-lasting TDP-43 de-mixing has been documented to occur in cell culture [66].
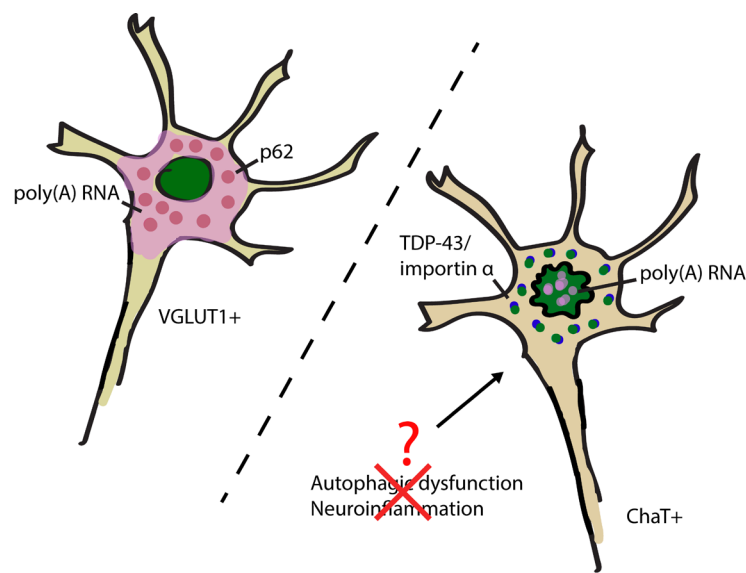
Figure 4.18 TDP-43 cytoplasmic mislocalization in NPC. TDP-43 cytoplasmic mislocalization and autophagic substrate accumulation occur independently and in distinct neuron subpopulations. VGLUT1+ neurons accumulated p62, while ChAT+ neurons accumulated mislocalized TDP-43 and importin α. These neurons were also marked with impaired poly(A) RNA export and abnormal nuclear membrane morphology. Autophagic dysfunction and neuroinflammation were not sufficient to drive TDP-43 mislocalization in NPC and point to the presence of other biological stressors involved.

Prior work has linked TDP-43 proteinopathy to LSDs in the context of progranulin mutations [22] and has suggested the occurrence of slightly diminished nuclear TDP-43 in cerebellar neurons of *Npc1*^{-/-} mice [90]. Our findings strengthen this connection with LSDs and expand the spectrum of TDP-43 proteinopathy in neurodegenerative brains by providing a first in vivo demonstration of stable cytoplasmic mislocalization that does not progress to ubiquitinated aggregates, even over several months. These observations indicate that while certain stressors are sufficient to induce TDP-43 mislocalization, distinct stressors are needed to promote its

cytoplasmic aggregation. This is in line with data from in vitro models where exposure of neurons to fragmented amyloid-like fibrils promotes TDP-43 de-mixing while additional sodium arsenite-induced stress converts these liquid droplets to gels/solids that later recruit p62 [66].

TDP-43 mislocalization occurs independently from the accumulation of autophagic cargo in the NPC brain. This conclusion is based on finding that these pathologies occur in distinct populations of neurons in *Npc1*^{-/-} mice and that *Npc1-I1061T* mice accumulate autophagic cargo but not mislocalized TDP-43. This was unexpected as autophagic dysfunction has been postulated to mediate TDP-43 proteinopathy [11-13], as mutations in autophagy genes cause ALS/FTD [15], and as inhibiting autophagy induces cytoplasmic accumulation of pathologic TDP-43 [65]. Furthermore, we demonstrate the occurrence of preferential susceptible to either TDP-43 proteinopathy (cholinergic) or autophagic dysfunction (glutamatergic) in distinct subpopulations of neurons, highlighting differential contributions to disease pathogenesis. Notably, neuroinflammation, as reflected by micogliosis, complement expression, and immunoproteasome induction, is insufficient to account for TDP-43 mislocalization in the NPC brain. Identifying the biological stressors in NPC that induce TDP-43 mislocalization without progression to insoluble aggregates emerges as an important unknown to be addressed by future research.

One intriguing hypothesis is that our observed cytoplasmic TDP-43 mislocalization represents a physiological response to neuronal injury. While TDP-43 cytoplasmic mislocalization without concomitant nuclear depletion and progression to aggregates is an unusual finding, it has been detected in motor neurons following axotomy. In these injured neurons, TDP-43 expression was upregulated and showed prominent cytosolic localization, findings that were restored following neuron recovery [91]. This was proposed to be due in part to TDP-43's involvement in neurofilament mRNA metabolism and transport to facilitate axonal

repair [92]. Thus, investigating the relationship between neuronal injury and TDP-43 cytoplasmic mislocalization could provide important insights on physiologic and/or pathologic roles of TDP-43 mislocalization in NPC.

Finally, our studies also provide the first demonstration of nuclear pathology in an LSD. Importin α mislocalizes with cytoplasmic TDP-43 in $Npc1^{-/-}$ neurons. These neurons also exhibit impaired nuclear export of RNA and abnormal nuclear membrane morphology. Similar disruption of nucleocytoplasmic transport and abnormalities of nuclear membrane architecture have been documented in other disorders with TDP-43 pathology [66,74,87,88]. Our observations suggest that shared mechanisms of lysosomal dysfunction and TDP-43 proteinopathy impair neuronal function in diverse degenerative disorders, including both LSDs and ALS/FTD. These shared disease mechanisms may provide future opportunities for therapeutic interventions that will benefit patients affected by these relentlessly progressive disorders.

4.6 Acknowledgements

References

1   Arai, T. *et al.* TDP-43 is a component of ubiquitin-positive tau-negative inclusions in frontotemporal lobar degeneration and amyotrophic lateral sclerosis. *Biochem Biophys Res Commun* **351**, 602-611, doi:10.1016/j.bbrc.2006.10.093 (2006).

2   Neumann, M. *et al.* Ubiquitinated TDP-43 in frontotemporal lobar degeneration and amyotrophic lateral sclerosis. *Science* **314**, 130-133, doi:10.1126/science.1134108 (2006).

3   Ling, S. C., Polymenidou, M. & Cleveland, D. W. Converging mechanisms in ALS and FTD: disrupted RNA and protein homeostasis. *Neuron* **79**, 416-438, doi:10.1016/j.neuron.2013.07.033 (2013).

4   Iguchi, Y. *et al.* Loss of TDP-43 causes age-dependent progressive motor neuron degeneration. *Brain* **136**, 1371-1382, doi:10.1093/brain/awt029 (2013).

5   Kraemer, B. C. *et al.* Loss of murine TDP-43 disrupts motor function and plays an essential role in embryogenesis. *Acta Neuropathol* **119**, 409-419, doi:10.1007/s00401-010-0659-0 (2010).

6   Swarup, V. *et al.* Pathological hallmarks of amyotrophic lateral sclerosis/frontotemporal lobar degeneration in transgenic mice produced with TDP-43 genomic fragments. *Brain* **134**, 2610-2626, doi:10.1093/brain/awr159 (2011).

7   Wils, H. *et al.* TDP-43 transgenic mice develop spastic paralysis and neuronal inclusions characteristic of ALS and frontotemporal lobar degeneration. *Proc Natl Acad Sci U S A* **107**, 3858-3863, doi:10.1073/pnas.0912417107 (2010).

8   Barmada, S. J. *et al.* Cytoplasmic mislocalization of TDP-43 is toxic to neurons and enhanced by a mutation associated with familial amyotrophic lateral sclerosis. *J Neurosci* **30**, 639-649, doi:10.1523/JNEUROSCI.4988-09.2010 (2010).

9   Lee, E. B., Lee, V. M. & Trojanowski, J. Q. Gains or losses: molecular mechanisms of TDP43-mediated neurodegeneration. *Nat Rev Neurosci* **13**, 38-50, doi:10.1038/nrn3121 (2011).

10   Johnson, B. S. *et al.* TDP-43 is intrinsically aggregation-prone, and amyotrophic lateral sclerosis-linked mutations accelerate aggregation and increase toxicity. *J Biol Chem* **284**, 20329-20339, doi:10.1074/jbc.M109.010264 (2009).

11   Scotter, E. L. *et al.* Differential roles of the ubiquitin proteasome system and autophagy in the clearance of soluble and aggregated TDP-43 species. *J Cell Sci* **127**, 1263-1278, doi:10.1242/jcs.140087 (2014).

12   Urushitani, M., Sato, T., Bamba, H., Hisa, Y. & Tooyama, I. Synergistic effect between proteasome and autophagosome in the clearance of polyubiquitinated TDP-43. *J Neurosci Res* **88**, 784-797, doi:10.1002/jnr.22243 (2010).

13   Wang, X. *et al.* Degradation of TDP-43 and its pathogenic form by autophagy and the ubiquitin-proteasome system. *Neurosci Lett* **469**, 112-116, doi:10.1016/j.neulet.2009.11.055 (2010).

14   Barmada, S. J. *et al.* Autophagy induction enhances TDP43 turnover and survival in neuronal ALS models. *Nat Chem Biol* **10**, 677-685, doi:10.1038/nchembio.1563 (2014).

15   Deng, Z., Sheehan, P., Chen, S. & Yue, Z. Is amyotrophic lateral sclerosis/frontotemporal dementia an autophagy disease? *Mol Neurodegener* **12**, 90, doi:10.1186/s13024-017-0232-6 (2017).

16   Deng, H. X. *et al.* Mutations in UBQLN2 cause dominant X-linked juvenile and adult-onset ALS and ALS/dementia. *Nature* **477**, 211-215, doi:10.1038/nature10353 (2011).

17   Fecto, F. *et al.* SQSTM1 mutations in familial and sporadic amyotrophic lateral sclerosis. *Arch Neurol* **68**, 1440-1446, doi:10.1001/archneurol.2011.250 (2011).

18   Johnson, J. O. *et al.* Exome sequencing reveals VCP mutations as a cause of familial ALS. *Neuron* **68**, 857-864, doi:10.1016/j.neuron.2010.11.036 (2010).

19   Maruyama, H. *et al.* Mutations of optineurin in amyotrophic lateral sclerosis. *Nature* **465**, 223-226, doi:10.1038/nature08971 (2010).

20   Murray, M. E. *et al.* Clinical and neuropathologic heterogeneity of c9FTD/ALS associated with hexanucleotide repeat expansion in C9ORF72. *Acta Neuropathol* **122**, 673-690, doi:10.1007/s00401-011-0907-y (2011).

21   Van Mossevelde, S. *et al.* Clinical features of TBK1 carriers compared with C9orf72, GRN and non-mutation carriers in a Belgian cohort. *Brain* **139**, 452-467, doi:10.1093/brain/awv358 (2016).

22   Gotzl, J. K. *et al.* Common pathobiochemical hallmarks of progranulin-associated frontotemporal lobar degeneration and neuronal ceroid lipofuscinosis. *Acta Neuropathol* **127**, 845-860, doi:10.1007/s00401-014-1262-6 (2014).

23   Pentchev, P. G. *et al.* A defect in cholesterol esterification in Niemann-Pick disease (type C) patients. *Proc Natl Acad Sci U S A* **82**, 8247-8251, doi:10.1073/pnas.82.23.8247 (1985).

24   Carstea, E. D. *et al.* Niemann-Pick C1 disease gene: homology to mediators of cholesterol homeostasis. *Science* **277**, 228-231 (1997).

25   Infante, R. E. *et al.* NPC2 facilitates bidirectional transfer of cholesterol between NPC1 and lipid bilayers, a step in cholesterol egress from lysosomes. *Proc Natl Acad Sci U S A* **105**, 15287-15292, doi:10.1073/pnas.0807328105 (2008).

26   Kwon, H. J. *et al.* Structure of N-terminal domain of NPC1 reveals distinct subdomains for binding and transfer of cholesterol. *Cell* **137**, 1213-1224, doi:10.1016/j.cell.2009.03.049 (2009).

27   Li, X. *et al.* Structure of human Niemann-Pick C1 protein. *Proc Natl Acad Sci U S A* **113**, 8212-8217, doi:10.1073/pnas.1607795113 (2016).

28   Qian, H. *et al.* Structural Basis of Low-pH-Dependent Lysosomal Cholesterol Egress by NPC1 and NPC2. *Cell* **182**, 98-111 e118, doi:10.1016/j.cell.2020.05.020 (2020).

29   Vanier, M. T. & Millat, G. Niemann-Pick disease type C. *Clin Genet* **64**, 269-281 (2003).

30   Davidson, C. D. *et al.* Chronic cyclodextrin treatment of murine Niemann-Pick C disease ameliorates neuronal cholesterol and glycosphingolipid storage and disease progression. *PLoS One* **4**, e6951, doi:10.1371/journal.pone.0006951 (2009).

31   Liu, B. *et al.* Reversal of defective lysosomal transport in NPC disease ameliorates liver dysfunction and neurodegeneration in the npc1-/- mouse. *Proc Natl Acad Sci U S A* **106**, 2377-2382, doi:10.1073/pnas.0810895106 (2009).

32   Vite, C. H. *et al.* Intracisternal cyclodextrin prevents cerebellar dysfunction and Purkinje cell death in feline Niemann-Pick type C1 disease. *Sci Transl Med* **7**, 276ra226, doi:10.1126/scitranslmed.3010101 (2015).

33   Schultz, M. L. *et al.* Synthetic high-density lipoprotein nanoparticles for the treatment of Niemann-Pick diseases. *BMC Med* **17**, 200, doi:10.1186/s12916-019-1423-5 (2019).

34   Chung, C., Puthanveetil, P., Ory, D. S. & Lieberman, A. P. Genetic and pharmacological evidence implicates cathepsins in Niemann-Pick C cerebellar degeneration. *Hum Mol Genet* **25**, 1434-1446, doi:10.1093/hmg/ddw025 (2016).

35   Davis, O. B. *et al.* NPC1-mTORC1 Signaling Couples Cholesterol Sensing to Organelle Homeostasis and Is a Targetable Pathway in Niemann-Pick Type C. *Dev Cell*, doi:10.1016/j.devcel.2020.11.016 (2020).

36   Liu, E. A. *et al.* Fbxo2 mediates clearance of damaged lysosomes and modifies neurodegeneration in the Niemann-Pick C brain. *JCI Insight* **5**, doi:10.1172/jci.insight.136676 (2020).

37   Yu, T., Shakkottai, V. G., Chung, C. & Lieberman, A. P. Temporal and cell-specific deletion establishes that neuronal Npc1 deficiency is sufficient to mediate neurodegeneration. *Hum Mol Genet* **20**, 4440-4451, doi:10.1093/hmg/ddr372 (2011).

38   Yu, T. & Lieberman, A. P. Npc1 acting in neurons and glia is essential for the formation and maintenance of CNS myelin. *PLoS Genet* **9**, e1003462, doi:10.1371/journal.pgen.1003462 (2013).

39   Lopez, M. E., Klein, A. D., Dimbil, U. J. & Scott, M. P. Anatomically defined neuron-based rescue of neurodegenerative Niemann-Pick type C disorder. *J Neurosci* **31**, 4367-4378, doi:10.1523/JNEUROSCI.5981-10.2011 (2011).

40   Lieberman, A. P. *et al.* Autophagy in lysosomal storage disorders. *Autophagy* **8**, 719-730, doi:10.4161/auto.19469 (2012).

41   Elrick, M. J., Yu, T., Chung, C. & Lieberman, A. P. Impaired proteolysis underlies autophagic dysfunction in Niemann-Pick type C disease. *Hum Mol Genet* **21**, 4876-4887, doi:10.1093/hmg/dds324 (2012).

42   Ko, D. C. *et al.* Cell-autonomous death of cerebellar purkinje neurons with autophagy in Niemann-Pick type C disease. *PLoS Genet* **1**, 81-95, doi:10.1371/journal.pgen.0010007 (2005).

43   Liao, G. *et al.* Cholesterol accumulation is associated with lysosomal dysfunction and autophagic stress in Npc1 -/- mouse brain. *Am J Pathol* **171**, 962-975, doi:10.2353/ajpath.2007.070052 (2007).

44   Maetzel, D. *et al.* Genetic and chemical correction of cholesterol accumulation and impaired autophagy in hepatic and neural cells derived from Niemann-Pick Type C patient-specific iPS cells. *Stem Cell Reports* **2**, 866-880, doi:10.1016/j.stemcr.2014.03.014 (2014).

45   Meske, V., Erz, J., Priesnitz, T. & Ohm, T. G. The autophagic defect in Niemann-Pick disease type C neurons differs from somatic cells and reduces neuronal viability. *Neurobiol Dis* **64**, 88-97, doi:10.1016/j.nbd.2013.12.018 (2014).

46   Ordonez, M. P. *et al.* Disruption and therapeutic rescue of autophagy in a human neuronal model of Niemann Pick type C1. *Hum Mol Genet* **21**, 2651-2662, doi:10.1093/hmg/dds090 (2012).

47   Pacheco, C. D., Kunkel, R. & Lieberman, A. P. Autophagy in Niemann-Pick C disease is dependent upon Beclin-1 and responsive to lipid trafficking defects. *Hum Mol Genet* **16**, 1495-1503, doi:10.1093/hmg/ddm100 (2007).

48   Sarkar, S. *et al.* Impaired autophagy in the lipid-storage disorder Niemann-Pick type C1 disease. *Cell Rep* **5**, 1302-1315, doi:10.1016/j.celrep.2013.10.042 (2013).

49   Elrick, M. J. *et al.* Conditional Niemann-Pick C mice demonstrate cell autonomous Purkinje cell neurodegeneration. *Hum Mol Genet* **19**, 837-847, doi:10.1093/hmg/ddp552 (2010).

50   Praggastis, M. *et al.* A murine Niemann-Pick C1 I1061T knock-in model recapitulates the pathological features of the most prevalent human disease allele. *J Neurosci* **35**, 8091-8106, doi:10.1523/JNEUROSCI.4173-14.2015 (2015).

51   de Jong, A., Schuurman, K. G., Rodenko, B., Ovaa, H. & Berkers, C. R. Fluorescence-based proteasome activity profiling. *Methods Mol Biol* **803**, 183-204, doi:10.1007/978-1-61779-364-6_13 (2012).

52   Zhu, Y. *et al.* Ablation of NF1 function in neurons induces abnormal development of cerebral cortex and reactive gliosis in the brain. *Genes Dev* **15**, 859-876, doi:10.1101/gad.862101 (2001).

53   Maday, S. Mechanisms of neuronal homeostasis: Autophagy in the axon. *Brain Res* **1649**, 143-150, doi:10.1016/j.brainres.2016.03.047 (2016).

54   Maday, S. & Holzbaur, E. L. Autophagosome biogenesis in primary neurons follows an ordered and spatially regulated pathway. *Dev Cell* **30**, 71-85, doi:10.1016/j.devcel.2014.06.001 (2014).

55   Maday, S., Wallace, K. E. & Holzbaur, E. L. Autophagosomes initiate distally and mature during transport toward the cell soma in primary neurons. *J Cell Biol* **196**, 407-417, doi:10.1083/jcb.201106120 (2012).

56   Komatsu, M. *et al.* Essential role for autophagy protein Atg7 in the maintenance of axonal homeostasis and the prevention of axonal degeneration. *Proc Natl Acad Sci U S A* **104**, 14489-14494, doi:10.1073/pnas.0701311104 (2007).

57   Nishiyama, J., Miura, E., Mizushima, N., Watanabe, M. & Yuzaki, M. Aberrant membranes and double-membrane structures accumulate in the axons of Atg5-null Purkinje cells before neuronal death. *Autophagy* **3**, 591-596, doi:10.4161/auto.4964 (2007).

58   Gowrishankar, S. *et al.* Massive accumulation of luminal protease-deficient axonal lysosomes at Alzheimer's disease amyloid plaques. *Proc Natl Acad Sci U S A* **112**, E3699-3708, doi:10.1073/pnas.1510329112 (2015).

59   Nixon, R. A. *et al.* Extensive involvement of autophagy in Alzheimer disease: an immuno-electron microscopy study. *J Neuropathol Exp Neurol* **64**, 113-122, doi:10.1093/jnen/64.2.113 (2005).

60   Tammineni, P., Jeong, Y. Y., Feng, T., Aikal, D. & Cai, Q. Impaired axonal retrograde trafficking of the retromer complex augments lysosomal deficits in Alzheimer's disease neurons. *Hum Mol Genet* **26**, 4352-4366, doi:10.1093/hmg/ddx321 (2017).

61   Xie, Y. *et al.* Endolysosomal Deficits Augment Mitochondria Pathology in Spinal Motor Neurons of Asymptomatic fALS Mice. *Neuron* **87**, 355-370, doi:10.1016/j.neuron.2015.06.026 (2015).

62   Kennedy, B. E. *et al.* Adaptations of energy metabolism associated with increased levels of mitochondrial cholesterol in Niemann-Pick type C1-deficient cells. *J Biol Chem* **289**, 16278-16289, doi:10.1074/jbc.M114.559914 (2014).

63   Wos, M. *et al.* Mitochondrial dysfunction in fibroblasts derived from patients with Niemann-Pick type C disease. *Arch Biochem Biophys* **593**, 50-59, doi:10.1016/j.abb.2016.02.012 (2016).

64   Kane, L. A. *et al.* PINK1 phosphorylates ubiquitin to activate Parkin E3 ubiquitin ligase activity. *J Cell Biol* **205**, 143-153, doi:10.1083/jcb.201402104 (2014).

65   Chang, M. C. *et al.* Progranulin deficiency causes impairment of autophagy and TDP-43 accumulation. *J Exp Med* **214**, 2611-2628, doi:10.1084/jem.20160999 (2017).

66   Gasset-Rosa, F. *et al.* Cytoplasmic TDP-43 De-mixing Independent of Stress Granules Drives Inhibition of Nuclear Import, Loss of Nuclear TDP-43, and Cell Death. *Neuron* **102**, 339-357 e337, doi:10.1016/j.neuron.2019.02.038 (2019).

67   Nana, A. L. *et al.* Neurons selectively targeted in frontotemporal dementia reveal early stage TDP-43 pathobiology. *Acta Neuropathol* **137**, 27-46, doi:10.1007/s00401-018-1942-8 (2019).

68   Conicella, A. E., Zerze, G. H., Mittal, J. & Fawzi, N. L. ALS Mutations Disrupt Phase Separation Mediated by alpha-Helical Structure in the TDP-43 Low-Complexity C-Terminal Domain. *Structure* **24**, 1537-1549, doi:10.1016/j.str.2016.07.007 (2016).

69   Harrison, A. F. & Shorter, J. RNA-binding proteins with prion-like domains in health and disease. *Biochem J* **474**, 1417-1438, doi:10.1042/BCJ20160499 (2017).

70   Colombrita, C. *et al.* TDP-43 is recruited to stress granules in conditions of oxidative insult. *J Neurochem* **111**, 1051-1061, doi:10.1111/j.1471-4159.2009.06383.x (2009).

71   Li, Y. R., King, O. D., Shorter, J. & Gitler, A. D. Stress granules as crucibles of ALS pathogenesis. *J Cell Biol* **201**, 361-372, doi:10.1083/jcb.201302044 (2013).

72   Parker, S. J. *et al.* Endogenous TDP-43 localized to stress granules can subsequently form protein aggregates. *Neurochem Int* **60**, 415-424, doi:10.1016/j.neuint.2012.01.019 (2012).

73   Mann, J. R. *et al.* RNA Binding Antagonizes Neurotoxic Phase Transitions of TDP-43. *Neuron* **102**, 321-338 e328, doi:10.1016/j.neuron.2019.01.048 (2019).

74   Chou, C. C. *et al.* TDP-43 pathology disrupts nuclear pore complexes and nucleocytoplasmic transport in ALS/FTD. *Nat Neurosci* **21**, 228-239, doi:10.1038/s41593-017-0047-3 (2018).

75   Lin, T. W. *et al.* Regulation of Synapse Development by Vgat Deletion from ErbB4-Positive Interneurons. *J Neurosci* **38**, 2533-2550, doi:10.1523/JNEUROSCI.0669-17.2018 (2018).

76   Vanier, M. T. Niemann-Pick disease type C. *Orphanet J Rare Dis* **5**, 16, doi:10.1186/1750-1172-5-16 (2010).

77   Gelsthorpe, M. E. *et al.* Niemann-Pick type C1 I1061T mutant encodes a functional protein that is selected for endoplasmic reticulum-associated degradation due to protein misfolding. *J Biol Chem* **283**, 8229-8236, doi:10.1074/jbc.M708735200 (2008).

78   Schultz, M. L. *et al.* Coordinate regulation of mutant NPC1 degradation by selective ER autophagy and MARCH6-dependent ERAD. *Nat Commun* **9**, 3671, doi:10.1038/s41467-018-06115-2 (2018).

79   Cunningham, C. Microglia and neurodegeneration: the role of systemic inflammation. *Glia* **61**, 71-90, doi:10.1002/glia.22350 (2013).

80   Hickman, S., Izzy, S., Sen, P., Morsett, L. & El Khoury, J. Microglia in neurodegeneration. *Nat Neurosci* **21**, 1359-1369, doi:10.1038/s41593-018-0242-x (2018).

81   Hanisch, U. K. & Kettenmann, H. Microglia: active sensor and versatile effector cells in the normal and pathologic brain. *Nat Neurosci* **10**, 1387-1394, doi:10.1038/nn1997 (2007).

82   Zhang, J. *et al.* Neurotoxic microglia promote TDP-43 proteinopathy in progranulin deficiency. *Nature* **588**, 459-465, doi:10.1038/s41586-020-2709-7 (2020).

83   Moritz, K. E. *et al.* The role of the immunoproteasome in interferon-gamma-mediated microglial activation. *Sci Rep* **7**, 9365, doi:10.1038/s41598-017-09715-y (2017).

84   Orre, M. *et al.* Reactive glia show increased immunoproteasome activity in Alzheimer's disease. *Brain* **136**, 1415-1431, doi:10.1093/brain/awt083 (2013).

85   Wagner, L. K. *et al.* Immunoproteasome deficiency alters microglial cytokine response and improves cognitive deficits in Alzheimer's disease-like APPPS1 mice. *Acta Neuropathol Commun* **5**, 52, doi:10.1186/s40478-017-0453-5 (2017).

86   Ferrington, D. A. & Gregerson, D. S. Immunoproteasomes: structure, function, and antigen presentation. *Prog Mol Biol Transl Sci* **109**, 75-112, doi:10.1016/B978-0-12-397863-9.00003-1 (2012).

87   Freibaum, B. D. *et al.* GGGGCC repeat expansion in C9orf72 compromises nucleocytoplasmic transport. *Nature* **525**, 129-133, doi:10.1038/nature14974 (2015).

88   Zhang, K. *et al.* The C9orf72 repeat expansion disrupts nucleocytoplasmic transport. *Nature* **525**, 56-61, doi:10.1038/nature14973 (2015).

89   Woerner, A. C. *et al.* Cytoplasmic protein aggregates interfere with nucleocytoplasmic transport of protein and RNA. *Science* **351**, 173-176, doi:10.1126/science.aad2033 (2016).

90   Dardis, A. *et al.* Altered localization and functionality of TAR DNA Binding Protein 43 (TDP-43) in niemann- pick disease type C. *Acta Neuropathol Commun* **4**, 52, doi:10.1186/s40478-016-0325-4 (2016).

91   Moisse, K. *et al.* Divergent patterns of cytosolic TDP-43 and neuronal progranulin expression following axotomy: implications for TDP-43 in the physiological response to neuronal injury. *Brain Res* **1249**, 202-211, doi:10.1016/j.brainres.2008.10.021 (2009).

92   Moisse, K. *et al.* Cytosolic TDP-43 expression following axotomy is associated with caspase 3 activation in NFL-/- mice: support for a role for TDP-43 in the physiological response to neuronal injury. *Brain Res* **1296**, 176-186, doi:10.1016/j.brainres.2009.07.023 (2009).

Chapter 5

Conclusion

In this dissertation, I investigated mechanisms of neurodegeneration in Niemann-Pick type C disease (NPC). I demonstrated that NPC cells are more sensitive to lysosomal damage, and that this sensitivity is dependent upon lipid storage. Furthermore, I described a novel role of Fbxo2 in lysophagy and show that depletion of Fbxo2 in NPC mice exacerbates disease phenotypes. My data support a model in which increased levels of lysosomal damage in NPC makes neurons vulnerable to lysosomal membrane permeabilization (LMP), necessitating functional lysophagy to prevent cytotoxicity. Additionally, I provide a detailed characterization of TDP-43 pathology in NPC. I show that TDP-43 mislocalization persists for months in vivo and resembles TDP-43 de-mixing rather than ubiquitinated aggregates. I show that this pathology occurs independently of autophagic dysfunction and is associated with nuclear membrane and nucleocytoplasmic transport abnormalities. In this final chapter, I will discuss questions that remain from this work and suggest future directions.

5.1 Lysosomal damage and lysophagy in NPC

In Chapter 3, I highlighted the importance of functioning lysophagy to protect against lysosomal membrane permeabilization in NPC. Our interest in this work began as LMP has been implicated in an increasing number of lysosomal diseases [1-7]. Prior work in our lab also

demonstrated mislocalization of lysosomal cathepsins outside the lysosomal compartment in NPC neurons and showed that NPC mice deficient in cystatin B, an inhibitor of cathepsins, exhibited exacerbated cerebellar degeneration [2]. I sought to build on this work and examine factors that cause increased sensitivity to lysosomal damage in NPC and investigate mechanisms the cell uses to respond to LMP and reduce its cytotoxic effects.

As autophagy defects are well described in NPC, I examined whether inability to clear damaged lysosomes by lysophagy could explain the increased numbers of damaged lysosomes. Through time-course experiments, I showed that lysophagy progresses at a similar rate to controls, indicating that impaired lysophagy is not the primary driver of the increased lysosomal damage. LMP can be induced by numerous endogenous and exogenous factors, including oxidative stress, pathogens and lysosomotropic drugs [8]. Notably, accumulated lipids have been shown to trigger LMP [3-5,9-11]. I showed that reduction of cholesterol storage with cyclodextrin significantly reduced the level of lysosomal damage triggered by LLOMe, supporting a role for stored lipids in altering lysosomal membrane integrity. In contrast, studies have also described the importance of lipids in membrane rigidity and lysosomal membrane stability, and others have shown that reducing lysosomal cholesterol sensitizes cells to lysosomal damage [12-14]. This raises questions as to the extent to which stored lipids either exacerbate or guard against LMP in NPC. Notably, the absence of functional NPC1 protein is expected to impair the movement of luminal cholesterol into the limiting membrane of the lysosome, leading to luminal cholesterol accumulation. Still, NPC1 deficient cells also accumulate cholesterol in the lysosomal limiting membrane, which is deposited from the ER through organelle membrane contact sites [15]. Thus, there may be opposing effects between destabilizing effects of luminal cholesterol and stabilizing effects of membrane cholesterol, although, increased lipid content in membranes could also alter

membrane fluidity and impact membrane stability. Defining the role of altered luminal versus lysosomal membrane lipid composition and their effects on lysosomal membrane stability, in addition to the mechanisms by which cholesterol transfers between different compartments, will be important in furthering our understanding of lysosomal dysfunction in NPC.

In this study I also identified a novel role for Fbxo2 in the clearance of damaged lysosomes in the brain. Depletion of Fbxo2 exacerbated the disease phenotype in NPC mice and *Fbxo2*^{-/-} neurons exhibited delayed clearance of damaged lysosomes and increased toxicity in response to LLOMe. This work highlights the critical importance of functioning lysophagy in NPC where there exists a background of increased lysosomal damage. An important next step would be to identify methods of targeting the lysophagy pathway to determine whether enhancing lysophagy or modulating the pathway could protect against neuron death in NPC. Overexpression of Fbxo27, previously shown to function in the SCF complex to ubiquitinate glycoproteins and target damaged lysosome for degradation, increased ubiquitination of glycoproteins [16]. However, it is unclear whether this could also enhance clearance of damaged lysosomes. Similarly, the question arises as to whether increased expression of Fbxo2 could impact lysophagy progression in the brain. However, overexpression of Fbxo2 has been shown to be detrimental in other systems, as it leads to aberrant glucose homeostasis and promotes proliferation of endometrial cancer by promoting ubiquitination and degradation of essential proteins [17,18] . Thus, balancing a possible induction of lysophagy with off target effects of ubiquitination would be a likely challenge. Notably, depletion of Fbxo2 did not completely abolish lysophagy progression in neurons, but rather delayed it. Additional pathways likely function to mediate lysophagy in the brain, and other proteins been shown to function in lysophagy and ubiquitination, including TRIM16 [19]. Investigating additional factors at play

would open up targets for lysophagy modulation. On a broader level, it is still an area of investigation as to how modulation of autophagy impacts disease pathogenesis in NPC, as both induction and inhibition have been shown to be detrimental and beneficial [20-23]. Autophagy inhibition impairs lysophagy progression [24,25], which could contribute to worsening disease phenotypes as it increases levels of lysosomal damage. Thus, investigating how autophagy modulation impacts lysosomal damage and lysophagy in NPC would provide insight on optimal autophagy modulation methods to improve disease phenotypes.

In examining lysosomal damage, I focused on characterizing lysophagy, which is important to clear damaged lysosomes. However, damaged lysosomes can also be repaired by the Endosomal Sorting Complex Required for Transport (ESCRT) machinery [26,27]. ESCRT-mediated repair is thought to be an early event in "low damage" conditions; lysosomes that are not repaired are degraded by lysophagy [19]. A recent study showed increased accumulation of ESCRT III components, including CHMP1A and CHMP2B, on lysosomes, a finding that indicates ongoing lysosomal damage [28]. However, despite recruitment of ESCRT machinery, the extent to which ESCRT repair functions adequately to repair damaged in lysosomes in NPC is not determined. Investigating the ESCRT repair pathway in NPC, the extent to which it functions and the effects of modulation would be an interesting future direction and open up the possibility of another pathway that can be targeted to minimize lysosomal damage in NPC.

5.2 Neuron autophagy dysregulation and TDP-43 proteinopathy

In Chapter 4, I characterized TDP-43 mislocalization in the NPC brain, factors that contribute to its development, and its functional effects. I found that TDP-43 mislocalization begins at an early stage in the disease course in $Npc1^{-/-}$ mice and resembles TDP-43 de-mixing

rather than cytoplasmic aggregates. Despite the connection between autophagic dysfunction and TDP-43 pathology, I found that TDP-43 mislocalization occurs independently of autophagy defects in NPC. Similarly, microgliosis and complement activation, also implicated in TDP-43 pathology, were not sufficient to drive TDP-43 pathology. These data raise questions as to the biological stressors that drive TDP-43 mislocalization without progression to ubiquitinated aggregates and nuclear depletion in $Npc1^{-/-}$ mice. TDP-43 mislocalization has been described in an NPC human neuronal model, where it was shown that oxidative stress and stored lipids contribute TDP-43 cytoplasmic accumulation [29]. Another possibility arises from alternative degradative pathways that have been implicated in clearing TDP-43. In yeast and human cell lines, TDP-43 turnover, aggregation and toxicity strongly depend on endocytosis [30]. TDP-43 co-localizes with multiple endocytosis proteins, TDP-43 expression impairs endocytosis, and enhancing endocytosis rescues TDP-43 levels and toxicity [30]. Although in human cells, endocytosis and autophagic pathways typically converge prior to lysosomal fusion [31], Rab5 overexpression, while blocking autophagy, reduced TDP-43 protein to pre-treatment levels, indicating that a Rab5-enhanced, autophagy-independent mechanism exists to clear TDP-43 [30]. Additionally, TDP-43 was found to co-localize with VCP in ALS patient tissue, and VCP facilitated endocytic function to regulate TDP-43 toxicity and turnover [32]. NPC1 deficient cells also display disruption in endocytosis [33]. Whether this contributes to TDP-43 mislocalization is not described, but could shed insight on mechanisms of TDP-43 proteinopathy in NPC.

Although I found that autophagic dysfunction occurred independently of TDP-43 mislocalization, the finding of autophagic substrate accumulation within axonal spheroids is of interest as it implies a defect in axonal transport during neuronal autophagy. Autophagosomes are formed in the distal axon and undergo retrograde transport towards the cell body where they

are degraded [34]. Impairments in neuron autophagy lead to accumulation of autophagosomes within swollen axons [35]. This is often linked to defects in retrograde transport, suggesting that impaired cargo motility leads to accumulation of dysfunctional organelles along axons [36]. Consistent with this hypothesis, inhibition of dynein leads to the accumulation of autophagosomes and axonal swellings [37]. Deficiency in JIP3, a motor scaffolding protein, leads to accumulation of autophagic vacuoles [38] and JIP3 KO neurons accumulate axonal swellings [39]. Similarly, deletion of Snapin, another scaffolding protein, leads to retention of autophagic vacuoles in distal axons, while overexpression of Snapin rescues impairments in retrograde transport and reduces the accumulation of autophagic vacuoles in Alzheimer disease neurons [40]. Exploring the extent to which axonal transport is impaired and its contribution to axonal pathology, mechanisms of dysregulation of axonal transport, and ways to modulate transport and rescue autophagic dysfunction are interesting directions to pursue.

Furthermore, my work provided the first description of nuclear pathology in an LSD. I showed that TDP-43 mislocalization is associated with abnormal nuclear membrane morphology, mislocalization of importin α and impaired mRNA export. A next step would be to investigate other proteins that could exhibit altered trafficking in TDP-43 mislocalized neurons. Importin α mislocalization is expected to lead to impaired import of other NLS-containing proteins. Furthermore, importin α has been demonstrated to be involved in functions in addition to nuclear import, including spindle formation, retrograde axonal transport in neurons, stress granule assembly, and nuclear envelope and lamin assembly [41]. Exploring other downstream effects of TDP-43 and importin α mislocalization would shed greater insight on disease mechanisms. Another major function of TDP-43 is in RNA processing. TDP-43 binds to over 6000 pre-mRNAs and affects levels of 601 mRNAs and splicing of another 965 [42]. Some ALS-

linked TDP-43 mutations also cause altered RNA splicing and promote motor neuron disease without cytoplasmic aggregation or loss of nuclear TDP-43 [43]. Thus, despite lack of TDP-43 aggregates or nuclear clearing seen in NPC, mislocalized TDP-43 could impact normal RNA processing in neurons. In addition to impaired mRNA export, altered splicing would have large effects on gene expression. This would be an important future direction to investigate.

With the observation that TDP-43 mislocalization occurs in a separate subset of neurons than those that accumulate autophagic substrates, I sought to identify affected neuron populations. Interestingly, I found that brainstem cholinergic neurons were preferentially affected by TDP-43 mislocalization, while brainstem glutamatergic neurons exhibited hallmarks of autophagic dysfunction. Although cholinergic neurons comprise less than one percent of neurons in the nervous system, their influence is vast as almost every brain region and peripheral target receives a cholinergic input, and cholinergic neurons are involved in functions from gross movement to consciousness [44]. Descending projections from mesopontine cholinergic neurons play a role in decreasing muscle tone during rapid eye movement (REM) sleep, and ascending projections play roles in higher cognitive function [44]. Sleep abnormalities have also been observed in NPC patients, including REM sleep behavior disorder [45,46]. This raises the possibility that TDP-43 mislocalization in cholinergic neurons could contribute to disrupted sleep in NPC. Lower motor neurons in the brainstem and spinal cord are also cholinergic and lesions in lower motor neurons lead to paralysis [47]. TDP-43 proteinopathy is also localized in spinal cord motor neurons in ALS. My studies focused on examining TDP-43 pathology in the brainstem, but its presence in cholinergic neurons raises the possibility of similar pathology within spinal cord lower motor neurons. Spinal cord and lower motor neuron pathology is not well characterized in NPC. Thus, characterizing spinal cord pathology would provide insight on mechanisms of

neurodegeneration and motor impairment in NPC. Further investigation of TDP-43

proteinopathy in human patients will also be of importance, particularly as it relates to the wide

spectrum of patient mutations.

5.3 Concluding Remarks

Niemann-Pick type C is an autosomal recessive lipid storage disorder that causes

neurodegeneration and early death. Currently, there are no FDA approved treatments.

Understanding cellular mechanisms of disease is vital to uncover therapeutic targets to combat

this devastating disease. In my thesis, I examined the effects of lysosomal damage and the

importance of lysophagy in disease, while defining a new function for Fbxo2. Furthermore, I

provided a detailed characterization of TDP-43 proteinopathy in the NPC brain and its functional

effects as it relates to nucleocytoplasmic transport and nuclear pathology. I hope the work I

described will enhance our understanding of disease mechanisms and enable the development of

targeted and effective treatments for NPC patients.

References

1   Amritraj, A. *et al.* Increased activity and altered subcellular distribution of lysosomal enzymes determine neuronal vulnerability in Niemann-Pick type C1-deficient mice. *Am J Pathol* **175**, 2540-2556, doi:10.2353/ajpath.2009.081096 (2009).
2   Chung, C., Puthanveetil, P., Ory, D. S. & Lieberman, A. P. Genetic and pharmacological evidence implicates cathepsins in Niemann-Pick C cerebellar degeneration. *Hum Mol Genet* **25**, 1434-1446, doi:10.1093/hmg/ddw025 (2016).
3   Gabande-Rodriguez, E., Boya, P., Labrador, V., Dotti, C. G. & Ledesma, M. D. High sphingomyelin levels induce lysosomal damage and autophagy dysfunction in Niemann Pick disease type A. *Cell Death Differ* **21**, 864-875, doi:10.1038/cdd.2014.4 (2014).
4   Gabande-Rodriguez, E. *et al.* Lipid-induced lysosomal damage after demyelination corrupts microglia protective function in lysosomal storage disorders. *EMBO J* **38**, doi:10.15252/embj.201899553 (2019).

5   Kirkegaard, T. *et al.* Hsp70 stabilizes lysosomes and reverts Niemann-Pick disease-associated lysosomal pathology. *Nature* **463**, 549-553, doi:10.1038/nature08710 (2010).

6   Micsenyi, M. C., Sikora, J., Stephney, G., Dobrenis, K. & Walkley, S. U. Lysosomal membrane permeability stimulates protein aggregate formation in neurons of a lysosomal disease. *J Neurosci* **33**, 10815-10827, doi:10.1523/JNEUROSCI.0987-13.2013 (2013).

7   Vitner, E. B. *et al.* Altered expression and distribution of cathepsins in neuronopathic forms of Gaucher disease and in other sphingolipidoses. *Hum Mol Genet* **19**, 3583-3590, doi:10.1093/hmg/ddq273 (2010).

8   Papadopoulos, C. & Meyer, H. Detection and Clearance of Damaged Lysosomes by the Endo-Lysosomal Damage Response and Lysophagy. *Curr Biol* **27**, R1330-R1341, doi:10.1016/j.cub.2017.11.012 (2017).

9   Magtanong, L., Ko, P. J. & Dixon, S. J. Emerging roles for lipids in non-apoptotic cell death. *Cell Death Differ* **23**, 1099-1109, doi:10.1038/cdd.2016.25 (2016).

10   Rajamaki, K. *et al.* Cholesterol crystals activate the NLRP3 inflammasome in human macrophages: a novel link between cholesterol metabolism and inflammation. *PLoS One* **5**, e11765, doi:10.1371/journal.pone.0011765 (2010).

11   Cantuti-Castelvetri, L. *et al.* Defective cholesterol clearance limits remyelination in the aged central nervous system. *Science* **359**, 684-688, doi:10.1126/science.aan4183 (2018).

12   Appelqvist, H. *et al.* Attenuation of the lysosomal death pathway by lysosomal cholesterol accumulation. *Am J Pathol* **178**, 629-639, doi:10.1016/j.ajpath.2010.10.030 (2011).

13   Appelqvist, H. *et al.* Sensitivity to lysosome-dependent cell death is directly regulated by lysosomal cholesterol content. *PLoS One* **7**, e50262, doi:10.1371/journal.pone.0050262 (2012).

14   Repnik, U., Hafner Cesen, M. & Turk, B. Lysosomal membrane permeabilization in cell death: concepts and challenges. *Mitochondrion* **19 Pt A**, 49-57, doi:10.1016/j.mito.2014.06.006 (2014).

15   Lim, C. Y. *et al.* ER-lysosome contacts enable cholesterol sensing by mTORC1 and drive aberrant growth signalling in Niemann-Pick type C. *Nat Cell Biol* **21**, 1206-1218, doi:10.1038/s41556-019-0391-5 (2019).

16   Yoshida, Y. *et al.* Ubiquitination of exposed glycoproteins by SCF(FBXO27) directs damaged lysosomes for autophagy. *Proc Natl Acad Sci U S A* **114**, 8574-8579, doi:10.1073/pnas.1702615114 (2017).

17   Che, X. *et al.* FBXO2 Promotes Proliferation of Endometrial Cancer by Ubiquitin-Mediated Degradation of FBN1 in the Regulation of the Cell Cycle and the Autophagy Pathway. *Front Cell Dev Biol* **8**, 843, doi:10.3389/fcell.2020.00843 (2020).

18   Liu, B. *et al.* Aberrant Expression of FBXO2 Disrupts Glucose Homeostasis Through Ubiquitin-Mediated Degradation of Insulin Receptor in Obese Mice. *Diabetes* **66**, 689-698, doi:10.2337/db16-1104 (2017).

19   Papadopoulos, C., Kravic, B. & Meyer, H. Repair or Lysophagy: Dealing with Damaged Lysosomes. *J Mol Biol* **432**, 231-239, doi:10.1016/j.jmb.2019.08.010 (2020).

20   Elrick, M. J., Yu, T., Chung, C. & Lieberman, A. P. Impaired proteolysis underlies autophagic dysfunction in Niemann-Pick type C disease. *Hum Mol Genet* **21**, 4876-4887, doi:10.1093/hmg/dds324 (2012).

21   Maetzel, D. *et al.* Genetic and chemical correction of cholesterol accumulation and impaired autophagy in hepatic and neural cells derived from Niemann-Pick Type C

patient-specific iPS cells. *Stem Cell Reports* **2**, 866-880, doi:10.1016/j.stemcr.2014.03.014 (2014).

22   Ordonez, M. P. *et al.* Disruption and therapeutic rescue of autophagy in a human neuronal model of Niemann Pick type C1. *Hum Mol Genet* **21**, 2651-2662, doi:10.1093/hmg/dds090 (2012).

23   Sarkar, S. *et al.* Impaired autophagy in the lipid-storage disorder Niemann-Pick type C1 disease. *Cell Rep* **5**, 1302-1315, doi:10.1016/j.celrep.2013.10.042 (2013).

24   Maejima, I. *et al.* Autophagy sequesters damaged lysosomes to control lysosomal biogenesis and kidney injury. *EMBO J* **32**, 2336-2347, doi:10.1038/emboj.2013.171 (2013).

25   Papadopoulos, C. *et al.* VCP/p97 cooperates with YOD1, UBXD1 and PLAA to drive clearance of ruptured lysosomes by autophagy. *EMBO J* **36**, 135-150, doi:10.15252/embj.201695148 (2017).

26   Radulovic, M. *et al.* ESCRT-mediated lysosome repair precedes lysophagy and promotes cell survival. *EMBO J* **37**, doi:10.15252/embj.201899753 (2018).

27   Skowyra, M. L., Schlesinger, P. H., Naismith, T. V. & Hanson, P. I. Triggered recruitment of ESCRT machinery promotes endolysosomal repair. *Science* **360**, doi:10.1126/science.aar5078 (2018).

28   Davis, O. B. *et al.* NPC1-mTORC1 Signaling Couples Cholesterol Sensing to Organelle Homeostasis and Is a Targetable Pathway in Niemann-Pick Type C. *Dev Cell* **56**, 260-276 e267, doi:10.1016/j.devcel.2020.11.016 (2021).

29   Dardis, A. *et al.* Altered localization and functionality of TAR DNA Binding Protein 43 (TDP-43) in niemann- pick disease type C. *Acta Neuropathol Commun* **4**, 52, doi:10.1186/s40478-016-0325-4 (2016).

30   Liu, G. *et al.* Endocytosis regulates TDP-43 toxicity and turnover. *Nat Commun* **8**, 2092, doi:10.1038/s41467-017-02017-x (2017).

31   Tooze, S. A., Abada, A. & Elazar, Z. Endocytosis and autophagy: exploitation or cooperation? *Cold Spring Harb Perspect Biol* **6**, a018358, doi:10.1101/cshperspect.a018358 (2014).

32   Liu, G. *et al.* Cdc48/VCP and Endocytosis Regulate TDP-43 and FUS Toxicity and Turnover. *Mol Cell Biol* **40**, doi:10.1128/MCB.00256-19 (2020).

33   Wheeler, S. & Sillence, D. J. Niemann-Pick type C disease: cellular pathology and pharmacotherapy. *J Neurochem* **153**, 674-692, doi:10.1111/jnc.14895 (2020).

34   Hill, S. E. & Colon-Ramos, D. A. The Journey of the Synaptic Autophagosome: A Cell Biological Perspective. *Neuron* **105**, 961-973, doi:10.1016/j.neuron.2020.01.018 (2020).

35   Nixon, R. A. *et al.* Extensive involvement of autophagy in Alzheimer disease: an immuno-electron microscopy study. *J Neuropathol Exp Neurol* **64**, 113-122, doi:10.1093/jnen/64.2.113 (2005).

36   Maday, S. Mechanisms of neuronal homeostasis: Autophagy in the axon. *Brain Res* **1649**, 143-150, doi:10.1016/j.brainres.2016.03.047 (2016).

37   Ikenaka, K. *et al.* dnc-1/dynactin 1 knockdown disrupts transport of autophagosomes and induces motor neuron degeneration. *PLoS One* **8**, e54511, doi:10.1371/journal.pone.0054511 (2013).

38   Hill, S. E. *et al.* Maturation and Clearance of Autophagosomes in Neurons Depends on a Specific Cysteine Protease Isoform, ATG-4.2. *Dev Cell* **49**, 251-266 e258, doi:10.1016/j.devcel.2019.02.013 (2019).

39   Gowrishankar, S., Wu, Y. & Ferguson, S. M. Impaired JIP3-dependent axonal lysosome transport promotes amyloid plaque pathology. *J Cell Biol* **216**, 3291-3305, doi:10.1083/jcb.201612148 (2017).

40   Tammineni, P., Ye, X., Feng, T., Aikal, D. & Cai, Q. Impaired retrograde transport of axonal autophagosomes contributes to autophagic stress in Alzheimer's disease neurons. *Elife* **6**, doi:10.7554/eLife.21776 (2017).

41   Oka, M. & Yoneda, Y. Importin alpha: functions as a nuclear transport factor and beyond. *Proc Jpn Acad Ser B Phys Biol Sci* **94**, 259-274, doi:10.2183/pjab.94.018 (2018).

42   Polymenidou, M. *et al.* Long pre-mRNA depletion and RNA missplicing contribute to neuronal vulnerability from loss of TDP-43. *Nat Neurosci* **14**, 459-468, doi:10.1038/nn.2779 (2011).

43   Arnold, E. S. *et al.* ALS-linked TDP-43 mutations produce aberrant RNA splicing and adult-onset motor neuron disease without aggregation or loss of nuclear TDP-43. *Proc Natl Acad Sci U S A* **110**, E736-745, doi:10.1073/pnas.1222809110 (2013).

44   Woolf, N. J. & Butcher, L. L. Cholinergic systems mediate action from movement to higher consciousness. *Behav Brain Res* **221**, 488-498, doi:10.1016/j.bbr.2009.12.046 (2011).

45   Rangel, D. M., Sobreira-Neto, M. A., Nepomuceno, C. R., Marques, E. R. & Braga-Neto, P. Sleep disorders in NiemannPick disease type C, beyond cataplexy. *Sleep Med* **57**, 122-127, doi:10.1016/j.sleep.2019.02.007 (2019).

46   Vankova, J. *et al.* Sleep disturbances and hypocretin deficiency in Niemann-Pick disease type C. *Sleep* **26**, 427-430, doi:10.1093/sleep/26.4.427 (2003).

47   Stifani, N. Motor neurons and the generation of spinal motor neuron diversity. *Front Cell Neurosci* **8**, 293, doi:10.3389/fncel.2014.00293 (2014).